# Advancing tendon-to-bone enthesis repair

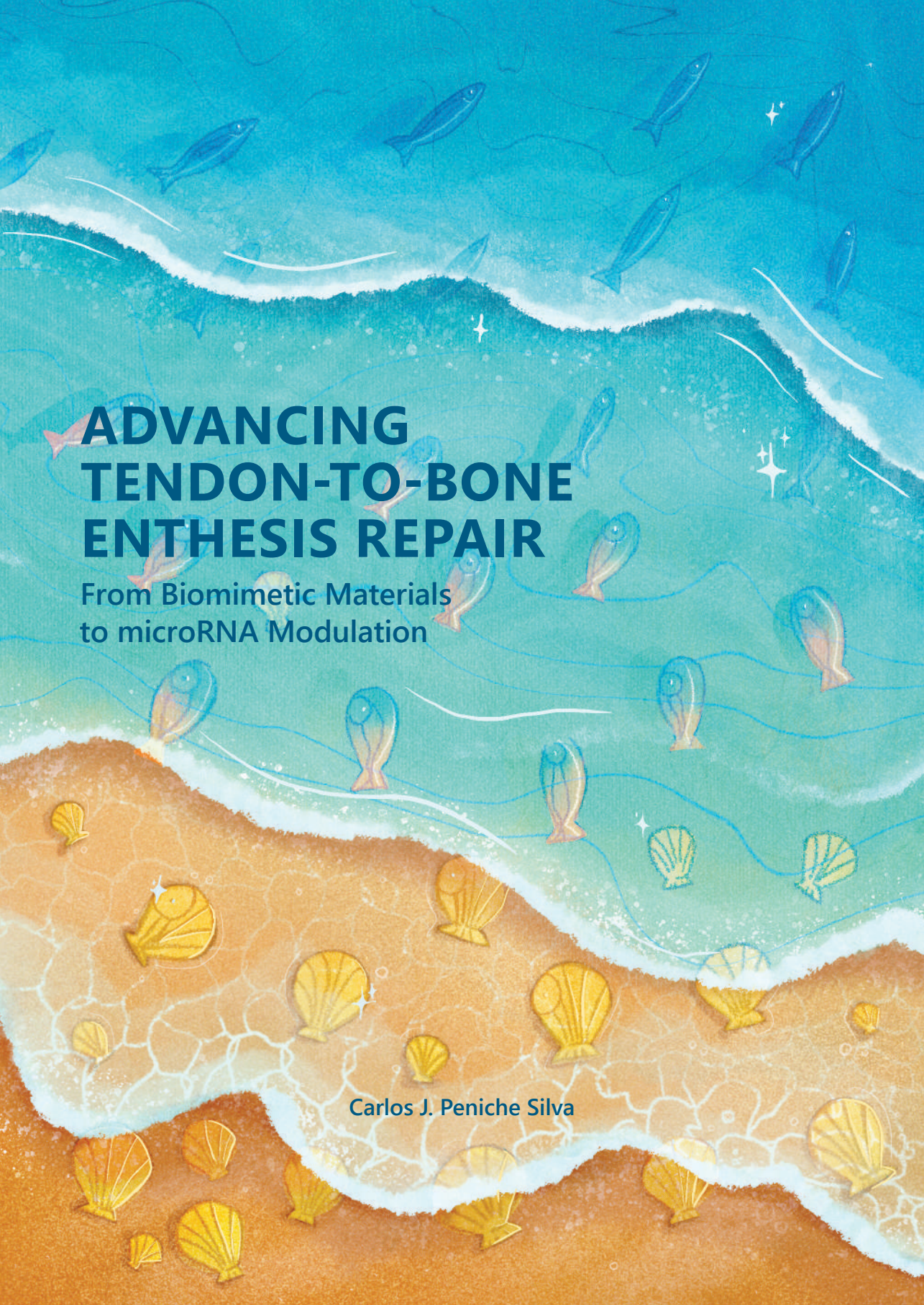

# ADVANCING TENDON-TO-BONE ENTHESIS REPAIR

## From Biomimetic Materials to microRNA Modulation

Carlos J. Peniche Silva

# ADVANCING TENDON-TO-BONE ENTHESIS REPAIR:

## From Biomimetic Materials to microRNA Modulation

The work presented in this thesis was funded by LINK (Limburg invests in its Knowledge Economy) and partially funded by the ON Foundation (p20-105) and the 2022 Mobility Grant from the European Society of Clinical Investigation (ESCI).




**ISBN**
978-94-93330-75-7

**Cover design**
Irma B. Peniche Silva

**Printing**
Proefschriftspecialist | proefschriftspecialist.nl

**Layout**
Anna | persoonlijkproefschrift.nl

# Advancing Tendon-to-Bone Enthesis Repair: From Biomimetic Materials to microRNA Modulation

## Dissertation

to obtain the degree of Doctor at Maastricht University
on the authority of the Rector Magnificus, Prof. Dr. Pamela Habibović in
accordance with the decision of the Board of Deans, to be defended in public on
**Wednesday, 17th of April 2024, at 16:00 hours**

by

**Carlos Julio Peniche Silva**

Born on the 5th of July 1990, in Havana, Cuba

**Supervisors:**

Prof. Dr. Martijn van Griensven (Maastricht University)
Prof. Dr. Elizabeth Rosado Balmayor (RWTH University Hospital Aachen, Germany)

**Assessment Committee:**

Prof. Dr. Roman Truckenmüller (Chair, Maastricht University)
Dr. Berta Cillero-Pastor (Maastricht University)
Prof. Dr. Denitsa Docheva (University of Wuerzburg, Germany)
Dr. Pieter Emans (Maastricht University)
Prof. Dr. Dimitrios Zevgolis (University College Dublin, Ireland)

## TABLE OF CONTENTS

CHAPTER 1

# General Introduction

# 1 INTRODUCTION

The human body possesses the remarkable ability to heal in response to various injuries. For centuries, we have attempted to improve such healing capabilities by different means, some more successful than others. Practices that today are given for granted, such as the cleansing and debridement of wounds, have their origins in ancient civilizations. Early cultures utilized natural remedies based on the use of herbs, milk, vinegar, or even wine as antibiotic solutions to sanitize and protect the injured tissue from infections and improve the healing of the wounded area. Furthermore, some of the first pieces of evidence of realistic medical science approaches to treat complex injuries date back over 2,000 years. Such are the records of skin graft procedures by the Indian physician Sushruta to treat facial and dental injuries [1]. Likewise, the miraculous transplantation of a limb, estimated to have happened around 474 CE, was forever immortalized by the Italian artist Matteo di Pacino back in the 14$^{th}$ century with his famous painting "Miracle of the Black Leg" as a testament to the pursuit of innovative solutions to restore the function of damaged or diseased tissues.

As our understanding of human biology grew, we came up with more sophisticated ideas to improve the healing of injured tissues that would not regenerate by themselves. Today, an emerging field known as Regenerative Medicine deals with the development of therapeutic strategies that combine tissue engineering approaches with biomaterial design to improve the healing and regeneration of complex tissues. One of these complex tissues, the enthesis, is the main subject of study of this thesis.

The enthesis is an interphase tissue that connects tendons and ligaments to bone [2]. It plays a crucial role in transmitting mechanical force from tendons or ligaments to bone and ensuring the functional integrity of this transition. However, injuries to the enthesis often undergo limited healing, which usually involves the formation of a scar at the site of the injury that compromises tissue functionality [3,4].

The majority of entheses-related injuries occur during or as a consequence of, the practice of sports. This is mostly due to the functional relevance of the tendon-to-bone entheses for locomotion and movement in general and the increased load sustained by the joints during the practice of sports. Records show that by the first editions of the Greek Olympics, approximately around the year 800 BCE, tendon and entheses injuries were acknowledged as some of the most common sports-related injuries. To help prevent such injuries and improve recovery after workouts, ancient Olympic athletes used to massage their muscles and tendons

with olive oil after training [5]. However, once an injury occurred, the options for treatment were very limited, and more often than not, resulted in poor recovery.

Over two thousand years have passed since the first celebration of the Greek Olympics, and we are still learning new ways to improve the healing of injured tendons and tendon-to-bone entheses. Unfortunately, and despite the current efforts, the regeneration of the tendon-to-bone enthesis remains a challenge [4,6]. Hence, this thesis aims to further explore novel therapeutic strategies, from the use of biomimetic scaffolds to the potential applications of microRNAs (miRNAs) as molecular cues to aid the healing and regeneration of the enthesis.



Nowadays, injured tendons and entheses can be treated conservatively, with the use of anti-inflammatory drugs, shock wave therapy, or via surgical intervention, which usually relies on the use of sutures or bone anchors to re-attach torn tendons to the bone [3,7]. Additionally, a plethora of biomaterials (e.g. collagen, silk, PLGA, GelMA, etc.) has been explored for their potential to aid the process of enthesis regeneration and healing [8,9]. **Chapter 2** of this thesis provides an overview of the state of the art in the context of tissue engineering applications for tendon and enthesis regeneration. Furthermore, we specifically address the most significant progress made in the field of silk biomaterials for tendon and enthesis tissue engineering.

**Chapter 3** deals with the comparative characterization between the three most clinically relevant sites of enthesis injuries (i.e. the supraspinatus enthesis, the patellar tendon enthesis, and the Achilles tendon enthesis) in a rodent model. Here, the biomechanical, morphological, and genetic differences between the three localizations are investigated and discussed. Such characterization revealed that the rotator cuff enthesis was the smallest, narrower, and weaker enthesis while the patellar tendon enthesis was the strongest and showed the largest enthesis cross-sectional area. Important morphological differences between the interphases investigated are herein described. The patellar tendon enthesis and the supraspinatus tendon enthesis showed a cartilaginous transition at the tendon-to-bone interphase while the Achilles enthesis showed a more abrupt transition from tendon to bone. As a key result of this chapter, the patellar tendon enthesis was chosen as the enthesis model to be used for further studies.

Precisely in **Chapter 4**, an injury in the patellar tendon enthesis of our rodent model was created and the defect was treated by implanting two versions of a biphasic silk fibroin scaffold. One version presented an abrupt transition between the phases while the other one showed an interconnected transition between the tendon and bony phases of the scaffold. This chapter demonstrates that the use of a biomimetic enthesis scaffold that presents an interconnected

transition between the phases promotes superior enthesis healing with a better recapitulation of the native enthesis morphology than the biphasic scaffold with an abrupt transition between the phases.

**Chapter 5** describes the healing process of an injured patellar enthesis at time points 1 day and 10 days after the creation of the injury by investigating the patterns of expression of fibrosis-related miRNAs. Target prediction for the dysregulated miRNAs was performed, which allowed for the establishment of potential regulatory effects for the herein-found dysregulated miRNAs and their respective predicted mRNA targets. Furthermore, it was possible to localize the upregulation of at least one of the investigated miRNAs (i.e. miR-16-5p) in the injured areas of the enthesis via *in situ* hybridization. This result served as an inspiration to investigate the therapeutic potential of miR-16-5p in enthesis tissue-engineering applications.

Consequently, in **Chapter 6**, we developed a magnetic-responsive GelMA-based bioink loaded with either mimics or inhibitors of miR-16-5p. Herewith, we evaluated the effects of the upregulation or inhibition of miR-16-5p on the tenogenic differentiation of adipose-derived mesenchymal stem cells AdMSCs encapsulated within the GelMA bioink. The encapsulated cells were able to uptake the miRNA mimics or inhibitors from the hydrogel and the effects on the regulation of the mRNA targets (e.g. SMAD3, COL1A1, and MKX) were sustained for at least 21 days of culture. The results herein described represent a significant advance towards the development of a bioactive bioink for enthesis tissue-engineering applications.

Finally, **Chapter 7**, consists of a general discussion of the inhere described results. A critical analysis of the investigation and the most significant conclusions are given. This chapter is followed by the valorization potential of this research, main conclusions, and future perspectives.

## 2 REFERENCES


1. Singh, V. Sushruta: The father of surgery. National Journal of Maxillofacial Surgery 2017, 8.
2. Apostolakos, J.; Durant, T.J.; Dwyer, C.R.; Russell, R.P.; Weinreb, J.H.; Alaee, F.; Beitzel, K.; McCarthy, M.B.; Cote, M.P.; Mazzocca, A.D. The enthesis: a review of the tendon-to-bone insertion. Muscles, ligaments and tendons journal 2014, 4, 333-342.
3. Bunker, D.L.; Ilie, V.; Ilie, V.; Nicklin, S. Tendon to bone healing and its implications for surgery. Muscles Ligaments Tendons J 2014, 343-350, doi:10.11138/mltj/2014.4.3.343.
4. Derwin, K.A.; Galatz, L.M.; Ratcliffe, A.; Thomopoulos, S. Enthesis Repair: Challenges and Opportunities for Effective Tendon-to-Bone Healing. J Bone Joint Surg Am 2018, 100, e109-e109, doi:10.2106/JBJS.18.00200.
5. Nomikos, N.N.; Nomikos, G.N.; Kores, D.S. Review paper. The use of deep friction massage with olive oil as a means of prevention and treatment of sports injuries in ancient times. Archives of Medical Science 2010, 6, 642-645, doi:10.5114/aoms.2010.17074.
6. Patel, S.; Caldwell, J.M.; Doty, S.B.; Levine, W.N.; Rodeo, S.; Soslowsky, L.J.; Thomopoulos, S.; Lu, H.H. Integrating soft and hard tissues via interface tissue engineering. J Orthop Res 2018, 36(4), 1069-1077, doi: 10.1002/jor.23810.
7. Jiang, N.; Wang, B.; Chen, A.; Dong, F.; Yu, B. Operative versus nonoperative treatment for acute Achilles tendon rupture: a meta-analysis based on current evidence. International Orthopaedics 2012, 36, 765-773.
8. Sun, W.; Gregory, D.A.; Tomeh, M.A.; Zhao, X. Silk Fibroin as a Functional Biomaterial for Tissue Engineering. International Journal of Molecular Sciences 2021, 22, doi:10.3390/ijms22031499.
9. Hou, J.; Yang, R.; Vuong, I.; Li, F.; Kong, J.; Mao, H.-Q. Biomaterials strategies to balance inflammation and tenogenesis for tendon repair. Acta Biomaterialia 2021, 130, 1-16, doi:https://doi.org/10.1016/j.actbio.2021.05.043.

CHAPTER 2

# Silk Biomaterials for Tendon and Tendon-to-Bone Enthesis Tissue Engineering

C. J. Peniche Silva, E. R. Balmayor, M. van Griensven

*Book Title: Silk-Based Biomaterials for Tissue Engineering, Regenerative and Precision Medicine, Second Edition. Editors: Subhas C. Kundu and Rui L. Reis. 2023*

## ABSTRACT

Tendons and tendon-to-bone entheses are frequent injury sites among athletes, accounting for up to 50% of all sports-related injuries. Additionally, about 2% to 5% of the general population is affected by tendinopathies up to some degree due to overuse, sport-related injuries, and/or degeneration. This situation is likely to worsen in the coming years due to the increasing popularity of sports practice among the middle-aged and elderly population. Unfortunately, the success rate of clinical intervention to treat tendinopathies is far from desirable, with surgical repair failure rates ranging from 20% to 90% in many cases. In this chapter, we review the perspective of tissue engineering to tackle the challenge that represents the successful treatment of injured tendon/enthesis. Furthermore, we look into the potential use of silk biomaterials in tendon and enthesis tissue engineering.

## 1 INTRODUCTION

Tendons are in charge of transferring force from the muscle to the bony skeleton, allowing the movement and stabilization of joints [1]. Tendons have evolved in many different shapes and sizes to perform their function. Some can be flat in appearance, such as the patellar or the supraspinatus tendons, while others are round, as is the case of the *flexor digitorum profundus* [2]. Generally, over 90% of the cells populating tendons are tenocytes and tenoblasts. In comparison, the remaining 10% consists of chondrocytes populating the tendon-to-bone interphase, synovial cells of the tendon sheath, and endothelial and smooth muscle cells [3]. The predominant structural components of the tendon are the fibril-forming collagen type I and proteoglycans, although other collagens are also present (e.g., collagens type II, III, V, VI, IX, XI) [4]. Three molecules of collagen type I combine to form a tropocollagen molecule. A pack of five tropocollagens comprises a microfibril and microfibrils aggregate together to form fibrils. Similarly, fibrils group into fibers, and fibers group into fiber bundles [2]. This structure is represented in Fig. 1 (left). Such design allows the tendon to withstand longitudinal deformation while the proteoglycan content is responsible for the viscoelastic behavior of the tendon [5].

The muscle-to-tendon interphase is termed the myotendinous junction [6]. Here, myocytes of the muscle tissue connect to the tendon's collagen fibrils via finger-like processes, which are interdigitations of the sarcolemma of muscle cells where actin filaments interact with the collagen type I-rich extracellular matrix (ECM) of the tendon [7].

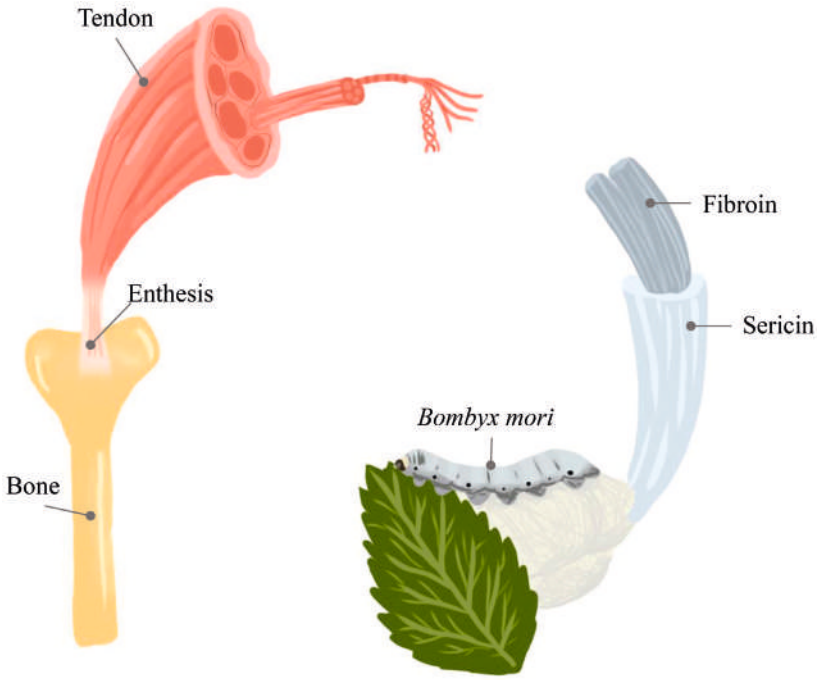


**Figure 1:** Representation of the hierarchical structure of the tendon (left) and the structural organization of the silk protein (right).

The tendon-to-bone interphase, or enthesis, presents a more complex structure. Since the enthesis acts as the connection point between the tendon and the bone, the leading role of the enthesis is to equalize the differences in elastic modulus between these two tissues [8]. Therefore, the anatomy of this transition includes both a tendon and a bony side localized at each (respective) opposing end of the enthesis. The interphase area, from tendon to bone, is characterized by a progressive loss of the longitudinal alignment of the collagen fibers towards a more disorganized bony-like structure. As the longitudinal arrangement of the collagen fibers decreases, the mineral content increases towards the bony end of the enthesis [9]. Entheses are usually classified as fibrous when the tendon-to-bone interphase is characterized by dense connective tissue. Alternatively, the enthesis is classified as fibrocartilaginous enthesis when the interphase is characterized by a collagen type II-rich fibrocartilaginous transition [10].

The physiological function of the tendon comes with a caveat; tendons and their tendon-to-bone attachment sites are prone to inflammation, disease, and rupture [1, 3]. Perhaps the most common cause of tendons and entheses injuries is the practice of regular physical activity [3]. It has been estimated that almost 50% of all sports-related injuries are related to tendon or enthesis injuries [11, 12]. However, many risk factors contribute to the incidence of tendon and

enthesis injury other than the practice of sports. Some of which are age, nutrition, metabolic diseases, and genetics [13].

The highly specialized biology of the tendon makes the tendon and its enthesis a challenging site of injury [3, 9, 14, 15]. Tendon injuries are treated conservatively or by surgical intervention [9, 16-18]. However, it has been demonstrated that non-surgical treatment is often followed by operative management of the injury due to the unsuccessful outcome of conservative treatments [6, 19]. Unfortunately, the landscape of surgical intervention to treat tendon or enthesis injuries doesn't look any brighter. It has been estimated that 20% to 90% of surgically treated patients suffer recurrent ruptures in the treated tendon after surgery [20-22]. Such a situation makes the critical need clear for developing novel therapies that can effectively improve the healing of the tendon and its enthesis.



## 2 TENDINOPATHIES: CURRENT THERAPIES AND LIMITATIONS

Tendinopathies are invalidating conditions that affect an alarming fast-growing number of people in today's society [23]. Around 30% of all musculoskeletal consultations are due to tendon injury or tendinopathy [24, 25]. This includes acute tendon injuries such as tendon/enthesis rupture or inflammation and chronic tendinopathies due to overuse and/or degeneration.

In an attempt to understand how the mechanical properties of a tendon behave and how strain patterns can lead to tendon rupture, Nagelli *et al.* investigated the mechanical properties of fresh Achilles tendons harvested from young human cadavers. Their study described the accumulation of lateral strain early in the loading cycle while longitudinal strain remained low. However, the high longitudinal strain was observed in the weakest part of the Achilles tendon, the mid-substance, immediately before rupture. These new insights advance the understanding of the mechanical behavior of tendons as they are stretched to failure. However, further research is needed to understand how aging and tendinopathy affect this behavior as older individuals and people with tendinopathy are significantly more likely to sustain a tendon rupture [26].

The native mechanism of healing of the tendon tissue is also a significant subject of study [8, 25]. It is known that the healing process is mainly dictated by the tendon cells and the surrounding ECM. Typically, such a process includes an inflammatory phase followed by cell proliferation and remodeling of the ECM. Regrettably, the general outcome of the healing is scar tissue that doesn't replicate the mechanical properties nor the functionality of the uninjured tissue [15].

Tendinopathies are usually dealt with via conservative treatments or surgical intervention. Traditional treatments of tendinopathies include but are not restricted to, the use of non-steroidal anti-inflammatory drugs (NSAIDs), corticosteroids, platelet-rich plasma, eccentric exercise, extracorporeal shock wave therapy (ESWT), and ultrasound [27, 28]. Alternatively, surgical approaches rely on reincorporating the tendon into the bone via sutures or bone anchors [21, 29].

Invalidating symptoms such as pain and dysfunction can be effectively relieved with NSAIDs or corticosteroids. However, the long-term use of such drugs is not recommended due to damaging the tissue and their application is therefore limited to short-term pain reduction. Furthermore, some reports indicate that the use of NSAIDs may exert both beneficial and detrimental effects on tendon healing depending on the timing of the application [30, 31]. Similarly, there is evidence of potential adverse effects of the use of corticosteroids on the biomechanical properties of the tendons, which increases the risk of spontaneous tendon rupture [32, 33]. Other forms of non-surgical therapy, such as ESWT, have been used to treat chronic calcic tendinopathy with some controversial results. Some authors have described a complete resolution of calcification in patients suffering from calcic shoulder tendinitis, which significantly decreased pain and improved shoulder function in the treated patients [34, 35]. However, the lack of standardized treatment protocols and long follow-ups is a limiting factor in determining these treatments' effectiveness [36]. Non-surgical intervention for acute tendon rupture has been suggested to be associated with a significant increase in the incidence of recurrent rupture compared to surgical treatment [37]. Or at least that has been the case for acute and chronic Achilles tendon ruptures [37, 38].

Surgical intervention is common in partial tears, full-thickness rotator cuff tears, and Achilles tendon and patellar tendon rupture cases since disability is high in patients suffering from such injuries. However, the success of such interventions is questionable [21]. A recent study reviewing nine trials involving 1007 patients failed to demonstrate that surgical intervention provided clinically meaningful benefits to people with symptomatic rotator cuff tears [39]. Surgical repair is also the most common treatment for ruptured Achilles tendon [40]. Nonetheless, it has been reported that, even though gait speed, stride length, and peak ankle moment and power can be significantly increased after surgical intervention of a ruptured Achilles tendon, patients might still exhibit impairments one year after the surgery, including decreased power in the knee and ankle compared with healthy controls [40].

Surgical management of ruptured patellar tendon seems to have a better prognosis, and failure is usually associated with technical errors during surgery

or delayed diagnosis and treatment [41]. Yet, a recent review of the performance-based outcomes following patellar tendon repair in professional athletes revealed that American football, basketball, and soccer athletes suffered from a significant drop in their performance and shortening of their professional sport carriers after surgical treatment of their patellar tendon injuries [42].

## 3 TISSUE ENGINEERING FOR TENDON AND ENTHESIS REPAIR

Tissue engineering (TE) combines scaffolds, cells, and biologically active molecules to promote the generation or regeneration of functional tissue [43]. This concept has witnessed significant improvements in the last couple of decades with novel TE strategies resulting in commercially available tissue-engineered products, including several scaffolds, hydrogels, matrices, and sponges developed by different techniques and with a wide range of potential applications [44, 45].



As described in the previous section of this chapter, the surgical reconstruction of the tendon and the tendon-to-bone enthesis is challenging and often fails. Therefore, it is not hard to understand the recent surge of TE-based strategies specifically tailored to tackle tendon and enthesis regeneration. The ever-growing character of TE offers almost unlimited opportunities for exploring new techniques and biomaterials to pursue therapeutic solutions to improve tendon regeneration. However, very few make the transit from the lab to the clinic.

In particular, developing biomaterials to produce biomimetic constructs for tendon and enthesis regeneration has come a long way. In the context of tendon and enthesis-TE, biomaterials are expected to supply mechanical support to the engineered construct until the affected tissue can re-take the load corresponding to its anatomic role [46]. Such materials should deliver the necessary platform for cell infiltration, proliferation, and ECM deposition. For this purpose, biomaterials are desired to be (1) biocompatible; (2) biomimetic; and (c) biodegradable. The biomaterials used in tendon and enthesis-TE can have a natural or synthetic origin. They are often combined with chemical and physical factors to improve their pro-healing capabilities [43].

Synthetic polymers such as poly-ε-caprolactone (PCL), poly(lactic acid) (PLA), poly(glycolic acid) (PGA), and poly(lactic-co-glycolic acid) (PLGA) are desirable. They can be manufactured with precise control, producing biomimetic microstructures with excellent mechanical properties and high area-to-volume ratios [47-49]. However, such synthetic biomaterials lack cell-binding ligands and their hydrolysis releases acidic products that have been proven toxic to tenocytes and osteoblasts [50, 51].

Natural polysaccharide polymers are popular alternatives used in tendon repair [52-54]. They are highly biocompatible, favor cell adhesion, and their biochemical cues can even exert immunomodulatory effects [55-57]. Commonly used biopolymers are hyaluronic acid (HA), chondroitin sulfate, chitosan, and alginate [58-60]. They present high charge density, which allows for the complexation with therapeutic agents. At the same time, their tunable hydrophobicity makes them suitable for producing a wide range of constructs, from hydrophilic injectable hydrogels to solid scaffolds [61-63]. Despite their desirable properties, for many years, polysaccharide polymers were solely considered to target hard-tissue regeneration such as cartilage and bone [64, 65]. Hence, the use of these polymers in tendon and enthesis-TE is short-lived and there is much that we do not understand yet regarding the role of these materials in cell signaling and immune recognition. Additionally, molecular weight or purity variables tend to vary amongst samples of the same material, thus hindering reproducibility [66].

Another attractive option as biomaterials for tendon and enthesis-TE are proteins such as collagen, fibrin, and silk. Of the three, collagen is perhaps the most widely used, as collagen constitutes the main component of the tendon ECM. Fibrin is a polymer naturally composed during wound healing. Both collagen and fibrin are present to bind the sites for cells and growth factors. This favors cell migration, adhesion, growth, and differentiation [67-70]. Fibrin has been used as a matrix to deliver stem cells in, for instance, a patellar tendon defect [71]. However, collagen scaffolds' mechanical strength and structural stability decrease upon hydration [72], and their degradation rate can be too high to allow the deposition of new tissue. Thus, collagen scaffolds are chemically or physically modified to reduce solubility and improve their biomechanics [73, 74]. Platelet-rich-fibrin scaffolds exhibit excellent elasticity and offer the additional benefits of prolonged release of growth factors and other hemocomponents to the site of injury that has proven to induce pro-healing effects [75, 76]. Yet, using these scaffolds for tendon repair has yielded conflicting results between animal models and clinical trials, possibly due to the lack of standardization of the preparation protocols and distinct differences between donors [76, 77].

Alternatively, silk offers exceptional mechanical properties in strength, toughness, and elasticity comparable to that of tendons and ligaments [78]. Moreover, silk is non-toxic, biocompatible, and hemocompatible, and it promotes cell adhesion and proliferation [78, 79]. Hence, silk-based composites are some of the most promising materials for fabricating scaffolds and biomimetic constructs [80]. Furthermore, silk can be manufactured into fiber bundles with tunable degradation rates and solubility, which makes it ideal for tendon and enthesis tissue engineering [81-83]. As a consequence, tendon and enthesis-TE have benefited from the use of silk-based constructs in recent years. Hereafter, we

will try to summarize some of the most relevant advances related to the role of silk in tendon and enthesis-TE.

## 4 SILK AND SILK FIBROIN IN TENDON TISSUE ENGINEERING

Silk is a biopolymer produced by many members of the arthropod family, including spiders, silkworms, flies, and silverfish. Each of these arthropods has silk components with particular amino acid composition and structural properties [84, 85]. Even within the same species, silk's composition and mechanical properties can vary due to certain environmental conditions or variations in the arthropod's nutrition [86].



The most commonly used silk in biomedical applications is one produced by silkworms, in particular from the *Bombyx mori* silkworm [84]. The essential structural components of the *B. mori* silk are the proteins fibroin and sericin, as represented in Fig. 1 (right). Fibroin is hydrophobic and forms microfibrils that assemble into filaments. The hydrophilic sericin glues these filaments together to form silk fibers [87]. Of the two proteins, only fibroin is used in biomedical applications and its use in the United States has been approved by the FDA [88]. Sericin, however, is known to be immunogenic. Therefore, silk must be processed, and the sericin removed [89]. This process yields a regenerated silk fibroin solution similar to the state of the fibroin in the glands of the arthropods before being spun [90].

Regenerated silk fibroin solutions are the starting material for silk fibroin sponges or scaffolds. In its water-soluble form, fibroin solutions can be processed in mild conditions without the need for harmful chemicals, preserving the excellent biocompatibility of the materials [84, 91]. It is possible to obtain a broad range of structures from silk fibroin solutions, including porous constructs, ropes, textured yarns, membranes, and so on.

In 2009, Fang *et al.* obtained a braided silk fibroin scaffold to treat tendon defects [92]. Their study demonstrated that the material promoted the adhesion and propagation of tenocytes *in vitro*. Furthermore, they tested the scaffolds *in vivo* by implanting them into a defect created in the Achilles tendon of New Zealand rabbits. They observed that after 16 weeks, neo-tendon tissue was formed at the site of the injury with a predominant composition of collagen type I and morphological features that resembled those from the native tendon.

In a more recent study, Yao *et al.* demonstrated that silk fibroin could also be used to fabricate membranes with different porosity. Using a rat Achilles tendon rupture suture wrapping model, they showed that these membranes could

reduce inflammation and promote ECM production *in vivo* [93]. Furthermore, they observed that, by decreasing the porosity of their silk fibroin membranes, they improved tendon repair and the regeneration capabilities of the biomaterial. Similarly, Lu *et al*. exploited the versatility offered by silk fibroin solutions to prepare silk fibroin films with biomimetic microstructure [94]. Here, silk fibroin films with tendon-like microstructure were obtained by casting and drying silk fibroin solutions on polydimethylsiloxane (PDMS) molds with a microstructure of parallel grooves whose width and depth corresponded to the normal tendon structure. They observed that, when seeding tendon stem/progenitor cells on the surface of the biomimetic silk fibroin films, the cells adopted a more slender morphology and expressed tenogenic markers such as scleraxis, tenascin-C, tenomodulin, and collagen type I at higher levels than the cells seeded onto silk fibroin films with a smooth surface.

These and many other examples support silk fibroin as a promising biomaterial suitable for tendon-TE applications. Moreover, these examples relied solely on the intrinsic properties of silk as a biomaterial. In the next section of this book chapter, we will explore how silk can be combined with other polymers and factors to improve the material's regeneration capabilities further.

## 5 SILK COMPOSITES FOR TENDON TISSUE ENGINEERING

Silk fibroin is usually combined with other biomaterials to enhance bioactivity and improve mechanical properties [95-97]. Additionally, the versatility offered by silk allows for the production of complex structures with excellent control in pore sizes and/or fiber alignments. However, silk composites are most commonly used to increase cell attachment capabilities of silk fibroin constructs since the silk protein extracted from *B. mori* does not contain an RGD sequence, also known as the site for integrin-mediated cell adhesion [98, 99]. This can be solved by surface coating or chemical coupling with RGD peptides [99-101]. In 2006, Kardestuncer *et al.* tested the effects of RGD-coating on silk fibroin sutures on the adhesion, proliferation, and differentiation of tenocytes. They found that cell proliferation and expression levels of collagen type I and decorin were increased in silk-RGD substrates [102]. A few years later, Yang *et al.* demonstrated that by fusing an RGD peptide with a recombinant mussel adhesive protein (MAP-RGD) it was possible to obtain MAP-RGD-blended silk fibroin fibers with improved hydrophilicity and biodegradability without affecting the mechanical properties of the silk fibroin fibers. Furthermore, the coated fibers exhibited enhanced cell adhesion and proliferation [101].

Another possibility to improve cell attachment is the use of lectin. Lectin obtained from wheat germ agglutinin can be covalently bound to fibroin using carbodiimide.

This modification increased attachment by 17-fold of stem cells. Furthermore, the cells attached so well that they were more resistant to shear stress [103].

Alternatively, gelatin, fibronectin, and collagen type I can be used to surface coat silk and improve cell attachment. Maghdouri-White *et al.* produced a nanofiber scaffold blending electrospun silk fibroin and collagen resulting in a biologically enhanced matrix with the mechanical properties of silk fibroin and the biocompatibility of collagen type I. Moreover, they demonstrated that, by incorporating BMP-13 into their engineered construct, cell migration, attachment, and viability of both human tenocytes and human adipose-derived stem cells were improved [96]. A different approach was followed by Qian *et al*. They produced a collagen scaffold with knitted silk that improved the healing of the tendon-to-bone enthesis in a rabbit model *in vivo* [104]. The designed scaffold performed significantly better than the alternative collagen scaffold without the silk, possibly due to the biphasic construct's superior biocompatibility, biodegradability, and mechanical properties.



Similarly, Xue *et al*. combined silk and gelatin methacryloyl sheets to produce nanofibrous scaffolds for tendon regeneration. By optimizing the ratio between silk fibroin and gelatin methacryloyl, they demonstrated improved proliferation of tenocytes with evidence of tenogenesis and enhanced *in vivo* tendon tissue regeneration [105]. The combination of silk fibroin and gelatin has also been explored using extrusion-based three-dimensional bioprinting [106]. Trucco *et al.* encapsulated hMSCs in silk fibroin-gelatin-based hydrogels to bio-print cell-laden constructs capable of sustaining chondrogenic differentiation in the presence of TGFβ-3. This principle demonstrated the potential of the combination of silk and gelatin to regenerate articular cartilage and the cartilaginous tendon-to-bone enthesis [106].

Another promising silk fibroin composite was tested by Young-Kwon Seo *et al*. They produced a silk scaffold containing lyophilized collagen-hyaluronan (HA) and wrapped it with an amniotic membrane before implanting it into an Achilles tendon defect created in New Zealand rabbits. Explants were harvested 12 weeks after the surgery and analyzed by histology, which allowed the authors to conclude that the rabbits treated with the composite silk-HA scaffold wrapped by amniotic membrane developed denser collagen bundles with a more linear and parallel organization of their fibers when compared to the groups treated with the silk scaffold alone and the silk scaffold-HA composite without the amniotic membrane [107].

Silk fibroin has also been combined with polymers such as PCL or poly-3-hydroxybutyrate (P3HB) to produce hybrid structures with tunable mechanical

properties specifically designed to treat tendon and ligament defects. That was the case with the nano/micro hybrid scaffold developed by Naghashzargar *et al*. [97]. By electrospinning PCL or P3HB onto twisted silk fibroin fibers, they obtained hybrid structures with superior mechanical properties and cell viability than the uncoated silk fibroin yarns. Unfortunately, the authors did not include *in vivo* applications of their hybrid constructs in their published study. Nevertheless, the fabrication method described appears suitable for tendon tissue engineering.

Another attractive silk fibroin-polymer composite was developed by Sahoo *et al*. [108]. They produced a hybrid scaffold combining knitted silk microfibers and electrospun bFGF-releasing PLGA nanofibers. This combination resulted in a construct that exhibited robust mechanical properties and a slow degradation rate of the silk and an ECM-like architecture achieved by electrospinning of the PLGA nanofibers. Furthermore, the coating with bFGF allowed for a sustained release of this factor that simulated the role of the native ECM, resulting in enhanced proliferation and tenogenic differentiation of the seeded BMSCs *in* vitro. Furthermore, the increased expression of collagen and other ECM markers contributed to improving the mechanical properties of the construct, which could well be an indication of the potential of this hybrid construct to be used in tendon-TE applications.

## 6 SILK BIOMATERIALS FOR ENTHESIS REPAIR

As previously discussed in this chapter, the tendon-to-bone enthesis is a challenging injury site. The stratified morphology of the tendon-to-bone transition makes this interphase tissue particularly hard to regenerate [21, 109]. Therefore, tissue engineers have explored the advantages offered by silk fibroin to create biomimetic constructs that recapitulate the opposing collagen fiber alignment and mineralization gradients found at the entheses. In some instances, the focus has been directed exclusively to the replication of the mineralization gradient at the interphase, as is the case of the biomineralized silk fibroin nanofibrous scaffold developed by Chen *et al*. [110]. Here, they produced an electrospun silk fibroin scaffold with a mineral gradient achieved by placing the construct vertically in a beaker containing simulated body fluid solution and allowing the solution to gradually flow out of the construct, which resulted in different mineral deposition on different areas of the scaffold. As a control, they produced another scaffold with a homogenous mineralization content and they used both versions to treat an Achilles tendon enthesis defect in a rat model. They observed that the gradient scaffold showed better osteointegration of the Achilles tendon with increased fibrocartilage formation at the enthesis area compared to the homogenous scaffold.

Alternately, Font Tellado *et al*. focused on producing a silk fibroin scaffold that simulated the morphology of the tendon-to-bone enthesis. Their study obtained a biphasic silk fibroin scaffold showing a smooth interconnected transition between the tendon-like portion and the bony-like portion of the scaffold by combining directional freezing, salt leaching, and freeze-drying. When seeded with adipose-derived mesenchymal stem cells (AdMSCs), the scaffold could support cell migration, proliferation, and differentiation *in vitro* [81]. Later, Peniche Silva *et al*. used this scaffold to treat a patellar enthesis defect in a rat model *in vivo*. The biphasic silk fibroin scaffold supported tissue growth and differentiation, allowing for the recapitulation of the patellar tendon-to-bone enthesis's highly complex morphological features and mechanical properties, demonstrating the promising potential of silk fibroin-based scaffolds in tendon and enthesis-TE [82].



Additionally, it was shown *in vitro* that the described effects of the topological features of the obtained biphasic silk fibroin scaffold on seeded AdMSCs could be further enhanced by incorporating the growth factors TGF-β2 and GDF5 in the tendon and bony portion of the scaffold, respectively. The synergic effect of the scaffold morphology and the growth factors lead to a further increase in the differentiation of AdMSCs towards an enthesis phenotype and genotype in a zone-specific fashion. Furthermore, functionalization of the scaffold with heparin increased the retention of the growth factors onto the surface of the scaffold, allowing the maximisation of the observed biological effects [111].

Another attractive silk scaffold was developed and tested by Teuschl *et al*. Their rope-like version of a silk fiber-based scaffold effectively promoted osteointegration and *de novo* tissue formation [112, 113]. Although the treated tissue was a ligament-to-bone interphase on this occasion, more specifically the anterior cruciate ligament (ACL) and its enthesis, the same principle and similar design could be applied to treat the tendon-to-bone enthesis of small, round-shaped tendons that integrate abruptly to the bone. In their study, Teuschl *et al*. created a multilayer silk scaffold with a core consisting of two strands of braided silk wrapped by a tubular sheathing structure. The scaffold was used to reconstruct the ACL in a sheep animal model. The ACL regeneration and osteointegration were evaluated for 12 months. It was observed that the ACL scaffold promoted the infiltration of regenerative cells from the surrounding tissues, which allowed for the regeneration of an ACL-like tissue that eventually would replace the scaffold after the complete degradation of the silk [112]. Furthermore, osteointegration was confirmed by forming a fibrous interzone at the scaffold-tibia insertion site, comparable to the tendon-to-bone healing observed after autographs and allographs [113].

## 7 CONCLUSIONS

Unlike bones or muscles, tendons have an inferior regeneration capacity. As a consequence, injured tendons and entheses take longer to heal, and usually, such healing does not regenerate the structure and mechanical properties of the native tissue. Tendon and enthesis-focused tissue engineering strategies have been directed to alleviate this situation by providing the injured tissue with the necessary architectural and biochemical cues in the shape of tissue-engineered constructs to speed up and guide the regeneration process. The advantages of silk as a biomaterial for tendon and enthesis-TE, have been exploited throughout the last couple of decades to produce films, particles, hydrogel, scaffolds, and other biomimetic constructs designed to replicate the aligned and parallel orientation of the collagen fibers of the tendon or the stratified but interconnected morphology of the tendon-to-bone enthesis. The combination of the mechanical strength of silk with its high degree of biocompatibility and tunable degradation rate has allowed for the obtention of constructs with promising tendon/enthesis regenerative capacity. Additionally, the relatively well-standardized process of silk extraction and preparation, and the associated low production cost, make this protein a very attractive biomaterial for tendon and enthesis-TE applications. However, the natural origin of silk constitutes a challenge on its own. Different species of arthropods will produce silk proteins with different amino acid sequences, which can affect the mechanical properties and biocompatibility of the protein. Moreover, other individuals within the same species can produce silk proteins with different qualities. Therefore, reproducibility is often a concern that may get its answer in genetically engineered silk protein.

Nevertheless, the advantages of working with silk far exceed the disadvantages. One of the major perks of working with silk is the ability to produce composites by mixing silk with other relevant biomaterials or chemical factors. By doing so, properties such as biocompatibility, bioactivity, and biomechanics have been enhanced, and the regeneration capacity of the tissue-engineered construct has increased significantly. Such promising outcomes have inspired the creation of more complex and ambitious constructs that replicate with more detail the intricate biology of the tendon and the enthesis, allowing for a more precise recapitulation of the features of the native tissue, which usually translates into better healing.

## 8 REFERENCES


1. Elliott, D.H., Structure and funtion of mammalian tendon. Biological Reviews, 1965. 40(3): p. 392-421.
2. Benjamin, M., S. Kaiser E Fau - Milz, and S. Milz, Structure-function relationships in tendons: a review. Journal of anatomy, 2008(1469-7580 (Electronic)).
3. Sharma, P. and N. Maffulli, Basic biology of tendon injury and healing. The Surgeon, 2005. 3(5): p. 309-316.
4. Ottani, V., et al., Hierarchical structures in fibrillar collagens. Micron, 2002. 33(7-8): p. 587-596.
5. Robinson, P.S., et al., Strain-rate sensitive mechanical properties of tendon fascicles from mice with genetically engineered alterations in collagen and decorin. J. Biomech. Eng., 2004. 126(2): p. 252-257.
6. Wu, F., M. Nerlich, and D. Docheva, Tendon injuries: Basic science and new repair proposals. 2017(2058-5241 (Print)).
7. Charvet, B., D. Ruggiero F Fau - Le Guellec, and D. Le Guellec, The development of the myotendinous junction. A review. 2012(2240-4554 (Print)).
8. Bunker, D.L., et al., Tendon to bone healing and its implications for surgery. Muscles Ligaments Tendons J, 2014(2240-4554 (Print)): p. 343-50.
9. Lu, H.H. and S. Thomopoulos, Functional Attachment of Soft Tissues to Bone: Development, Healing, and Tissue Engineering. Annual Review of Biomedical Engineering, 2013. 15(1): p. 201-226.
10. Tresoldi, I., et al., Tendon's ultrastructure. Muscles, ligaments and tendons journal, 2013. 3(1): p. 2.
11. Kannus, P., Theme: Tendon injuries and other tendon disorders in sports and exercise: Editorial. Scandinavian Journal of Medicine & Science in Sports, 1997. 7(2): p. 53-54.
12. Abat, F., et al., Current trends in tendinopathy: consensus of the ESSKA basic science committee. Part I: biology, biomechanics, anatomy and an exercise-based approach. Journal of Experimental Orthopaedics, 2017. 4(1): p. 18.
13. Aicale, R., A. Oliviero, and N. Maffulli, Management of Achilles and patellar tendinopathy: what we know, what we can do. Journal of Foot and Ankle Research, 2020. 13(1): p. 59.
14. Moffat, K.L., et al., Orthopedic Interface Tissue Engineering for the Biological Fixation of Soft Tissue Grafts. Clinics in Sports Medicine, 2009. 28(1): p. 157-176.
15. Chartier, C., et al. Tendon: Principles of Healing and Repair. in Seminars in Plastic Surgery. 2021. Thieme Medical Publishers, Inc.
16. Holm, C., M. Kjaer, and P. Eliasson, Achilles tendon rupture – treatment and complications: A systematic review. Scandinavian Journal of Medicine & Science in Sports, 2015. 25(1): p. e1-e10.
17. Greis Patrick, E., C. Holmstrom Michael, and A. Lahav, Surgical Treatment Options for Patella Tendon Rupture, Part I: Acute. Orthopedics, 2005. 28(7): p. 672-679.
18. El Hawary, R., W.D. Stanish, and S.L. Curwin, Rehabilitation of Tendon Injuries in Sport. Sports Medicine, 1997. 24(5): p. 347-358.
19. Zafar, M.S., A. Mahmood, and N. Maffulli, Basic science and clinical aspects of achilles tendinopathy. Sports medicine and arthroscopy review, 2009. 17(3): p. 190-197.

20. Clement, N.D., Y.X. Nie, and J.M. McBirnie, Management of degenerative rotator cuff tears: a review and treatment strategy. Sports Medicine, Arthroscopy, Rehabilitation, Therapy & Technology, 2012. 4(1): p. 1-5.
21. Derwin, K.A., et al., Enthesis Repair: Challenges and Opportunities for Effective Tendon-to-Bone Healing. The Journal of bone and joint surgery. American volume, 2018. 100(16): p. e109-e109.
22. Rhee, Y.G., N.S. Cho, and J.H. Yoo, Clinical outcome and repair integrity after rotator cuff repair in patients older than 70 years versus patients younger than 70 years. Arthroscopy, 2014(1526-3231 (Electronic)).
23. Kujala, U.M., S. Sarna, and J. Kaprio, Cumulative incidence of achilles tendon rupture and tendinopathy in male former elite athletes. Clinical Journal of Sport Medicine, 2005. 15(3): p. 133-135.
24. Jordan, K.P., et al., International comparisons of the consultation prevalence of musculoskeletal conditions using population-based healthcare data from England and Sweden. Annals of the Rheumatic Diseases, 2014. 73(1): p. 212.
25. Andarawis-Puri, N., E.L. Flatow, and L.J. Soslowsky, Tendon basic science: Development, repair, regeneration, and healing. Journal of Orthopaedic Research, 2015. 33(6): p. 780-784.
26. Nagelli, C., et al., Mechanical and strain behaviour of human Achilles tendon during in vitro testing to failure. European Cells & Materials, 2022. 43: p. 153-161.
27. Arvind, V. and A.H. Huang, Reparative and Maladaptive Inflammation in Tendon Healing. Frontiers in Bioengineering and Biotechnology, 2021. 9.
28. Yang, S.-M. and W.-S. Chen, Conservative Treatment of Tendon Injuries. American Journal of Physical Medicine & Rehabilitation, 2020. 99(6).
29. Holwein, C., et al., No healing improvement after rotator cuff reconstruction augmented with an autologous periosteal flap. Knee Surgery, Sports Traumatology, Arthroscopy, 2019. 27(10): p. 3212-3221.
30. Chan, K.-M. and S.-C. Fu, Anti-inflammatory management for tendon injuries - friends or foes? BMC Sports Science, Medicine and Rehabilitation, 2009. 1(1): p. 23.
31. Connizzo, B.K., et al., The Detrimental Effects of Systemic Ibuprofen Delivery on Tendon Healing Are Time-Dependent. Clinical Orthopaedics and Related Research®, 2014. 472(8).
32. Speed, C.A., Fortnightly review: Corticosteroid injections in tendon lesions. BMJ, 2001(0959-8138 (Print)).
33. Wong, M.W.N., et al., Triamcinolone Suppresses Human Tenocyte Cellular Activity and Collagen Synthesis. Clinical Orthopaedics and Related Research®, 2004. 421.
34. Bannuru, R.R., et al., High-Energy Extracorporeal Shock-Wave Therapy for Treating Chronic Calcific Tendinitis of the Shoulder. Annals of Internal Medicine, 2014. 160(8): p. 542-549.
35. Harniman, E., et al., Extracorporeal shock wave therapy for calcific and noncalcific tendonitis of the rotator cuff: a systematic review. Journal of Hand Therapy, 2004. 17(2): p. 132-151.
36. Lee, S.-Y., B. Cheng, and K. Grimmer-Somers, The midterm effectiveness of extracorporeal shockwave therapy in the management of chronic calcific shoulder tendinitis. Journal of Shoulder and Elbow Surgery, 2011. 20(5): p. 845-854.
37. Wu, Y., et al., Is surgical intervention more effective than non-surgical treatment for acute Achilles tendon rupture? A systematic review of overlapping meta-analyses. International Journal of Surgery, 2016. 36: p. 305-311.

38. Jiang, N., et al., Operative versus nonoperative treatment for acute Achilles tendon rupture: a meta-analysis based on current evidence. International orthopaedics, 2012. 36(4): p. 765-773.
39. Karjalainen, T.V., et al., Surgery for rotator cuff tears. 2019(1469-493X (Electronic)).
40. Nordenholm, A., et al., Surgical treatment of chronic Achilles tendon rupture results in improved gait biomechanics. Journal of Orthopaedic Surgery and Research, 2022. 17(1): p. 67.
41. Hsu, H. and R.M. Siwiec, Patellar Tendon Rupture. 2022, BTI - StatPearls: StatPearls Publishing.
42. Nguyen, M.T. and W.K. Hsu, Performance-based outcomes following patellar tendon repair in professional athletes. The Physician and Sportsmedicine, 2020. 48(1): p. 110-115.
43. Moshiri, A. and A. Oryan, Role of tissue engineering in tendon reconstructive surgery and regenerative medicine: current concepts, approaches and concerns. Hard Tissue, 2012. 1(2): p. 11.
44. Laurencin, C.T. and Y. Khan, Regenerative Engineering. Science Translational Medicine, 2012. 4(160): p. 160ed9-160ed9.
45. Goldenberg, D., et al., Regenerative Engineering: Current Applications and Future Perspectives. Frontiers in Surgery, 2021. 8.
46. Hou, J., et al., Biomaterials strategies to balance inflammation and tenogenesis for tendon repair. Acta Biomaterialia, 2021. 130: p. 1-16.
47. Calejo, I., et al., A textile platform using continuous aligned and textured composite microfibers to engineer tendon-to-bone interface gradient scaffolds. Advanced Healthcare Materials, 2019. 8(15): p. 1900200.
48. Rinoldi, C., et al., Mechanical and biochemical stimulation of 3D multilayered scaffolds for tendon tissue engineering. ACS biomaterials science & engineering, 2019. 5(6): p. 2953-2964.
49. Vuornos, K., et al., Human adipose stem cells differentiated on braided polylactide scaffolds is a potential approach for tendon tissue engineering. Tissue Engineering Part A, 2016. 22(5-6): p. 513-523.
50. Baldwin, M., et al., Augmenting endogenous repair of soft tissues with nanofibre scaffolds. Journal of the Royal Society Interface, 2018. 15(141): p. 20180019.
51. Vasiliadis, A.V. and K. Katakalos, The Role of Scaffolds in Tendon Tissue Engineering. Journal of Functional Biomaterials, 2020. 11(4): p. 78.
52. Younesi, M., et al., Tenogenic induction of human MSCs by anisotropically aligned collagen biotextiles. Advanced functional materials, 2014. 24(36): p. 5762-5770.
53. Zheng, Z., et al., Alignment of collagen fiber in knitted silk scaffold for functional massive rotator cuff repair. Acta biomaterialia, 2017. 51: p. 317-329.
54. Learn, G.D., et al., Woven collagen biotextiles enable mechanically functional rotator cuff tendon regeneration during repair of segmental tendon defects in vivo. Journal of Biomedical Materials Research Part B: Applied Biomaterials, 2019. 107(6): p. 1864-1876.
55. Jiang, D., J. Liang, and P.W. Noble, Hyaluronan as an immune regulator in human diseases. Physiological reviews, 2011. 91(1): p. 221-264.
56. Fong, D., et al., Lysosomal rupture induced by structurally distinct chitosans either promotes a type 1 IFN response or activates the inflammasome in macrophages. Biomaterials, 2017. 129: p. 127-138.

57. Jaibaji, M., Advances in the biology of zone II flexor tendon healing and adhesion formation. Annals of plastic surgery, 2000. 45(1): p. 83-92.
58. Ruppert, S., et al., Tissue integrity signals communicated by high-molecular weight hyaluronan and the resolution of inflammation. Immunologic research, 2014. 58(2): p. 186-192.
59. Vallières, M. and P. Du Souich, Modulation of inflammation by chondroitin sulfate. Osteoarthritis and Cartilage, 2010. 18: p. S1-S6.
60. Güdemez, E., et al., Chondroitin sulfate–coated polyhydroxyethyl methacrylate membrane prevents adhesion in full-thickness tendon tears of rabbits. The Journal of hand surgery, 2002. 27(2): p. 293-306.
61. Sundaram, M.N., et al., Chitosan hydrogel scaffold reinforced with twisted poly (l lactic acid) aligned microfibrous bundle to mimic tendon extracellular matrix. International journal of biological macromolecules, 2019. 122: p. 37-44.
62. Liu, R., S. Zhang, and X. Chen, Injectable hydrogels for tendon and ligament tissue engineering. Journal of Tissue Engineering and Regenerative Medicine, 2020. 14(9): p. 1333-1348.
63. Majima, T., et al., Alginate and chitosan polyion complex hybrid fibers for scaffolds in ligament and tendon tissue engineering. Journal of Orthopaedic Science, 2005. 10(3): p. 302-307.
64. Wang, L., et al., Evaluation of sodium alginate for bone marrow cell tissue engineering. Biomaterials, 2003. 24(20): p. 3475-3481.
65. Li, Z., et al., Chitosan–alginate hybrid scaffolds for bone tissue engineering. biomaterials, 2005. 26(18): p. 3919-3928.
66. Silva, M., et al., Biodegradable polymer nanocomposites for ligament/tendon tissue engineering. Journal of Nanobiotechnology, 2020. 18(1): p. 23.
67. González-Quevedo, D., et al., Nanostructured fibrin-based hydrogel membranes for use as an augmentation strategy in Achilles tendon surgical repair in rats. European cells & materials, 2022. 43: p. 162-178.
68. Wong, C.-C., et al., Cytokine and growth factor delivery from implanted platelet-rich fibrin enhances rabbit Achilles tendon healing. International journal of molecular sciences, 2020. 21(9): p. 3221.
69. Chen, P., et al., A bio-inductive collagen scaffold that supports human primary tendon-derived cell growth for rotator cuff repair. Journal of Orthopaedic Translation, 2021. 31: p. 91-101.
70. Yeung, D.A. and N.H. Kelly, The role of collagen-based biomaterials in chronic wound healing and sports medicine applications. Bioengineering, 2021. 8(1): p. 8.
71. Hankemeier, S., et al., Tissue engineering of tendons and ligaments by human bone marrow stromal cells in a liquid fibrin matrix in immunodeficient rats: results of a histologic study. Arch Orthop Trauma Surg, 2007. 127(9): p. 815-21.
72. Dong, C. and Y. Lv, Application of Collagen Scaffold in Tissue Engineering: Recent Advances and New Perspectives. Polymers, 2016. 8(2): p. 42.
73. Maslennikova, A., et al., Effects of gamma irradiation on collagen damage and remodeling. International Journal of Radiation Biology, 2015. 91(3): p. 240-247.
74. Takitoh, T., et al., Gamma-cross-linked nonfibrillar collagen gel as a scaffold for osteogenic differentiation of mesenchymal stem cells. Journal of bioscience and bioengineering, 2015. 119(2): p. 217-225.
75. Boswell, S.G., et al., Platelet-rich plasma: a milieu of bioactive factors. Arthroscopy: The journal of arthroscopic & related surgery, 2012. 28(3): p. 429-439.

76. Barbon, S., et al., Platelet-Rich Fibrin Scaffolds for Cartilage and Tendon Regenerative Medicine: From Bench to Bedside. International Journal of Molecular Sciences, 2019. 20(7): p. 1701.
77. Xiong, G., et al., Men and women differ in the biochemical composition of platelet-rich plasma. The American journal of sports medicine, 2018. 46(2): p. 409-419.
78. Sun, W., et al. Silk Fibroin as a Functional Biomaterial for Tissue Engineering. International Journal of Molecular Sciences, 2021. 22, DOI: 10.3390/ijms22031499.
79. Tao, W., M. Li, and C. Zhao, Structure and properties of regenerated Antheraea pernyi silk fibroin in aqueous solution. International Journal of Biological Macromolecules, 2007. 40(5): p. 472-478.
80. Tandon, S., B. Kandasubramanian, and S.M. Ibrahim, Silk-Based Composite Scaffolds for Tissue Engineering Applications. Industrial & Engineering Chemistry Research, 2020. 59(40): p. 17593-17611.
81. Font Tellado, S., et al., Fabrication and Characterization of Biphasic Silk Fibroin Scaffolds for Tendon/Ligament-to-Bone Tissue Engineering. Tissue Eng Part A, 2017. 23(1937-335X (Electronic)): p. 859-872.
82. Peniche Silva, C.J., et al., Enthesis Healing Is Dependent on Scaffold Interphase Morphology-Results from a Rodent Patellar Model. Cells, 2022. 11(11).
83. Yao, D., H. Liu, and Y. Fan, Silk scaffolds for musculoskeletal tissue engineering. Experimental biology and medicine, 2016. 241(3): p. 238-245.
84. Belda Marín, C., et al., Silk Polymers and Nanoparticles: A Powerful Combination for the Design of Versatile Biomaterials. Frontiers in Chemistry, 2020. 8.
85. Kundu, B., et al., Silk fibroin biomaterials for tissue regenerations. Advanced Drug Delivery Reviews, 2013. 65(4): p. 457-470.
86. Koh, L.-D., et al., Structures, mechanical properties and applications of silk fibroin materials. Progress in Polymer Science, 2015. 46: p. 86-110.
87. Poza, P., et al., Fractographic analysis of silkworm and spider silk. Engineering Fracture Mechanics, 2002. 69(9): p. 1035-1048.
88. Zhang, W., et al., Silk fibroin biomaterial shows safe and effective wound healing in animal models and a randomized controlled clinical trial. Adv Healthcare Mater 6 (10): 1–16. 2017.
89. Teuschl, A.H., M. van Griensven, and H. Redl, Sericin removal from raw Bombyx mori silk scaffolds of high hierarchical order. Tissue Eng Part C Methods, 2014. 20(5): p. 431-9.
90. Rockwood, D.N., et al., Materials fabrication from Bombyx mori silk fibroin. Nature Protocols, 2011. 6(10): p. 1612-1631.
91. Karageorgiou, V., et al., Porous silk fibroin 3-D scaffolds for delivery of bone morphogenetic protein-2 in vitro and in vivo. Journal of Biomedical Materials Research Part A: An Official Journal of The Society for Biomaterials, The Japanese Society for Biomaterials, and The Australian Society for Biomaterials and the Korean Society for Biomaterials, 2006. 78(2): p. 324-334.
92. Fang, Q., et al., In vitro and in vivo research on using Antheraea pernyi silk fibroin as tissue engineering tendon scaffolds. Materials Science and Engineering: C, 2009. 29(5): p. 1527-1534.
93. Yao, S., et al., Porous and nonporous silk fibroin (SF) membranes wrapping for Achilles tendon (AT) repair: Which one is a better choice? Journal of Biomedical Materials Research Part B: Applied Biomaterials, 2019. 107(3): p. 733-740.

94. Lu, K., et al., Bionic Silk Fibroin Film Promotes Tenogenic Differentiation of Tendon Stem/Progenitor Cells by Activating Focal Adhesion Kinase. Stem Cells International, 2020. 2020: p. 8857380.
95. Xue, Y., et al., Co-Electrospun Silk Fibroin and Gelatin Methacryloyl Sheet Seeded with Mesenchymal Stem Cells for Tendon Regeneration. Small, 2022: p. 2107714.
96. Maghdouri-White, Y., et al., Electrospun silk–collagen scaffolds and BMP-13 for ligament and tendon repair and regeneration. Biomedical Physics & Engineering Express, 2018. 4(2): p. 025013.
97. Naghashzargar, E., et al., Nano/Micro Hybrid Scaffold of PCL or P3HB Nanofibers Combined with Silk Fibroin for Tendon and Ligament Tissue Engineering. Journal of Applied Biomaterials & Functional Materials, 2015. 13(2): p. 156-168.
98. Maghdouri-White, Y., et al., Mammary epithelial cell adhesion, viability, and infiltration on blended or coated silk fibroin–collagen type I electrospun scaffolds. Materials Science and Engineering: C, 2014. 43: p. 37-44.
99. Chen, J., et al., Human bone marrow stromal cell and ligament fibroblast responses on RGD-modified silk fibers. Journal of Biomedical Materials Research Part A: An Official Journal of The Society for Biomaterials, The Japanese Society for Biomaterials, and The Australian Society for Biomaterials and the Korean Society for Biomaterials, 2003. 67(2): p. 559-570.
100. Unger, R., et al., Endothelialization of a non-woven silk fibroin net for use in tissue engineering: growth and gene regulation of human endothelial cells. Biomaterials, 2004. 25(21): p. 5137-5146.
101. Yang, Y.J., et al., Multifunctional Adhesive Silk Fibroin with Blending of RGD-Bioconjugated Mussel Adhesive Protein. Biomacromolecules, 2014. 15(4): p. 1390-1398.
102. Kardestuncer, T., et al., RGD-tethered Silk Substrate Stimulates the Differentiation of Human Tendon Cells. Clinical Orthopaedics and Related Research (1976-2007), 2006. 448.
103. Teuschl, A.H., et al., Enhanced cell adhesion on silk fibroin via lectin surface modification. Acta Biomater, 2014. 10(6): p. 2506-17.
104. Qian, S., et al., A Collagen and Silk Scaffold for Improved Healing of the Tendon and Bone Interface in a Rabbit Model. Med Sci Monit., 2019(1643-3750 (Electronic)).
105. Xue, Y., et al., Co-Electrospun Silk Fibroin and Gelatin Methacryloyl Sheet Seeded with Mesenchymal Stem Cells for Tendon Regeneration. Small, 2022. 18(21): p. 2107714.
106. Trucco, D., et al., Modeling and Fabrication of Silk Fibroin–Gelatin-Based Constructs Using Extrusion-Based Three-Dimensional Bioprinting. ACS Biomaterials Science & Engineering, 2021. 7(7): p. 3306-3320.
107. Seo, Y.-K., J.-H. Kim, and S.-R. Eo, Co-effect of silk and amniotic membrane for tendon repair. Journal of Biomaterials Science, Polymer Edition, 2016. 27(12): p. 1232-1247.
108. Sahoo, S., S.L. Toh, and J.C.H. Goh, A bFGF-releasing silk/PLGA-based biohybrid scaffold for ligament/tendon tissue engineering using mesenchymal progenitor cells. Biomaterials, 2010. 31(11): p. 2990-2998.
109. Calejo, I., et al., Enthesis Tissue Engineering: Biological Requirements Meet at the Interface. Tissue Engineering Part B: Reviews, 2019. 25(4): p. 330-356.
110. Chen, P., et al., Gradient Biomineralized Silk Fibroin Nanofibrous Scaffold with Osteochondral Inductivity for Integration of Tendon to Bone. ACS Biomaterials Science & Engineering, 2021. 7(3): p. 841-851.

111. Font Tellado, S., et al., Heparin functionalization increases retention of TGF-β2 and GDF5 on biphasic silk fibroin scaffolds for tendon/ligament-to-bone tissue engineering. Acta Biomaterialia, 2018. 72: p. 150-166.
112. Teuschl, A., et al., A Novel Silk Fiber–Based Scaffold for Regeneration of the Anterior Cruciate Ligament: Histological Results From a Study in Sheep. The American Journal of Sports Medicine, 2016. 44(6): p. 1547-1557.
113. Teuschl, A.H., et al., Osteointegration of a Novel Silk Fiber–Based ACL Scaffold by Formation of a Ligament-Bone Interface. The American Journal of Sports Medicine, 2019. 47(3): p. 620-627.

CHAPTER 3

# Enthesis: Not the same in each Localization: a Molecular, Histological, and Biomechanical Study

C. J. Peniche Silva, S. A. Müller, N. Quirk, R. E. De la Vega, M. J. Coenen, C. H. Evans, E. R. Balmayor, M. van Griensven

*European Cells & Materials, Vol. 44, 2022*

## ABSTRACT

The interphase between tendon and bone consists of a highly specialized tissue called enthesis. Typically, the enthesis is described as a succession of four different zones: tendon, unmineralized fibrocartilage, mineralized fibrocartilage, and bone. However, the microstructure of the entheses, cellular composition, and mechanical properties, vary depending on their anatomical localization. The present study aimed to characterize three of the most relevant sites of enthesis injury in a rat model: the patellar tendon enthesis, the Achilles tendon enthesis, and the supraspinatus enthesis, in terms of biomechanics, histology, and genetic expression. The patellar enthesis presented the highest ultimate load and lowest stiffness of the three, while the supraspinatus was the weakest and stiffest. The histological characterization revealed key differences at the insertion site for each enthesis. The patellar enthesis showed a large cartilaginous area at the tendon-to-bone interphase whilst this interphase was smaller in the supraspinatus entheses samples. Furthermore, the Achilles tendon enthesis displayed a more abrupt transition from tendon to bone. Additionally, each enthesis exhibited a particular and distinct pattern of expression of tenogenic, chondrogenic, and osteogenic markers. This study provided valuable insights for a better understanding of the three entheses at relevant anatomic sites. Moreover, the larger cross-sectional area of the patellar enthesis, the strong mechanical properties, and the easier surgical access to this localization lead us to conclude that the patellar tendon enthesis site could be most suitable for the development of a preclinical model for general enthesis regeneration studies in rats.

## 1 INTRODUCTION

The tendon attaches to bone through a highly specialized tissue called enthesis [1, 2]. The microscopical and macroscopical structures of the enthesis, its cellular composition, as well as the mechanical properties, vary depending on the anatomic localization to meet the mechanical demands at each insertion site [3]. Generally, the entheses can be classified as fibrous, or fibrocartilaginous entheses [2, 4, 5]. The fibrous entheses are common in tendons that attach directly to the bone or the bone's periosteum such as the deltoid attachment to the humerus and the *adductur magnus* to the *linea aspera* of the femur [1]. Fibrocartilaginous entheses are more frequently found attaching tendons to long bone's epiphyses or apophyses and are normally present at high-stress concentration sites associated with joint movement [4].



The majority of the entheses in the body are fibrocartilaginous entheses [4, 5]. Among these, the supraspinatus, the Achilles tendon, and the patellar tendon are considered some of the most frequent sites of enthesis injury due to acute trauma and/or tissue degeneration [6]. Regrettably, torn or injured entheses often require surgery, and the outcome of such is far from ideal, with high rupture recurrence rates and long-term complaints from the patients' side [6, 7]. This occurs mostly because of the complexity of the fibrocartilaginous structure of the tendon-to-bone enthesis and the intricacy of entheses' pathologies [7-9]. Additionally, the wide range of factors influencing the healing process of the different entheses varies from one anatomic localization to the other, as the risk factors and biology of the entheses are unique to the particular anatomic localization [6, 7, 10].

Important breakthroughs have been achieved in recent years by tissue engineers working on novel therapies to improve the healing of the tendon-to-bone entheses [11-15]. Most of these studies rely on the use of scaffolds or sponges combined with growth factors to promote the regeneration of the fibrocartilage zone of the enthesis [11, 16, 17]. Others, with limited success, have focused on the use of autografts and autologous periosteal flaps to regenerate the cartilaginous tendon-to-bone transition [18-20]. However, despite the efforts, the challenges still to overcome are many. They range from the lack of understanding of the development and healing mechanisms of the entheses to the need for a relevant animal model for the translation of novel treatments [6].

The use of experimental animals is an unfortunate yet necessary, phase in current biomedical research [21]. For many years, tissue engineers working on musculoskeletal regeneration have trusted animal-based research to learn, develop, and validate new concepts and novel therapies [14, 20, 22, 23]. Moreover,

enthesis-related research not only exploits different animal models but also focuses on different anatomical localizations [24-26], which makes the translation of the developed therapies somewhat difficult. This is why the establishment of a suitable animal model for entheses regeneration studies is of utmost importance to improve the quality of entheses research and the translation of new findings.

Focusing on this challenge, the present study aimed at the characterization in a rat model of the 3 most relevant sites of enthesis injury (*i.e.*, patellar tendon, Achilles tendon, and supraspinatus) in terms of biomechanics, histology, and gene expression, to gain overall knowledge. This may help in the future to select one as the ultimate model for basic enthesis regeneration studies.

## 2 MATERIALS AND METHODS

### 2.1 Collection of explants

10 male Sprague Dawley rats (Charles River Laboratories, Wilmington, MA, USA) weighing between 400 and 500 g (100–130 days of age) were used. The animals were sacrificed for reasons unrelated to our study while being in other studies that do not influence the enthesis.

After having received the sacrificed animals, sets of two samples of native (healthy) tendon-to-bone entheses from the patellar tendon, Achilles tendon, and supraspinatus tendon per rat were harvested for a total of 20 samples from each localization. The patellar enthesis sample included the patellar tendon and its insertion site at the tibia. The Achilles tendon-to-bone enthesis samples were harvested as a muscle-tendon unit containing the Achilles tendon and its insertion site into the calcaneus. Similarly, the supraspinatus samples comprised the supraspinatus tendon-muscle unit and its insertion site at the head of the humerus.

### 2.2 Biomechanical measurements and testing

Samples to be used for mechanical testing (n=12 per localization) were wrapped in a gauze soaked with saline and stored in a 15 ml Falcon tube at -20°C until the day of testing [27].

Before the testing, samples were thawed for 4 hours at room temperature while kept moist with saline. Afterward, the tendon length of each sample, from the tendon origin at the muscle to the enthesis, and the enthesis cross-sectional area (width x depth) were measured with an electronic Vernier caliper (Model CD-8 ASX, Mitutoyo, Japan).

For the mechanical testing, a custom-made small biological specimen mechanical-testing machine (Mayo Clinic, Rochester, MN, USA) with a 50 lbf loadcell limit

(Model MLP-2, Transducer Techniques, Temecula, CA, USA) and associated LabVIEW 2017 SP1 (National Instruments, Austin, TX, USA) was employed. Custom-made mounting fixtures were previously developed similar to other reported tissue testing clamps [28]. Samples from the Achilles tendon were tested through isolation of the calcaneus and ensuring the correct orientation of the tendon by utilizing custom-made foot support. The entheses samples from the patellar tendon and supraspinatus tendon were tested through clamping of the tibia and humerus respectively, allowing the alignment of the tendon. Custom-built cryo-clamps were used in conjunction with dry ice powder to secure sample muscle attachments proximally (Figure 1 d.1 and d.2).

During the freezing period, the temperature of the entheses and the proximal and middle tendons was monitored by utilizing a TrueRMS multi-meter (TrueRMS Supermeter, Newport, RI, USA) to ensure optimal fixation. The optimal temperature for enthesis testing was determined in a previous study [27]. A mean temperature of -1°C at the proximal tendon region assured sufficient muscle freezing to prevent the muscle to slip from the clamps. All samples were tested at a mean temperature of 10°C at the enthesis region, which ensured that the testing could be performed reproducibly while the samples were not frozen. Samples were preloaded to 3N prior to 200 mm/min failure tensile test [27]. During the mechanical testing, enthesis tears were monitored in real-time with a consistent single operator throughout. No tears occurred in the tendon or the bony part of any of the specimens tested for each group.

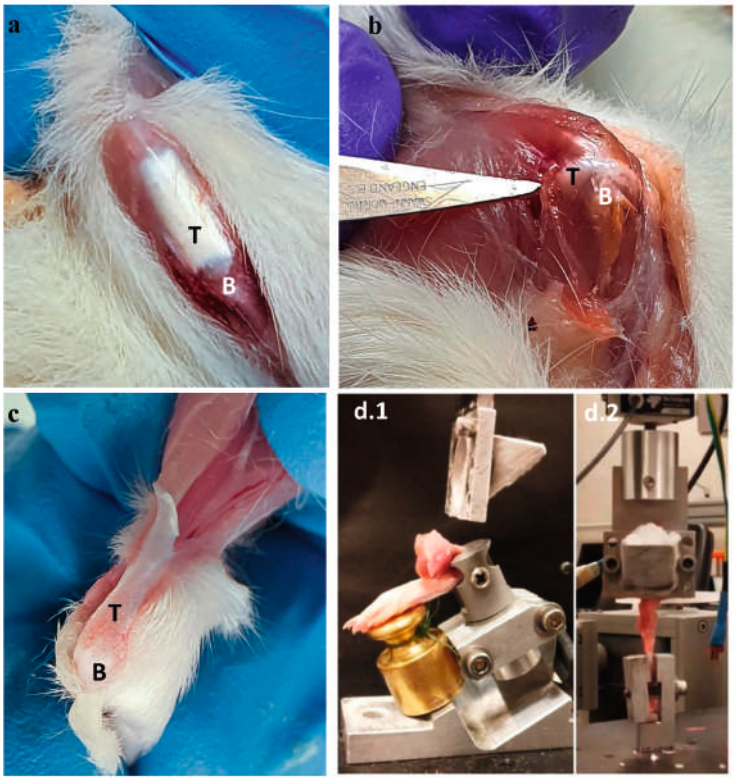


**Figure 1.** Representative images of the exposed entheses. (**a**) Patellar enthesis with associated tendon. (**b**) Achilles enthesis with associated tendon. (**c**) Supraspinatus enthesis with associated tendon. **T** and **B** indicate tendon and bone tissues at their respective sides of the enthesis. (**d**) Custom-made mechanical testing fixtures. **d.1** Achilles enthesis fixture. Calf muscle is not yet mounted to cryo-clamp, **d.2** Patellar and Supraspinatus testing set-up

Force-elongation curves were recorded, from which ultimate load (force at failure; N), stiffness (loading curve linear portion; N/mm), and tangent modulus ([force at failure/enthesis cross-sectional area]/[ultimate strain]; MPa) were calculated. Data were processed individually through Matlab 2016a (Mathworks, Natick, MA, USA), compiled in Microsoft Excel 2010 (Microsoft, Redmond, WA, USA), and statistically assessed by Graphpad Prism 8.0 (GraphPad Software, San Diego, CA, USA). Measurable data and calculated mechanical property data are reported through box plots (median, 1st, 3rd quartile ranges and outliers bounderies at 10-90 Percentile).

### 2.3 Histology and Immunohistochemistry (IHC)

Samples from the three entheses (n=8 per localization) were fixated in 4% paraformaldehyde (Sigma Aldrich, St. Louis, MO, USA) for 48 h, rinsed with PBS, and decalcified in 10% buffered EDTA (Sigma Aldrich, St. Louis, MO, USA) for

28 days. Buffer was exchanged every two to three days and the endpoint of the decalcification was determined by macroscopic inspection. For this, the tissue samples were inspected every five days by gently compressing the bony area of the sample by hand until a gel-like consistency was attained from all angles. After reaching the point where no sharp edges or hard tissue were perceived by compression, one sample was selected, cut with a scalpel, and thoroughly inspected to confirm that the decalcification endpoint was attained. After decalcification, samples were dehydrated in an ethanol series and embedded in paraffin. Longitudinal cross-sections were sliced at a thickness of 7 µm using a Leica RM 2165 microtome (Leica Biosystems, Nussloch, Germany). Afterward, hematoxylin and eosin (H&E), safranin O, toluidin blue, and picrosirius red stainings were performed.



Briefly, samples were rehydrated in descending ethanol series and distilled water. For the H&E staining, samples were incubated with hematoxylin solution for 10 mins and eosin for 2 mins (Carl Roth GmbH, Karlsruhe, Germany), dehydrated in ascending ethanol series, cleared with NeoClear-xylene substitute (Merck KGaA, Darmstadt, Germany), and mounted with UltraKit mounting media (Thermo Fisher Scientific, Landsmeer, the Netherlands). The toluidine blue staining was performed by incubating the rehydrated slides in a working solution of toluidine blue (0.1% Toluidine Blue, pH 2.5, Sigma Aldrich, St. Louis, MO, USA) for 3 min, followed by three washes with distilled water. Subsequently, the slides were dehydrated in an ascending ethanol series, cleared with NeoClear-xylene substitute, and mounted with Ultrakit mounting media.

For the safranin O staining, the rehydrated slides were stained with hematoxylin solution for 10 min, followed by 5 min staining with 0.1% fast green solution (Sigma Aldrich, St. Louis, MO, USA), rinsed with 0.1% acetic acid, and further stained with 0.1% safranin O solution for 10 min (Sigma Aldrich, St. Louis, MO, USA). Subsequently, the samples were dehydrated, cleared, and mounted as described before. The stained slides were imaged with a Nikon DS-Ri2 camera mounted on a Nikon Ti Slide Scanner Microscope (Nikon Instruments Europe BV, Amsterdam, the Netherlands).

The picrosirius red staining was conducted on slides that were previously rehydrated and stained with hematoxylin solution for 10 min. Incubation with 0.1% picrosirius red working solution (Sigma Aldrich, St. Louis, MO, USA) was done for 1 h followed by two washes with acidified water. Later, the samples were dehydrated, cleared, and mounted as previously described. Imaging was done using an inverted Nikon Ti-S/L100 microscope (Nikon Instruments Europe BV, Amsterdam, the Netherlands).

As part of the histological characterization, the orientation angle of the collagen fibers at the tendon-to-bone interphase of the enthesis was measured in the picrosirius-stained samples using Image J v1.53p (Nat. Inst. of Health, Bethesda, MD, USA). For this, the images of the stained samples were rotated to match the same orientation using the bony site of the entheses as the reference to set the horizontal line. Afterward, three different regions of interest (ROIs) were set at the tendon-to-bone interphase, ROI1 at the left end of the interphase, ROI2 at the middle portion of the cross-section, and ROI3 at the right end of the interphase. The orientation angle of each ROI was measured using the Image J plugin Orientation J_Measure-v2.0.4. The values were imported to Microsoft Excel 2016 (Microsoft, Redmond, WA, USA), and the variability of the orientation angle among the three ROIs was calculated for each anatomical localization.

For the IHC, all primary and secondary antibodies (Table 1), as well as the DAPI (ab285390) staining solutions were purchased from Abcam (Cambridge, UK). Antigen retrieval was performed on the rehydrated samples by incubation in 10 mM citrate buffer (pH 6) for 10 min at 95 °C followed by blocking with 1% BSA (Sigma Aldrich, St. Louis, USA) for 1 h at room temperature. Afterward, the slides were placed in a humidity chamber and incubated with the primary antibody diluted in blocking solution overnight at 4 °C, followed by incubation with the secondary antibody for 2 h at room temperature. Finally, counterstaining with DAPI was performed and the slides were mounted with Dako fluorescent mounting media (Agilent technology, Santa Clara, CA, USA).

The stained slides were imaged with a Nikon DS-Ri2 camera mounted on a Nikon Ti Slide Scanner Microscope (Nikon Instruments Europe BV, Amsterdam, the Netherlands).

**Table 1.** List of the antibodies and working dilutions used for IHC.

| Name | Abcam ID number | Working dilution |
|---|---|---|
| Anti-collagen type I | ab270993 | 1:250 |
| Anti-collagen type II | ab34712 | 1:50 |
| Anti-collagen type III | ab6310 | 1:250 |
| Anti-collagen type X | ab49945 | 1:100 |
| Rabbit IgG isotype control | ab172730 | 1:50 |
| Mouse IgM isotype control | ab18401 | 1:100 |
| Mouse IgG1 isotype control | ab170190 | 1:250 |
| Alexa Fluor 647 Goat anti-rabbit | ab190565 | 1:500 |
| Alexa Fluor 647 Goat anti-mouse | ab15015 | 1:500 |

### 2.4 Gene expression.

Immediately after the mechanical testing, the muscle-tendon unit and bony portions of the tissue samples were separated from the entheses leaving only the respective tendon-to-bone insertion site at the bony end of the entheses (n=12). Then, the entheses samples were homogenized with stainless steel beads in the presence of TRIzolTM Reagent (Thermo Scientific, Waltham, MA, USA) using a Qiagen TissueLyser LT (Qiagen GmbH, Hilden, Germany) set at 50 Hz for periods of 5 mins following a step of snap freeze with liquid nitrogen.

The extraction of the total RNA was performed by the well-established phenol/chloroform extraction protocol. The final concentration and purity of the obtained total RNA were measured with a BioDrop µLite UV/Vis spectrophotometer (BioDrop, Cambridge UK). The cut-off value for RNA purity (Ratios A260/230 and 260/280) was set to 2.0. All the samples yielded values of A260/230 and 260/280 ratios between 2.0 and 2.2.



The extracted RNA was the starting material for the cDNA synthesis. The cDNA synthesis was performed in a PeqLab Thermocycler (AvantorTM, Radnor, PA, USA) using the iScript cDNA synthesis kit (Bio-Rad Laboratories GmbH, Feldkirchen, Germany) following the manufacturer's instructions. The reaction mix was prepared with 10 µl of RNA template (250 ng), 4 µl of 5x iScript Reaction Mix, 1 µl of iScript Reverse transcription mix, and 5 µl of ultra-pure nuclease-free water for a total volume of 20 µl per reaction. The reaction mix was then incubated at 25 oC for 5 min, followed by 46 oC for 20 min and 95 oC for 1 min.

The gene expression of a selection of tenogenic, chondrogenic, and osteogenic markers (Table 2) was analyzed by single SYBR Green-based Real-time quantitative PCRs. The RT-PCR reactions were performed in a CFX96 Real-Time System Thermocycler (Bio-Rad Laboratories GmbH, Feldkirchen, Germany). For the RT-PCR reactions, 4 µl of cDNA template (5 ng) was added to the master mix containing: 10 µl of iQTM SYBER® Green Supermix (Bio-Rad Laboratories GmbH, Feldkirchen, Germany), 2 µl of forward primer, 2 µl of reverse primer (300 mM) and 2 µl of ultra-pure water for a reaction volume of 20 µl. PCR amplification was conducted by using the following program: 90 °C for 3 minutes and 40 cycles of 95 °C for 10 sec, 55 °C for 30 sec, and 95 °C for 30 sec. A melting curve was performed at the end of the last amplification cycle. For the analysis of the results, the Ct values higher than 35 were considered unreliable and therefore, not included in the calculations of relative gene expression. Ct values ≤ 35 were exported to Microsoft Excel 2016 (Microsoft, Redmond, WA, USA), and the ratio of expression between reference and target gene was calculated as $2^{(-\Delta CT)}$ where ΔCt was calculated as (Ct gene of interest - Ct reference gene). The statistical analysis of the gene expression was performed on the ΔCt values and

assessed by GraphPad Prism 8.0 (GraphPad Software, San Diego, CA, USA). The normalized gene expression data are reported as dot blots indicating mean and standard deviation of the ratio of expression 2(-ΔCT).

**Table 2.** Primers used for RT-PCRs

| Target | Forward 5'→3' | Reverse 5'→3' |
|---|---|---|
| *Col1a1* | TTTCCCCCAACCCTGGAAAC | CAGTGGGCAGAAAGGGACTT |
| *Col2a1* | CACGCCTTCCCATTGTTGAC | AGATAGTTCCTGTCTCCGCCT |
| *Col3a1* | TGCAATGTGGGACCTGGTTT | GGGCAGTCTAGTGGCTCATC |
| *Col10a1* | TCCCAGGATTCCCTGGATCTAA | TACCGCTGGGTAAGCTTTGG |
| *Mkx* | GACGACGGCTGAAGAACACTG | CCTCTTCGTTCATGTGAGTTCTTG |
| *Tnmd* | GTCCCACAAGTGAAGGTGGA | TTGCAAGGCATGATGACACG |
| *Scx* | GACCGCACCAACAGCGTGAA | GTGGACCCTCCTCCTTCTAACTTC |
| *Fn1* | CCCCAACTGGTTACCCTTCC | TGGTTCGCCTAAAGCCATGT |
| *Sparc* | CCTCAGACGGAAGCTGCAGAA | ACCAGGACGTTTTTGAGCCA |
| *Runx2* | CAAGGAGGCCCTGGTGTTTA | AAGAGGCTGTTTGACGCCAT |
| *Sox9* | CCTCCTACCCAACCATCACG | GAGCTGTGTGTAGACGGGTT |
| **β-Tubulin** | GAGGGCGAGGACGAGGCTTA | TCTAACAGAGGCAAAACTGAGCA |

β-tubulin was selected as the housekeeping gene by the ΔCt method for reference genes [29]. This method allows comparing the relative expression of "pairs of genes" within each sample to identify useful housekeeping genes. For this, β-actin, β2-Microglobulin, lactate dehydrogenase A, ribosomal protein stalk subunit P1, and β-tubulin were compared. As a result of this comparison, b-tubulin was the highest-scoring gene and, thus the one with the most stable expression among our analyzed samples.

### 2.5 Statistical analysis

Statistical analyisis was performed using GraphPad Prism 8.0 (GraphPad Software, San Diego, USA). Data were tested for normal distribution by the D'Agostino & Person and Shapiro-Wilk normality test. Since the data were normally distributed in all cases, statistically significant differences were determined by One-way ANOVA with Tukey's multiple comparison test ($p < 0.05$).

# 3 RESULTS

## 3.1 Mechanical testing

Before the biomechanical characterization, the length of the tendons of each enthesis and the entheses' cross-sectional area were measured (Fig. 2a,b). On the one hand, the patellar tendon was significantly longer ($p < 0.001$) than that of the supraspinatus while the Achilles showed the longest tendon of the three ($p < 0.001$). On the other hand, the cross-sectional area at the bony insertion site of the patellar enthesis resulted to be the largest one of the three ($p < 0.001$) with the Achilles and supraspinatus displaying less than half of the patellar enthesis cross-sectional area. (Fig. 2a,b).

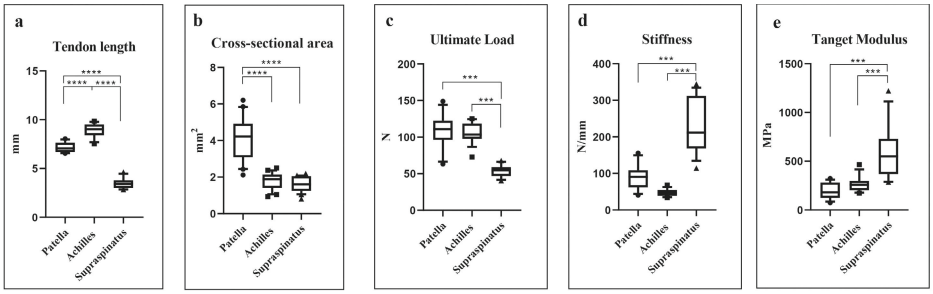


**Figure 2.** Measurements and biomechanics of the three native entheses. (**a**) Tendon length, (**b**) cross-sectional area, (**c**) ultimate load, (**d**) stiffness, (**e**) tangent Modulus. ****p < 0.0001.

The biomechanical testing revealed that the measured ultimate load (Fig. 2c) was similar in magnitude for the patellar and the Achilles entheses, which both had reported the longest tendons, whereas the supraspinatus with the shortest tendon of the three, resulted to be the weakest ($p < 0.001$). Conversely, the supraspinatus enthesis showed higher stiffness ($p < 0.001$) and higher tangent modulus whilst the patella and the Achilles were similar regarding both properties (Fig. 2d,e).

## 3.2 Histology

The H&E, toluidine blue, and safranin O staining exposed differences in the morphology of the tendon-to-bone insertion site among the three localizations (Figures 3 and 4). The patellar enthesis exhibited a tendon-to-bone transition characterized by a proteoglycan-rich cartilaginous interphase between the tendon and the bony ends. The Achilles enthesis displayed a more abrupt transition from tendon to bone at the insertion site, while the supraspinatus presented a well-defined cartilage-like transition zone between the tendon and the bone.

The insertion angle of the collagen fibers from tendon to bone was determined using the picrosirius red-stained sections (Table 3). The orientation angles of the three ROIs measured for the Achilles and patellar entheses reported uniform

values. The variation of the orientation angle among the ROIs of the patellar and the Achilles entheses showed no significant differences. However, the variation of the orientation angle among the ROIs of the supraspinatus was significantly higher than the variation measured in the patellar and the Achilles entheses ($p < 0.005$).

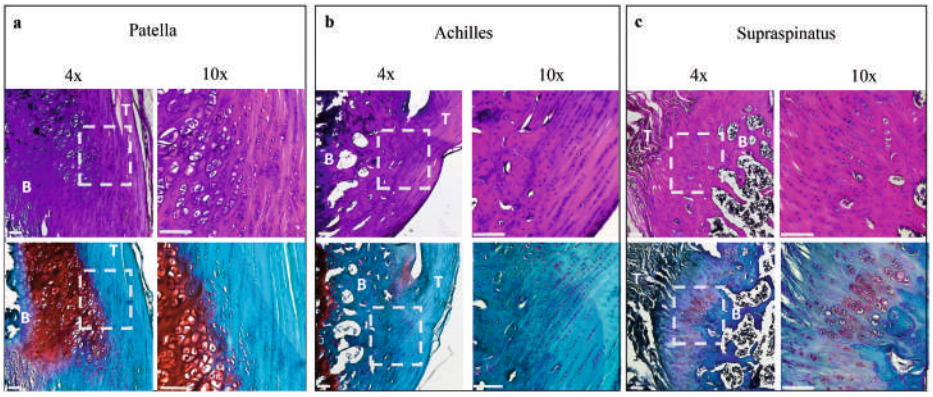


**Figure 3.** Histological staining of native entheses. (a) Patella, (b) Achilles, (c) supraspinatus. Top row: hematoxylin and eosin. Bottom row: safranin O. **T** and **B** indicate tendon and bone tissues at their respective zone of the enthesis. Dashed squares indicate the magnified area. Scale bar = 100 µm.

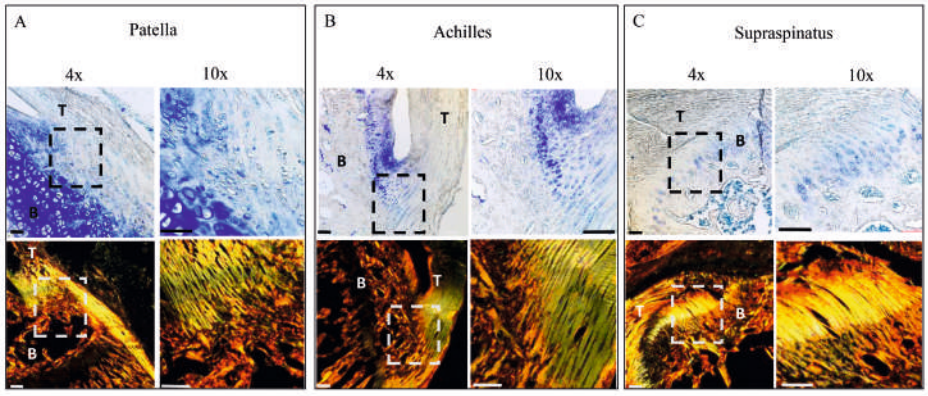


**Figure 4.** Histological staining of native entheses. (a) Patella, (b) Achilles, (c) supraspinatus. Top row: toluidine blue. Bottom row: picrosirius red. **T** and **B** indicate tendon and bone tissues at their respective zone of the enthesis. Dashed squares indicate magnified area. Scale bar = 100 µm.

**Table 3.** Orientation angle of the collagen fibers per localization. [a]Values with no statistical difference from one another. [b]Values with statistical differences from the others ($p < 0.05$).

| Enthesis | Orientation angle of the collagen fibers | Variation of orientation angle among ROIs |
|---|---|---|
| Achilles | 41.14 ± 1.6 | 7.12 ± 2.24[a] |
| Patella | 28.32 ± 5.25 | 3.19 ± 2.15[a] |
| Supraspinatus | 56.00 ± 8.60 | 19.68 ± 5.28[b] |

The IHC for the extracellular matrix collagens showed that, in the three instances, tendon and bone tissue were rich in collagen type I while the interface between these two tissues was positively stained for collagen type II. Interestingly, none of the three entheses showed visible deposition of collagen type III nor type X (Fig. 5).



### 3.3 Gene expression

The analysis of the gene expression from the three localizations revealed significant differences among them (Fig. 6). The expression of *Col1a1* was significantly higher in the Achilles entheses samples than in the patellar and supraspinatus samples ($p < 0.005$ and $p < 0.05$ respectively), while the expression in the patellar entheses was not different from that of the supraspinatus.

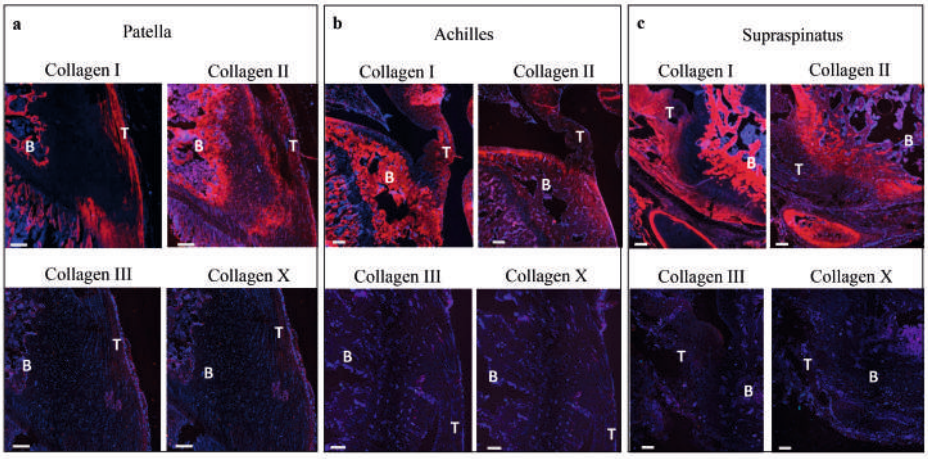


**Figure 5.** Immunostaining of extracellular matrix collagens. Staining with Alexa Fluor 647 of the respective target antigen for each antibody. T and B indicate tendon and bone tissues at their respective sides of the enthesis. Counter staining with DAPI. Scale bar = 200 µm.

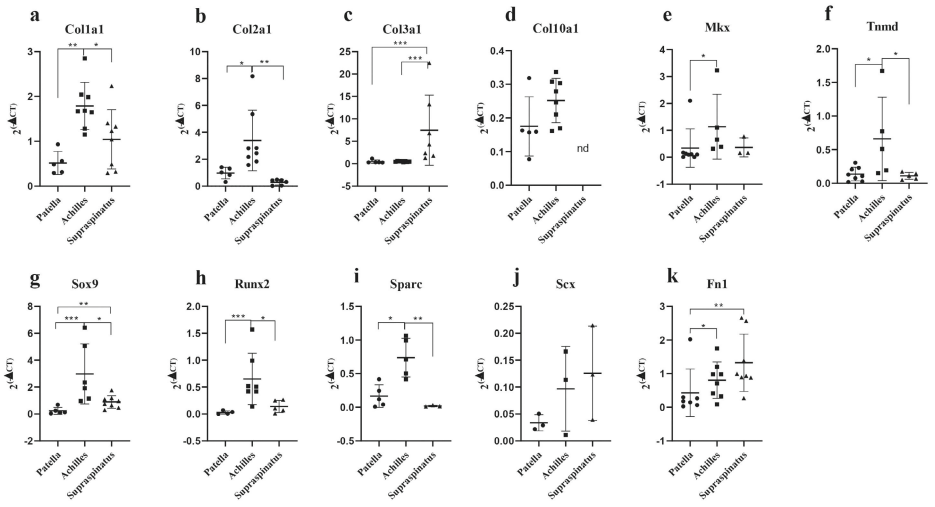


**Figure 6.** Normalized gene expression at each location. (a) *Col1a1*, (b) *Col2a1*, (c) *Col3a1*, (d) *Col10a1*, (e) *Mkx*, (f) *Tnmd*, (g) *Sox9*, (h) *Runx2*, (i) *Sparc*, (j) *Scx* and (k) *Fn1*. Reference gene used for normalization was β-tubulin. nd indicates non-detected, * $p < 0.05$, ** $p < 0.005$, *** $p < 0.001$. Lines indicate mean and standard deviation.

However, the expression of *Col2a1* was similar for the patellar and the Achilles entheses and in both cases, higher than that measured in the supraspinatus samples ($p < 0.05$ and $p < 0.005$ respectively). Conversely, the expression of *Col3a1* was the highest in the supraspinatus entheses samples ($p < 0.001$) while the entheses samples from the Achilles and the patella showed very similar levels of expression of *Col3a1*. Interestingly, *Col10a1* was not detected in the samples from the supraspinatus entheses and the *Col10a1* expression in the Achilles and patellar entheses was similar and rather low.

In addition to the collagens, other tenogenic, chondrogenic, and osteogenic markers were investigated (Fig. 6). The expression of *Mkx* and *Tnmd* was the highest in the Achilles samples ($p < 0.05$), while in the patella and the supraspinatus these two genes were found to be expressed at similar, lower levels. In the same way, *Sox9*, *Runx2*, and *Sparc* were highly expressed in the Achilles samples compared to the expression in the patella and supraspinatus entheses samples ($p < 0.05$). However, the expression of *Scx* was similar in the three localizations while the expression of *Fn1* was the lowest in the patellar entheses samples, followed by the Achilles and reaching the highest levels of expression in the supraspinatus entheses samples ($p < 0.05$).

## 4 DISCUSSION

The intricate biology of the tendon-to-bone enthesis has fascinated orthopedics and tissue engineers for decades [30-32]. The focus of the vast majority of enthesis-related studies lies on either the patellar enthesis, the Achilles tendon enthesis, or the supraspinatus enthesis [19, 33-36]. A plausible explanation for that is the fact that these three entheses are among the more frequently injured ones [1]. The present study aimed at a comparative characterization of all these three insertion sites using different techniques in one study. Overall, the aim was to select the ultimate anatomic localization for enthesis regeneration studies in the future.

Of the three analyzed anatomical localizations, the supraspinatus features the only intra-articular enthesis, while the patellar and Achilles tendons entheses are of extra-articular nature [6]. The intra-articular environment of the supraspinatus enthesis and its exposure to synovial fluid makes this insertion site an extraordinary challenging site for injury, susceptible to degenerative enthesopathies, and acute trauma [6, 37, 38]. Hence, this explains the abundance of clinical reports addressing supraspinatus tears. However, with the biomechanical characterization performed, it was observed the supraspinatus enthesis to be the smallest and weakest of the three. Furthermore, the supraspinatus enthesis at the rotator cuff is rather cumbersome to access surgically, which is especially relevant when working with animal models of relatively small size (e.g., mice and rats). Besides, entheses regeneration studies usually involve the development of sponges and multiphasic scaffolds to provide a physical space for the new tissue to grow upon the creation of an enthesis defect [12, 14, 26]. Therefore, the small size and weakness of the supraspinatus enthesis of adult rats impose an additional challenge during the in vivo evaluation of such scaffolds in this enthesis.

In the three investigated localizations, the first zone of the enthesis (*i.e.*, end of the tendon) was characterized by an arrangement of longitudinally aligned collagen type I bundles, clearly visible in the picrosirius red staining. This observation is in line with previous descriptions of the supraspinatus enthesis [39], the Achilles tendon enthesis [40, 41], and the patellar tendon enthesis [42]. Comparatively, the second zone of the enthesis, known as the fibrocartilaginous transition zone, was the less evident in the Achilles tendon enthesis, where the collagen bundles seem to connect more abruptly to the bone. However, the toluidine blue staining did show some positive staining for cartilage in the Achilles tendon enthesis, especially in the upper section of the tendon-to-bone interphase. A similar observation was done by Shaw *et al.* in samples of human Achilles entheses [43]. In their study, they describe a narrow fibrocartilaginous area more prominent in the superior part of the tendon-to-bone attachement as well as a sesamoid fibrocartilage zone in the section of the tendon immediately adjacent to the

enthesis. This area is also visible in our safranin O staining of the deep section of the tendon, proximal to the calcaneus. Such zone, nearby the retro calcaneal bursa, is likely to be a high stress concentration point were the friction between the tendon and the calcaneus yields a more chondrogenic phenotype [43, 44]. Hence, the more cartilaginous appearance of the tissue in this area.

The transition from the second to the third zone of the enthesis was noticeably different between the patellar enthesis and the enthesis of the Achilles tendon and the supraspinatus. In the case of the patellar enthesis, the non-mineralized fibrocartilage area led to the large proteoglycan rich zone of the tibial cartilage. This transition was similar in morphology to the proliferative and pre-hypertrophic zones observed in the growth plate of joints [45], where the chondrocytes are typically tightly packaged and arrange themselves into longitudinal columns. Liu *et al*. described a similar morphology of the insertion of a patellar tendon in mice [46]. Such a large proteoglycan-rich area was not noticeable in the entheses of the supraspinatus and the Achilles tendons. Instead, in the supraspinatus enthesis, the aligned collagen bundles of the tendon were followed by a narrow fibrochondrogenic transition zone that abruptly connected to the trabecular bone. This morphology of the supraspinatus tendon enthesis was also described by Bedi *et al*. in mice [47]. In the case of the Achilles tendon enthesis, the narrow rows of chondrocytes in between the collagen bundles connected the tendon directly to the perichondrium of the calcaneus. This was also observed in human samples of Achilles tendon entheses [43]. Moreover, such a direct link has been described to be highly efficient in the dissipation of stress [5]. This is supported by our mechanical data since the Achilles enthesis showed the highest ultimate load per $mm^2$ among the three studied localizations.

Interestingly, and despite the observed histological differences at the insertion sites between the patellar enthesis and the Achilles tendon enthesis, these two localizations showed comparable biomechanical properties. Both entheses were at least twice as strong and showed lower stiffness than the supraspinatus enthesis. Additionally, the variation of the orientation angle of the collagen fibers across the tendon-to-bone interphase of the Achilles and patellar enthesis was similar, while the supraspinatus showed a higher degree of variability of the orientation angle at the insertion site, which could contribute to the relatively poor performance of the supraspinatus enthesis during the tensile test. Furthermore, the insertion site of the patellar tendon displayed a cross-sectional area twice as big as that of the Achilles tendon and the supraspinatus entheses.

Up to this point, it is possible to argue that both the anatomy and biomechanical features of the rat patellar enthesis both support the selection of this enthesis to be used as a model for enthesis regeneration studies. Nevertheless, it is

worth pointing out that the ultimate load measured for the Achilles enthesis, if normalized to the enthesis cross-sectional area, is higher per $mm^2$ than that measured for the patellar entheses samples.

The histological analysis confirmed type I collagen-rich tendons that were inserted into the bone through a type II collagen-rich transition zone for all the three entheses studied. Yet, no noticeable deposition of collagen type III nor type X was observed in any of the three localizations studied. Our observation is partially in line with that of Dyment *et al*. In their work, they compared the deposition of collagen type I, II, and X in the patellar tendon, supraspinatus tendon, and Achilles tendon entheses at different maturation stages (i.e., postnatal day 1, 2 weeks, and 4 weeks). They observed similar patterns of collagen type I deposition to that described in the present work. However, after 4 weeks of entheses maturation, they did not observe collagen II expression at the enthesial interphase. Interestingly, the authors reported deposition of collagen type X within the mineralized fibrocartilage [48].



The gene expression data provided crucial insights into the collagen expression of the three localizations. On the one hand, the highest *Col1a1* expression was measured in the Achilles entheses samples. Collagen type I is the major component of the extracellular matrix of the tendons and is for the most part, responsible for the mechanical properties of this tissue [49, 50]. The elevated expression of *Col1a1* in the Achilles samples might explain the high ultimate load measured for this enthesis, which was comparable to that from the patellar enthesis while showing a fraction of the patellar tendon's cross-sectional area. On the other hand, the expression of *Col3a1* was the highest in the supraspinatus enthesis, which, displaying a similar cross-sectional area to that of the Achilles enthesis, performed poorly in the biomechanical test. In healthy tendons, collagen type III fibrils are associated with collagen type I [50]. However, disorganization and random orientation of the collagen type III fibers typically yield a weaker structure than collagen type I. The ratio of collagen type III/I has been shown to increase with aging and the presence of pathologies [51, 52].

The expression of the transcriptor factor *Mkx* was the highest in the Achilles enthesis. This observation goes in line with the *Col1a1* expression pattern previously described since *Mkx* acts as a positive regulator of collagen type I expression [53]. In a similar way, the higher expression of *Sox9* in the Achilles entheses samples could cause the high expression of *Col2a1* in this localization, since the expression of collagen type II by chondrocytes at the enthesis is activated by the transcription factor *Sox9* [54]. Interestingly, the gene expression of *Col2a1* in the patellar enthesis was similar to that of the Achilles enthesis while the expression of *Sox9* measured in the patellar sample was the lowest of

the three. However, the higher expression of *Col2a1* in the patellar tendon and the Achilles tendon entheses compared to the supraspinatus entheses could be related to the higher compressive loads at which the patellar tendon and Achilles entheses are exposed due to their anatomical localizations [49, 55]. Nevertheless, the tendon–to–bone transition zone of the three analyzed entheses stained positive for collagen type II.

The expression of *Scx* was low in the three localizations and only three samples per group showed values of expression high enough to render Ct values lower than our Cut-off value of 35. However, such low expression of *Scx* was expected in our entheses samples since this early marker of tenogenesis is usually expressed in tendons during the stages of organogenesis or at the early stages of healing [56, 57].

Overal, each of the three entheses showed a very distinctive pattern of gene expression. On the one hand, samples from the Achilles enthesis consistently showed higher levels of expression of chondrogenic, osteogenic, and tenogenic markers than the other two localizations. On the other hand, the expression of chondrogenic markers in the supraspinatus entheses samples was relatively higher than in the patellar tendon entheses. The observed differences between the three analyzed entheses illustrate how anatomical localization and function dictate the mechanical properties, morphology, and local gene expression. Additionally, we have demonstrated that the three entheses are essentially different, thus, a unique model to study enthesis, as an organ, might not always be suitable. This is, undeniably, one major limitation that tissue engineers face when studying tendon-to-bone entheses, especially in small animal models. The gained insight into such differences facilitates the translation of pre-clinical investigation for specific enthesis injury sites. However, there are practical limitations to this study associated with the challenge of working with interphase tissues from small animal models. Ensuring a clean preparation of the enthesis is difficult. For our study, a single/same operator performed all the sample preparation to ensure consistency. This procedure was extensively rehearsed. The measurements of the entheses and tendons were performed by the same operator utilizing high-accuracy equipment to conduct all measurements. Cross-sectional areas were assumed to be rectangular in nature and thus allowed standardization and assessment across the samples from each anatomic localization. We acknowledge this assumption as a limitation, however, we do not believe that higher accuracy assessments were practically feasible. Ultimately, the patellar samples showed the highest reported cross-sectional areas and thus expected higher failure loads corroborating our measurements.

## 5 CONCLUSION

The comparative characterization performed in the present study provides valuable insights for a better understanding of three entheses at relevant anatomic sites. To the best of the authors' knowledge, such a direct comparison of entheses tissues corresponding to three different anatomical localizations has not been reported before. On the one hand, the gene expression analysis allowed to compare the expression patterns of genes important for the healing of tendon, cartilage, and bone tissue in the three investigated localizations. On the other hand, biomechanical evaluations revealed that the patellar tendon enthesis and the Achilles enthesis featured the highest ultimate load resistance combined with the lowest stiffness. However, the large cross-sectional area of the patellar tendon at the enthesis and the convenient surgical accessibility to the patellar region, allowed us to conclude that the patellar tendon enthesis site would be most suitable for the development of a preclinical model for general enthesis regeneration studies in rats.



## 6 ACKNOWLEDGMENTS

This study has been partially funded by the ON Kick Starter Grant (project number 20-105). Dr. Evans's research is partly funded by the John and Posy Krehbiel Professorship in Orthopedics. This work was supported by the Province of Limburg, Limburg Invests in its Knowledge Economy (LINK).

## 7 REFERENCES


1. Apostolakos, J., et al., The enthesis: a review of the tendon-to-bone insertion. Muscles, ligaments and tendons journal, 2014. 4(3): pp. 333-342.
2. Benjamin, M., et al., The skeletal attachment of tendons—tendon 'entheses'. Comparative Biochemistry and Physiology Part A: Molecular & Integrative Physiology, 2002. 133(4): pp. 931-945.
3. Killian, M.L., Growth and mechanobiology of the tendon-bone enthesis. Seminars in Cell & Developmental Biology, 2021.
4. Benjamin, M., et al., Anatomy and biochemistry of entheses. Annals of the Rheumatic Diseases, 2000. 59(12): p. 995.
5. Benjamin, M., et al., Where tendons and ligaments meet bone: attachment sites ('entheses') in relation to exercise and/or mechanical load. Journal of Anatomy, 2006. 208(4): pp. 471-490.
6. Derwin, K.A., et al., Enthesis Repair: Challenges and Opportunities for Effective Tendon-to-Bone Healing. The Journal of bone and joint surgery. American volume, 2018. 100(16): p. e109-e109.
7. Calejo, I., et al., Enthesis Tissue Engineering: Biological Requirements Meet at the Interface. Tissue Engineering Part B: Reviews, 2019. 25(4): pp. 330-356.
8. Watad, A., et al., Enthesitis: Much More Than Focal Insertion Point Inflammation. Current rheumatology reports, 2018. 20(7): p. 41-41.
9. Rossetti, L., et al., The microstructure and micromechanics of the tendon-bone insertion. Nat Mater, 2017. 16(6): pp. 664-670.
10. Paxton, J., K. Baar, and L. Grover, Current Progress in Enthesis Repair: Strategies for Interfacial Tissue Engineering. Orthopedic & Muscular System, 2012.
11. Nowlin, J., et al., Engineering the hard-soft tissue interface with random-to-aligned nanofiber scaffolds. Nanobiomedicine, 2018. 5: p. 1849543518803538-1849543518803538.
12. Font Tellado, S., et al., Heparin functionalization increases retention of TGF-β2 and GDF5 on biphasic silk fibroin scaffolds for tendon/ligament-to-bone tissue engineering. Acta Biomaterialia, 2018. 72: pp. 150-166.
13. Su, W., et al., Promoting tendon to bone integration using graphene oxide-doped electrospun poly(lactic-co-glycolic acid) nanofibrous membrane. International journal of nanomedicine, 2019. 14: pp. 1835-1847.
14. Wang, W., et al., Type II Collagen Sponges Facilitate Tendon Stem/Progenitor Cells to Adopt More Chondrogenic Phenotypes and Promote the Regeneration of Fibrocartilage-Like Tissues in a Rabbit Partial Patellectomy Model. Frontiers in Cell and Developmental Biology, 2021. 9: p. 1805.
15. Bunker, D.L., et al., Tendon to bone healing and its implications for surgery. Muscles Ligaments Tendons J, 2014(2240-4554 (Print)): pp. 343-50.
16. Zhao, F., et al., Changes in scaffold porosity during bone tissue engineering in perfusion bioreactors considerably affect cellular mechanical stimulation for mineralization. Bone Reports, 2020. 12: p. 100265.
17. Font Tellado, S., et al., Fabrication and Characterization of Biphasic Silk Fibroin Scaffolds for Tendon/Ligament-to-Bone Tissue Engineering. Tissue Eng Part A, 2017. 23(1937-335X (Electronic)): pp. 859-872.

18. Holwein, C., et al., No healing improvement after rotator cuff reconstruction augmented with an autologous periosteal flap. Knee Surgery, Sports Traumatology, Arthroscopy, 2019. 27(10): pp. 3212-3221.
19. Lee, K.W., et al., Effective healing of chronic rotator cuff injury using recombinant bone morphogenetic protein-2 coated dermal patch in vivo. J Biomed Mater Res B Appl Biomater, 2017(1552-4981 (Electronic)).
20. Novakova, S.S., et al., Tissue-engineered tendon constructs for rotator cuff repair in sheep. Journal of Orthopaedic Research, 2018. 36(1): p. 289-299.
21. Baumans, V., Use of animals in experimental research: an ethical dilemma? Gene Therapy, 2004. 11(1): p. S64-S66.
22. Fan, L., et al., Histopathological changes in patellar tendon enthesis of rabbit induced by electrical stimulation intensity. Journal of Orthopaedic Science, 2020. 25(2): p. 344-348.
23. Rothrauff, B.B., et al., The effect of adipose-derived stem cells on enthesis healing after repair of acute and chronic massive rotator cuff tears in rats. Journal of Shoulder and Elbow Surgery, 2019. 28(4): p. 654-664.
24. Sun, Y., et al., Small Subchondral Drill Holes Improve Marrow Stimulation of Rotator Cuff Repair in a Rabbit Model of Chronic Rotator Cuff Tear. The American Journal of Sports Medicine, 2020. 48(3): p. 706-714.
25. Fu, S.-C., et al., Hydrogen peroxide induced tendinopathic changes in a rat model of patellar tendon injury. Journal of Orthopaedic Research, 2018. 36(12): p. 3268-3274.
26. Zhang, J., et al., A Novel Kartogenin-Releasing Polymer Scaffold Promotes Wounded Rat Achilles Tendon Enthesis Healing. Foot & Ankle Orthopaedics, 2018. 3(3).
27. Quirk, N.P., et al., Effects of freeze-thaw on the biomechanical and structural properties of the rat Achilles tendon. Journal of Biomechanics, 2018. 81: p. 52-57.
28. Wieloch, P., et al., A cryo-jaw designed for in vitro tensile testing of the healing Achilles tendons in rats. Journal of Biomechanics, 2004. 37(11): p. 1719-1722.
29. Silver, N., et al., Selection of housekeeping genes for gene expression studies in human reticulocytes using real-time PCR. BMC molecular biology, 2006. 7: p. 33-33.
30. Lu, H.H. and S. Thomopoulos, Functional Attachment of Soft Tissues to Bone: Development, Healing, and Tissue Engineering. Annual Review of Biomedical Engineering, 2013. 15(1): p. 201-226.
31. Schwartz, A.G., et al., Mineral distributions at the developing tendon enthesis. PloS one, 2012. 7(11): p. e48630-e48630.
32. Benjamin, M., E.J. Evans, and L. Copp, The histology of tendon attachments to bone in man. Journal of anatomy, 1986. 149: p. 89-100.
33. Nawata, K., et al., Development of the attachment zones in the rat anterior cruciate ligament: changes in the distributions of proliferating cells and fibrillar collagens during postnatal growth. 2002(0736-0266 (Print)).
34. Smietana, M.J., et al., Tissue-Engineered Tendon for Enthesis Regeneration in a Rat Rotator Cuff Model. BioResearch open access, 2017. 6(1): p. 47-57.
35. Mattap, S., et al., Patellar tendon enthesis abnormalities and their association with knee pain and structural abnormalities in older adults. Osteoarthritis and Cartilage, 2018. 26: p. S412-S413.
36. Baraliakos, X., et al., Achilles tendon enthesitis evaluated by MRI assessments in patients with axial spondyloarthritis and psoriatic arthritis: a report of the methodology of the ACHILLES trial. BMC Musculoskeletal Disorders, 2020. 21(1): p. 767.

37. Yamamoto, A., et al., Prevalence and risk factors of a rotator cuff tear in the general population. Journal of Shoulder and Elbow Surgery, 2010. 19(1): p. 116-120.
38. Bedi, A., et al., Differences in tendon graft healing between the intra-articular and extra-articular ends of a bone tunnel. HSS journal : the musculoskeletal journal of Hospital for Special Surgery, 2009. 5(1): p. 51-57.
39. Thomopoulos, S., et al., Collagen fiber orientation at the tendon to bone insertion and its influence on stress concentrations. Journal of Biomechanics, 2006. 39(10): p. 1842-1851.
40. Sartori, J., et al., Three-dimensional imaging of the fibrous microstructure of Achilles tendon entheses in Mus musculus. Journal of Anatomy, 2018. 233(3): p. 370-380.
41. Nourissat, G., et al., Mesenchymal stem cell therapy regenerates the native bone-tendon junction after surgical repair in a degenerative rat model. PloS one, 2010. 5(8): p. e12248-e12248.
42. Domínguez, D., et al., Generation of a new model of patellar tendinopathy in rats which mimics the human sports pathology: A pilot study. Apunts. Medicina de l'Esport, 2017. 52(194): p. 53-59.
43. Shaw, H.M., et al., Development of the human Achilles tendon enthesis organ. Journal of Anatomy, 2008. 213(6): p. 718-724.
44. Amadio, P.C., Friction of the gliding surface. Implications for tendon surgery and rehabilitation. Journal of hand therapy: Official Journal of the American Society of Hand Therapists, 2005. 18(2): p. 112-119.
45. Sun, M.M.-G. and F. Beier, Chondrocyte hypertrophy in skeletal development, growth, and disease. Birth Defects Research Part C: Embryo Today: Reviews, 2014. 102(1): p. 74-82.
46. Liu, C.-F., et al., A Role for Hedgehog Signaling in the Differentiation of the Insertion Site of the Patellar Tendon in the Mouse. PloS One, 2013. 8: p. e65411.
47. Bedi, A., et al., Cytokines in rotator cuff degeneration and repair. Journal of Shoulder and Elbow Surgery, 2012. 21(2): p. 218-227.
48. Dyment, N.A., et al., Gdf5 progenitors give rise to fibrocartilage cells that mineralize via hedgehog signaling to form the zonal enthesis. Dev Biol, 2015. 405(1): p. 96-107.
49. Franchi, M., et al., Collagen structure of tendon relates to function. TheScientificWorldJournal, 2007. 7: p. 404-420.
50. Buckley, M.R., et al., Distributions of types I, II and III collagen by region in the human supraspinatus tendon. Connective tissue research, 2013. 54(6): p. 374-379.
51. Smith, R.K., et al., Should equine athletes commence training during skeletal development?: changes in tendon matrix associated with development, ageing, function and exercise. Equine Veterinary Journal, 1999. 31(S30): p. 201-209.
52. Gonçalves-Neto, J., et al., Changes in collagen matrix composition in human posterior tibial tendon dysfunction. Joint Bone Spine, 2002. 69(2): p. 189-194.
53. Ito, Y., et al., The Mohawk homeobox gene is a critical regulator of tendon differentiation. Proc Natl Acad Sci U S A, 2010. 107(23): p. 10538-42.
54. Eames, B.F., P.T. Sharpe, and J.A. Helms, Hierarchy revealed in the specification of three skeletal fates by Sox9 and Runx2. Developmental Biology, 2004. 274(1): p. 188-200.
55. Docking, S., et al., Relationship between compressive loading and ECM changes in tendons. Muscles, ligaments and tendons journal, 2013. 3(1): p. 7-11.
56. Murchison, N.D., et al., Regulation of tendon differentiation by scleraxis distinguishes force-transmitting tendons from muscle-anchoring tendons. Development, 2007. 134(14): p. 2697-2708.

57. Shukunami, C., et al., Scleraxis is a transcriptional activator that regulates the expression of Tenomodulin, a marker of mature tenocytes and ligamentocytes. Scientific Reports, 2018. 8(1): p. 3155.

CHAPTER 4

# Enthesis Healing is Dependent on Scaffold Interphase Morphology: Results from a Rodent Patellar Model

C. J. Peniche Silva, S. A. Müller, N. Quirk, P. S. P. Poh, C. Mayer, A. Motta, C. Migliaresi, M. J. Coenen, C. H. Evans, E. R. Balmayor, M. van Griensven

*Cells, Vol. 11, 2022*

## ABSTRACT

The use of multiphasic scaffolds to treat injured tendon-to-bone entheses has shown promising results in vitro. Here, we used two versions of a biphasic silk fibroin scaffold to treat an enthesis defect created in a rat patellar model in vivo. One version presented a mixed transition between the bony and the tendon end of the construct (S-MT) while this transition was abrupt in the second version (S-AT). At 12 weeks after surgery, the S-MT scaffold promoted better healing of the injured enthesis, with minimal undesired ossification of the insertion area. The expression of tenogenic and chondrogenic markers was sustained for longer in the S-MT-treated group and the tangent modulus of the S-MT-treated samples was similar to the native tissue at 12 weeks while that of the S-AT-treated enthesis was lower. Our study highlights the important role of the transition zone of multiphasic scaffolds in the treatment of complex interphase tissues such as the tendon-to-bone enthesis.

## 1 INTRODUCTION

The enthesis is a fibrocartilaginous tissue that connects tendons and/or ligaments to bone. In particular, the tendon-to-bone enthesis is an interphase tissue that features a structural gradient of extracellular matrix (ECM). The opposing gradients of collagen molecule alignment and mineralization present at the enthesis allow smooth stress transfer from tendon to bone [1, 2]. This insertion site can be anatomically described as a succession of four different tissues/zones with region-specific cell types and mineral content [1]: tendon, non-mineralized fibrocartilage, mineralized fibrocartilage, and bone [2]. This structural complexity is essential for the enthesis' function in the body; it allows the transfer of mechanical loads between tendon and bone tissue and reduces stress at the insertion site. Regrettably, once the tendon-to-bone enthesis is damaged, its native structure is often not regenerated, resulting in scar formation, with poor mechanical properties and high rupture recurrence rates [2-5]. This damage often needs surgical repair, in which the injured tendon is reattached to its binding site in the bone using sutures or bone anchors [3, 6], which has proven to be insufficient for promoting the regeneration of the native enthesis structure [3, 7-9], as it relies purely on the reincorporation of the tendon into the bone at the enthesis without promoting the regeneration of the native tendon-to-bone transition [3]. One additional complication associated with the surgical intervention is the subsequent mineralization of the tendon area, usually involving endochondral ossification [10, 11], reported in animal studies [12, 13] as well as patient treatments [14]. The latter described a significant percentage of patients suffering from tendon mineralization after open augmented repair of the Achilles tendon or reconstruction of the anterior cruciate ligament [14, 15]. Tendon mineralization can result in pain and tendon weakness, increasing the probability of recurrent tendon/enthesis rupture in treated patients [10].

To overcome these limitations and to enhance the regeneration of the tendon-to-bone enthesis, tissue engineering strategies are increasingly growing in popularity [2, 16-20]. The combination of cells, biomaterials, and growth factors has shown promising results in studies whereby bone, tendon, and the enthesis tissue have been engineered in vitro and in vivo [2, 8, 21-23]. In the case of the enthesis, special attention has been directed to the design of scaffolds that mimic its native structural properties and complexity [23-26].

One example describes the fabrication of a tri-phasic scaffold using different combinations of PLGA and bioactive glass. This material promoted zone-specific distribution of cells in vitro [24] and stimulated fibrocartilage-like tissue deposition at the interphase region when evaluated in vivo [19]. Additionally, other reports of multiphasic scaffolds for enthesis regeneration describe

promising results only in vitro [27, 28], while others evaluated their constructs in vivo by implanting the scaffold subcutaneously rather than treating an actual enthesis defect [19, 29]. Thus, the in vivo evaluation of the functionality of such constructs for enthesis regeneration is still lacking.

Additionally, different manufacturing techniques and construct designs have been explored. For example, electrospinning is a widely used technique that allows the generation of fibers in the nanometer and micrometer range for the production of scaffolds [30-32]. However, it has been shown that the dense packing of fibers of electrospun scaffolds might result in poor cell infiltration and proliferation [33]. A similar limitation was reported by Lipner *et al*. when using an aligned electrospun PLGA scaffold with a mineral gradient in a rat model for supraspinatus tendon repair. As a result, the healing process was dominated by fibrosis and scar formation [34].

Although the fibrous morphology that is usually obtained in electrospun scaffolds mimics the fibrous morphology of tendon tissue, porous scaffolds mimic the 3D morphology of cartilage and bone tissue better [35-37].

Freeze-drying is a simple, cost-effective technique that allows the generation of porous scaffolds with a fair amount of control over the pore size and orientation [38, 39]. We have previously demonstrated that by combining directional freezing, freeze-drying, and salt leaching, it is possible to obtain biphasic scaffolds with the desired morphological structure and mechanical properties to mimic both, the tendon and bony morphology characteristic of the native enthesis [23]. Furthermore, we demonstrated that the obtained silk fibroin multiphasic scaffold for enthesis repair showed excellent in vitro biocompatibility and functionality [23, 36]. While designing our constructs, we exploited the formidable biomechanical properties and malleability of the silk fibroin, which allows the creation of scaffolds with high porosity without compromising the robustness of the construct. This is especially relevant for load-bearing scaffolds [23]. Additionally, this material shows a biocompatible, slow degradation rate due to proteolytic activity, that corresponds to the rate of new tissue deposition, which makes it ideal for tissue engineering applications [40, 41]. Interestingly, we observed a major impact of the interphase morphology on the mechanical properties of the scaffold [23]. Additionally, the presence of an interconnected transition zone promoted tissue-specific gene expression such as *Col1a1, Col2a1, Col3a1,* and *Sox9* along the scaffold in adipose-derived mesenchymal stem cells [23]. Our investigations and that of other groups pointed out a crucial role of the interphase morphology in enthesis scaffolds for cellular proliferation, cytoskeleton reorganization, and possibly, cell differentiation [18, 42, 43] in vitro. We hypothesize that the morphology of the transition zone in

engineered scaffolds will also have a significant impact on the healing process of the enthesis in vivo. Furthermore, we expect that the biocompatibility, the good mechanical properties, and tailorable degradability of the silk fibroin will play a favorable role for the healing process of the enthesis. Therefore, in this study, we developed a new enthesis injury model in the rat patella and enthesis defects were treated with silk fibroin multiphasic scaffolds that featured two distinctive interphase morphologies, smooth and abrupt. The fabrication technique was built upon our previously reported methodology [23]. Treated animals were observed for up to 12 weeks, and tissue healing was assessed using gene expression, μCT, histology, and mechanical testing. We found that a smooth transition between the bone and tendon-like phases of the enthesis scaffold induced region-specific cell morphology and matrix deposition, leading to de novo enthesis-like tissue formation.

## 2 MATERIALS AND METHODS



### 2.1 Biphasic Silk Fibroin Scaffolds

In the present study, a porous, biphasic silk fibroin scaffold featuring two distinct interface morphologies was used to treat a tendon-to-bone tissue defect at the enthesis site of a rat patella. The two different tendon-to-bone transitions recreated in the scaffolds featured either an abrupt phase transition or a mixed, smooth transition (Fig. 1A,B). Furthermore, the scaffolds feature site-mimicking structures and properties at the bony and the tendon sites. The scaffolds were fabricated using a methodology previously published by our group [23]. A complete characterization of the biphasic silk fibroin scaffolds, which included biomechanics and in vitro performance has been published in [23, 36].

Briefly, to produce the two versions of the biphasic scaffold, two different protocols were used. To obtain the scaffold with abrupt phase transition (hereafter termed as S-AT), the tendon zone of the scaffold, showing a lamellar-like structure of longitudinally oriented pores, was obtained first by directional freezing followed by freeze-drying. The pore sizes were controlled by adjusting the cooling rate of the 8% fibroin solution contained inside the molds. Thereafter, the tendon-like part was placed on top of a mixture of 8% silk fibroin solution containing 0.2 g of NaCl. After allowing for fibroin gelation to occur, the NaCl particles were removed from the scaffold by salt leaching with $ddH_2O$. A porous structure resembling bone architecture remained. The entire construct was frozen and freeze-dried. The final product consisted of a biphasic scaffold with an abrupt transition between the two distinct phases (Fig. 1A).

To obtain the scaffold with the mixed, smooth transition (hereafter termed as S-MT), the bony end of the scaffold showing randomly oriented pores was

produced first by salt leaching and freeze-drying as described for the S-AT scaffold in the second stage. Then, the bony-like sponge was placed at the bottom of a mold and covered with an 8% fibroin solution. Directional freezing was induced followed by freeze-drying to produce a zone of vertically oriented pores (tendon-like zone). This two-step approach yielded a biphasic scaffold with a large interconnected area of mixed porosity between the two types of pore orientation (Fig. 1B).

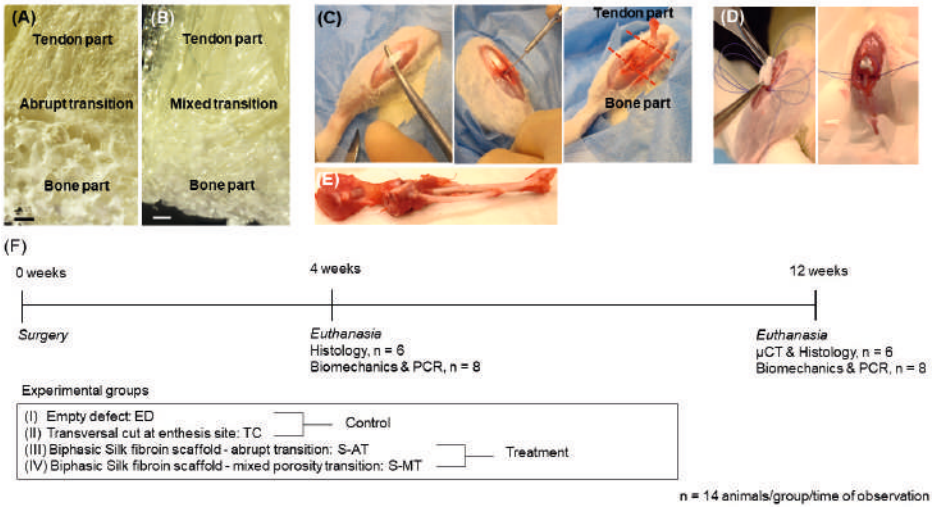


**Figure 1.** Schematic representation of the surgical approach. (**A**,**B**) Representative images of the biphasic silk fibroin scaffolds used for treatment, one with an interphase featuring an abrupt transition (S-AT) and one with an interphase presenting a mixed transition (S-MT; **B**). Scale bars represent 1 mm. (**C**) Exposure of the tendon and localization of the enthesis. Creation of the enthesis defect. (**D**) Scaffold implantation and fixation. (**E**) Representative image of the sample harvested at 12 weeks after surgery. (**F**) Timeline of surgery and subsequent times of observation. Specimens were collected for histology (n = 6) and biomechanics and PCR (n = 8). Samples at 12 weeks were also analyzed by µCT.

## 2.2 Rat Patellar Defect Model

Male Sprague Dawley rats (n = 112; Charles River Laboratories, Wilmington, MA, USA) weighing 400 g (100–115 d of age) were used in this study. The animals were allowed 48 h of acclimatization after arrival in the animal facilities. This study was approved by the Institutional Animal Care and Use Committee (IACUC, Protocol A00002479-17).

Prior to surgery, rats were placed in an anesthesia induction chamber with 3–4% isoflurane and an $O_2$ flow of 1.5–2.0 L/min. After reaching a deep anesthesia state, rats were transferred to a heat pad (37 °C). Anesthesia was maintained using a nose cone with 2–3% isoflurane and an $O_2$ flow of 1.5–2.0 L/min. Anesthesia depth

was constantly monitored in addition to the respiration rate. Before starting the surgical procedure, rats received subcutaneous injections with Buprenex (0.6 mg/kg body weight) and cefazolin (50 mg/kg body weight). The right leg was shaved from the inguinal area up to the malleoli. The leg was disinfected with iodine and 70% ethanol. In supine position, the knee was moved to a 60° angle and the foot was fixed with tape to the operation table. A para-patellar longitudinal incision was made from the distal femur to the proximal tibia. The bursal tissue was lifted and opened using scissors, thereby exposing the patellar tendon. In order to keep the length of the patellar tendon similar to its original length after transection, a McLaughlin procedure was performed using a loop through a drill hole in the proximal tibia and around the patella. Two sutures were made on the medial and lateral side of the patellar tendon. Subsequently, the patellar tendon was detached from the tibial insertion using a scalpel. At the tibial insertion side, a defect in the bone was created using a Gigli saw. In the scaffold treatment groups (S-MT or S-AT), the scaffolds were oriented with the bony part to the tibial plateau and the tendon part towards the patellar tendon. The scaffolds were secured into the defect using sutures guided over the bony bridge using the mediolateral drill hole in the tibia. In addition to our scaffold-treated groups, two control groups were included. For the first control group (empty defect—ED), the defect was created in the enthesis as described above but nothing was inserted. The patellar tendon was sutured back over the bone defect. Thus, the sutures were directly going through the tendon and the bone. For the second control group (transversal cut—TC), a transversal cut at the tendon near the enthesis was performed without damaging the bone and no treatment was provided. The incision was closed in layers.



After surgery, the animals were placed in a 37 °C recovery chamber for 30 min before being placed back in their cages. Animals were allowed to freely move in their cages without any restriction or immobilization after surgery. The wounds were inspected daily for the first 5 d. After that, wounds were checked two times per week until the end of the observation period (12 weeks). The surgical approach and experimental design are summarized in Fig. 1.

### 2.3 Mechanical Testing

For each of the four experimental groups, 14 animals were sacrificed at 4 and 12 weeks after surgery. Of these, 8 rats per sample group and time point of observation were used for the biomechanics and PCR studies. After sacrificing the rats, entire muscle–tendon–bone units were harvested (the distal fourth of the quadriceps muscle, the tendon, and the entire tibia including fibula).

Samples from the contralateral uninjured/healthy patellar enthesis were also harvested to be used as native tissue controls.

Before mechanical testing, the enthesis cross-sectional area (width ´ depth) and tendon length (muscle–tendon junction to bony insertion) were measured with an electronic CD-8 ASX Vernier caliper (Mitutoyo, Kawasaki, Japan). All measurements were conducted by a single operator. The sample length of interest was calculated as tendon length including the enthesis height.

Samples for mechanical testing were wrapped in a gauze soaked with saline and stored in a 15 mL Falcon tube at −20 °C until the day of testing [44]. Samples were thawed for 20–30 min at room temperature and kept moist with saline during the thawing period.

A custom-made, small biological specimen mechanical testing machine (Mayo Clinic, Rochester, NY, USA) with a MPL-2 50 lbf loadcell limit (Transducer Techniques, Temecula, CA, USA) and associated LabVIEW 2017 SP1 (National Instruments, Austin, TX, USA) was used for mechanical enthesis testing. The tibia was clamped by fixing the distal aspect rigidly whilst allowing neutral tendon alignment to the proximal attached muscle. The muscle was fixed by custom-built cryo-clamps [45]. Just before testing, muscles were frozen using dry ice powder to secure sample muscle attachments proximally. The temperature of proximal and middle tendon sections, as well as the enthesis, was monitored by a TrueRMS Supermeter multimeter (True RMS, Newport, RI, USA) during the freezing period to achieve optimal fixation. The optimal temperature for enthesis testing had been determined previously in a test study [44]. A mean temperature of −1 °C at the proximal tendon region assured sufficient muscle freezing in order to avoid muscle slippage. With a mean temperature of 10 °C at the enthesis region, mechanical testing could be performed reproducibly while the enthesis was not frozen. Samples were preloaded to 3 N prior to 200 mm/min failure tensile test [44]. Force–elongation curves were recorded, from which ultimate load (force at failure (N)), ultimate strain (elongation at failure/tendon length (%)), and tangent modulus ([force at failure/enthesis cross sectional area]/[ultimate strain] (MPa)) were calculated. Data were processed individually through Matlab 2016a (Mathworks, Natick, MA, USA), and compiled in Microsoft Excel 2010 (Microsoft, Redmond, WA, USA).

### 2.4 Micro-Computed Tomography (µ-CT) Analysis

Entheses samples (n = 6 per each of the 4 groups) harvested at 12 weeks after surgery were scanned using a Skyscan 1176 µCT (Bruker, Kontich, Belgium) at 90 kV and 277 µA. A 0.1 mm Cu filter was used. Images were acquired at a resolution of 35 µm. Image reconstruction was performed using NRecon v2.0.4 (Bruker, Kontich, Belgium), and analysis was performed using CTAn v1.13 (Bruker, Kontich, Belgium). Briefly, a region of interest (ROI) was selected by excluding the patella and tibia bones but including the area of the enthesis defect. Next,

global thresholding of 90 to 255 was implemented for the binarization of images and further calculations using built-in algorithms in CTAn.

### 2.5 Histology

Collected specimens at 4 and 12 weeks after surgery (n = 6 per group and time point) were decalcified in 10% buffered EDTA (Sigma Aldrich, St. Louis, MO, USA), dehydrated in ethanol, and embedded in paraffin. Longitudinal cross-sections of the tendon-to-bone enthesis (thickness 7 µm) were sliced using the Leica RM 2165 microtome (Leica Biosystems, Nussloch, Germany). Subsequently, hematoxylin and eosin (H&E), and Safranin O stainings were performed. Briefly, after rehydration of the samples in descending ethanol series and distilled water, H&E staining was performed by incubating the slides with hematoxylin solution for 10 min and eosin for 2 min (Carl Roth GmbH, Karlsruhe, Germany). Thereafter, samples were dehydrated in ascending ethanol series, cleared with NeoClear-xylene substitute (Merck KGaA, Darmstadt, Germany), and mounted with UltraKit mounting media (Thermo Fisher Scientific, Landsmeer, The Netherlands). This staining allows the visualization of tissue microanatomy by staining the nuclear components of the cells purplish blue and staining structures such as elastic fibers, collagens and muscle fibers different shades of pink.



For Safranin O staining, the rehydrated samples were stained with hematoxylin solution for 10 min followed by 5 min staining with fast green solution (Sigma Aldrich, St. Louis, MO, USA), rinsing with 0.1% acetic acid, and further staining with 0.1% Safranin O solution for 10 min (Sigma Aldrich, St. Louis, MO, USA). Subsequently, the samples were dehydrated, cleared, and mounted as described before. Safranin O staining is specific for cartilage tissue. Proteoglycan-rich cartilage stains orange to red (also the endochondral ossifications), nuclei are stained black and the background stains green to blue.

Additionally, sections were stained with Masson–Goldner trichrome using a commercial kit (Carl Roth GmbH, Karlsruhe, Germany) according to the manufacturer's protocol. When using this staining, dense collagen areas such as old bone appear dark green while cartilage and newly formed collagen-rich tissues appear pale green. Muscle and cell cytoplasm are stained red.

Images were taken with a Nikon DS-Ri2 camera mounted on a Nikon Ti Slide Scanner Microscope (Nikon Instruments Europe BV, Amsterdam, The Netherlands). In addition, sections were stained with picrosirius red to visualize collagens and their alignment by highlighting the natural birefringence of collagen fibers when exposed to polarized light. For the staining, sections were incubated for 1 h in a picric acid-saturated sirius red solution (Sigma Aldrich, St. Louis, MO, USA). Next, several washing steps were performed with acidified

water. Finally, excess water was removed and sections were dehydrated further cleared in xylene, and mounted with a cover slip. Images were taken under polarized light microscopy in an Olympus IX83 inverted microscope (Olympus, Westborough, MA, USA) using the cellSens Dimension Desktop software v2.2 (Olympus, Westborough, MA, USA).

### 2.6 Gene Expression; qPCR Array

Immediately after processing the samples for biomechanics, the tissue was harvested for the qPCRs (n = 8 per group and time point) in RNALater® solution (Sigma Aldrich, St. Louis, MO, USA). In order to guarantee that the quality of the RNA extracted from these samples would be as required by scientific standards, the equipment used for biomechanics, sample holder, and working table and surroundings were cleaned with ethanol 70% and RNAse AWAY® (Sigma Aldrich, St. Louis, MO, USA) prior mechanical testing and between each sample. In addition to the samples of the treatment and control groups, samples from the healthy/native patellar enthesis of each rat were also included as controls (n = 8). The samples were homogenized with steel beads in TRIzol (Sigma Aldrich, St. Louis, MO, USA) using a TissueLyser II set to 3 min at 30 Hz (Qiagen GmbH, Hilden, Germany). Total RNA isolation was performed by phenol-chloroform extraction. The concentration and purity of the RNA were measured using a NanoDrop spectrophotometer (NanoDrop Tech. Inc., Greenville, SC, USA). A baseline for RNA purity values was set to be 1.7 for the ratio 260/230 and 1.8 for the ratio 260/280. Samples showing lower purity values than the baseline were further purified with the Monarch RNA cleanup kit (New England BioLabs GmbH, Frankfurt, Germany). The final purity values of all RNA samples used were, in every case, according to scientific quality standards. cDNA synthesis was performed using the RT$^2$ First Strand Kit (Qiagen GmbH, Hilden, Germany) in a C1000 Touch Thermal Cycler (Eppendorf AG, Hamburg, Germany) following the manufacturer's instructions. The Osteogenic RT$^2$ Profiler PCR arrays (PARN-026Z) and the RT$^2$ SYBR Green Mastermix were purchased from Qiagen (Qiagen GmbH, Hilden, Germany). PCR assays were performed in a CFX 96 Real-Time System thermocycler (Bio-Rad, Hercules, CA, USA) following the instructions of the manufacturer. The melting curves displayed a well-defined single distinct peak for each amplified gene, indicating that the amplified PCR products are single discrete species.

Ct values were exported to an Excel file following Qiagen's instructions. This table was then uploaded to Qiagen's data analysis web portal at http://www.qiagen.com/geneglobe, accessed on 6 June 2021. Samples were assigned to control (native tissue) and test groups (ED, TC, S-AT, and S-MT). Ct values were normalized against the arithmetic mean of the Ct values from the reference genes *Ldha* and *Rplp1* included in the array setup.

The lower limit of detection was set to a Ct value of 35 using the "Set Cut-off" function in the web analysis portal. This function defines the upper limit of useful Ct values in calculating the fold change. All raw undetermined Ct values or Ct values greater than the set Ct cut-off value were automatically changed to the cut-off value. For the fold change calculations, genes that were not detected or showed a Ct value greater than the set cut-off value for both the control and test group samples were not considered. The data analysis web portal calculated fold change/regulation by means of the widely used delta delta Ct method (ΔΔCt), in which ΔCt is calculated as the difference between the Ct value of a gene of interest and that of a reference gene followed by ΔΔCt calculations (ΔCt(Test Group) − ΔCt(Control Group)). The fold change was then calculated using the 2(-ΔΔCt) formula. Treated data are displayed as fold regulation (FR) as this makes it easier to read and interpret. FR is the same as fold change (FC) for FC values > 1. For FC values < 1, FR is the inverse negative of FC. Additionally, a heat map was generated using Qiagen's data analysis web portal that indicates with a gradient of color from green to black to red, the fold regulation of each gene compared to the expression in the native tissue. Black indicates the same expression as native, grey indicates no expression, green indicates downregulation of the gene expression compared to the native tissue, and red indicates upregulation of the gene expression compared to the native tissue.



### 2.7 Statistical Analysis

The statistical analysis was performed using the GraphPad Prism 8.3.0 Software (GraphPad Software, San Diego, CA, USA). Measurable data are displayed as the mean ± SD.

For mechanical testing, the data on calculated mechanical properties are displayed through box plots (median, 1st, 3rd quartile ranges and outliers > 1.5 × IQR + Q 1/3). Statistical significance was determined by Kruskal–Wallis test and Dunn's multiple comparisons test, with a $p$ value < 0.05 indicating statistical significance. The µ-CT data were analyzed using a one-way analysis of variance (df = 4; F = 4.139) followed by Dunnett's multiple comparison test, with a $p$ value < 0.05 indicating statistical significance.

## 3 RESULTS

### 3.1 Rat Patellar Injury and Scaffold Treatment

All operations were successfully completed. All animals in all groups (i.e., scaffold abrupt transition, S-AT; mixed and smooth transition, S-MT; empty defect, ED; transversal cut, TC) remained healthy, assessed by twice-weekly checks, during the experimental period up to 12 weeks.

### 3.2 Mechanical Testing

The measurements of the associated tendon length at 4 and 12 weeks after surgery showed no significant differences between the scaffold-treated groups and the native tissue (Fig. 2A), while the cross-sectional area measured in the scaffold-treated groups and the controls was significantly larger ($p < 0.005$) than that of the native enthesis (Fig. 2B). Native tissue at 4 weeks after surgery showed the highest ultimate load compared to the S-MT, S-AT and TC groups ($p < 0.005$). The ED group was the exception, displaying values of ultimate load comparable to the native tissue as early as at 4 weeks after surgery. However, this result was not dependent on the tissue but solely on the suture material since the tendon was directly sutured back to the bone defect. In the scaffold-treated groups, the sutures did not go through the tendon nor through the scaffold. Thereby, the ED group seems to outperform the scaffold-treated groups. However, samples taken at 12 weeks after surgery from the scaffold-treated groups had similar ultimate loads as native tissue (Fig. 2C). Similarly, the tangent modulus determined for the scaffold-treated groups at 4 weeks after surgery was lower ($p < 0.05$) than that of the native tissue (Fig. 2D). Nevertheless, 12 weeks after surgery, the group treated with the S-MT scaffold showed a significant increase in the tangent modulus to values no longer statistically different to that of the native tissue, while the tangent modulus of the group treated with the S-AT scaffold remained lower ($p < 0.01$).

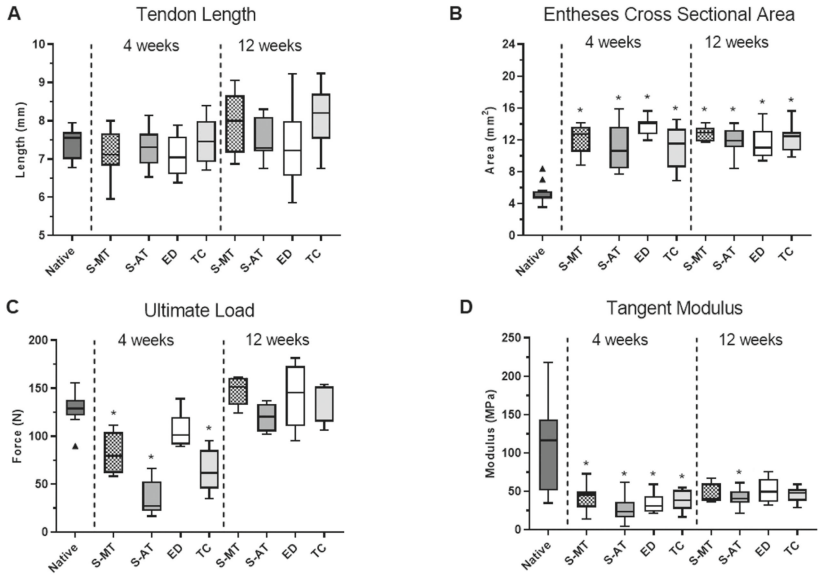


**Figure 2.** Measurements and mechanical testing of the samples at 4 and 12 weeks after surgery. (A) Tendon length, (B) enthesis cross sectional area, (C) ultimate load, and (D) tangent modulus. Tukey's box plots show 1st and 3rd quartile, median and outliers from eight samples. Significant differences with respect to the native tissue are shown. Obtained p values are indicated as * for $p < 0.05$ and outliers are indicated by (▲).

### 3.3 Micro-Computed Tomography (μCT) Analysis

μCT analysis performed at 12 weeks after surgery allowed the quantitative comparison of ectopic mineralization, an undesired complication during healing [10, 46-48], occurring in the tendon area of the samples from the treatments and control groups relative to native tissue (Fig. 3). This analysis revealed that the mineralization occurring in the tendon area of the samples treated with the S-MT scaffold was rather low and not of statistical significance. However, a significantly larger degree of mineralization was detected in the tendon of the samples from the TC and the S-AT groups ($p < 0.05$). Surprisingly, the control group ED showed a reasonably low degree of mineralization in the tendon.

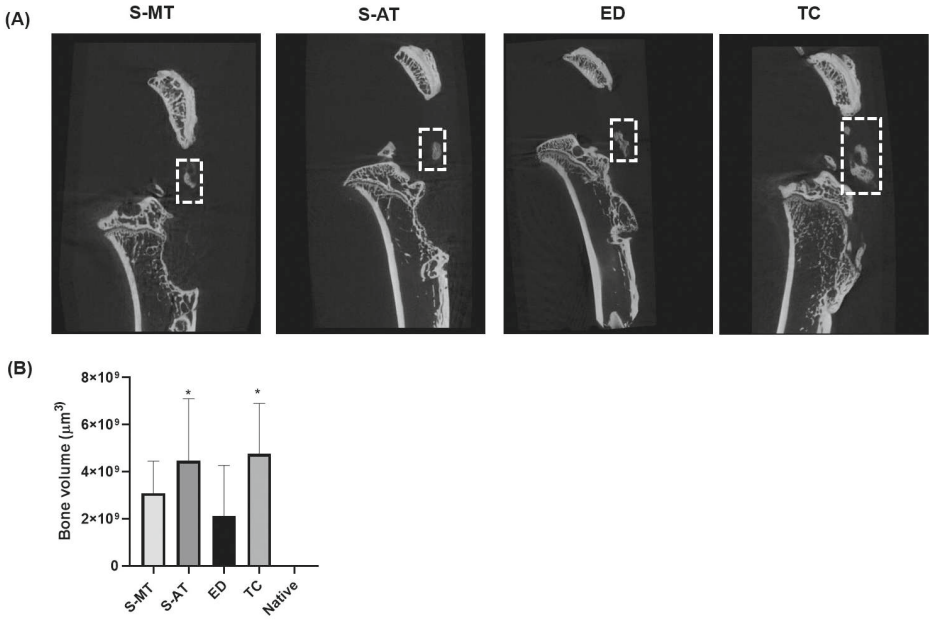


**Figure 3.** (**A**) μCT scans of the specimens harvested at 12 weeks after surgery. Detected ossification in the tendon tissue is indicated with dashed squares. (**B**) Comparison of bone volume (ossification) found in the tendon tissue for each of the treatment groups (S-AT with abrupt transition and S-MT with mixed transition) and the control groups (TC, transversal cut; ED, empty defect). Bone volume calculations are expressed relative to native tissue, with statistically significant differences denoted * $p \leq 0.05$ from 6 samples.

### 3.4 Histology

The histology performed on the samples treated with the S-MT scaffold revealed a smooth transition from the tendon to the bone in the insertion site as early as 4 weeks after scaffold implantation (Figures 4B, 5B and 6B). Furthermore, the Masson–Goldner trichrome staining showed that at 12 weeks after surgery, the samples treated with the S-MT scaffold presented a fully restored native-like

pattern of collagen deposition in the enthesis (Fig. 6B). Moreover, H&E staining of the newly regenerated tissue in the S-MT samples revealed a longitudinal alignment of the Sharpey fibers in the tendon area of the enthesis similar to that observed in the native tissue (Fig. 4B). Such a particular pattern was not observed in neither the samples of the S-AT nor in those from the control groups.

Safranin O staining revealed sites of cartilage deposition and endochondral ossification in the ED, TC, and S-AT groups that were absent in the S-MT group at both analyzed time points (Fig. 5). The group treated with the S-AT scaffold developed some ossification in the shape of a bulky bony structure that protruded into the tendon area at the insertion site of the enthesis, as well as some isolated spots near the enthesis, where mineralization in the tendon region was visible (Fig. 5C, 6C). A similar ossification pattern at the insertion site was also visible in the control groups (Fig. 5, 6). Additionally, both control groups developed scattered mineralization regions in the tendon area, particularly at 12 weeks after surgery.

Picrosirius red staining of the collagen fibers in the samples treated with the S-MT scaffold (Fig. 7B) confirmed the observations described above, highlighting a zone of longitudinally aligned collagen fibers in the tendon part of the enthesis at 4 weeks after surgery. At 12 weeks after surgery, these samples showed abundant staining of tightly packed collagen fibers where the scaffold had been implanted. This result indicated that the transition zone present in the S-MT scaffold effectively promoted the deposition and organization of the collagen fibers in the newly formed enthesis. In contrast, picrosirius red staining of the samples treated with the S-AT scaffold (Fig. 7C) showed a lower presence of collagen fibers in the defect region compared to the S-MT-treated group at 4 weeks. The differences between the two treatment groups remained visible at 12 weeks after surgery, with the S-AT-treated group showing a mesh-like pattern of collagen deposition in the defect site rather than the aligned and more homogenous pattern observed in the S-MT-treated group. Furthermore, both control groups showed a more disorganized and heterogenous collagen deposition pattern in the defect zone (Fig. 7D, E), more in line with tissue scarification than with the regeneration of the native enthesis tissue structure.

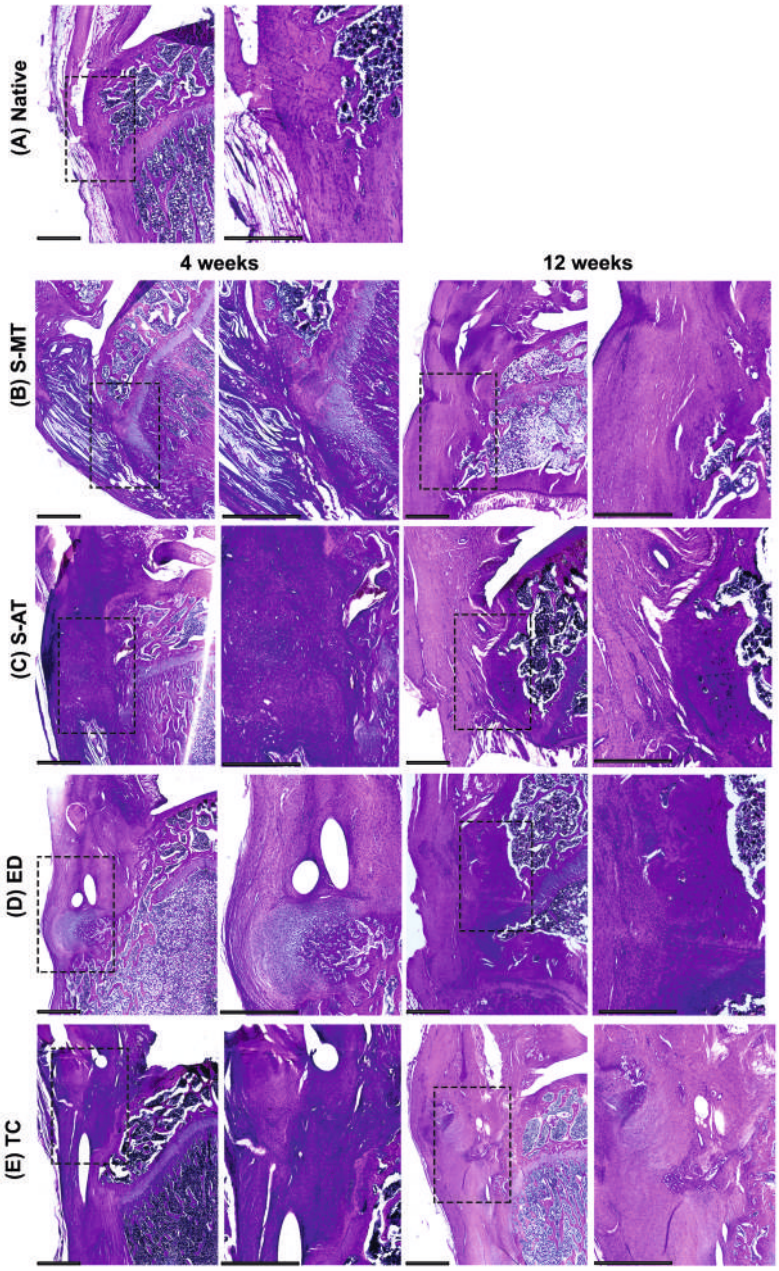


**Figure 4.** H&E staining. Representative images of the histological analysis of enthesis defects at the patellar region at 4 (left pairs) and 12 weeks (right pairs) after surgery, in (**A**) native enthesis, (**B**) S-MT with mixed transition, (**C**) S-AT with abrupt transition, (**D**) empty defect, and (**E**) transversal cut at enthesis site. Extracellular collagens and muscle fibers appear stained with different shades of pink. Dashed squares in the left pairs indicate the locations of the magnified areas shown on the respective right. Scale bars = 800 μm.

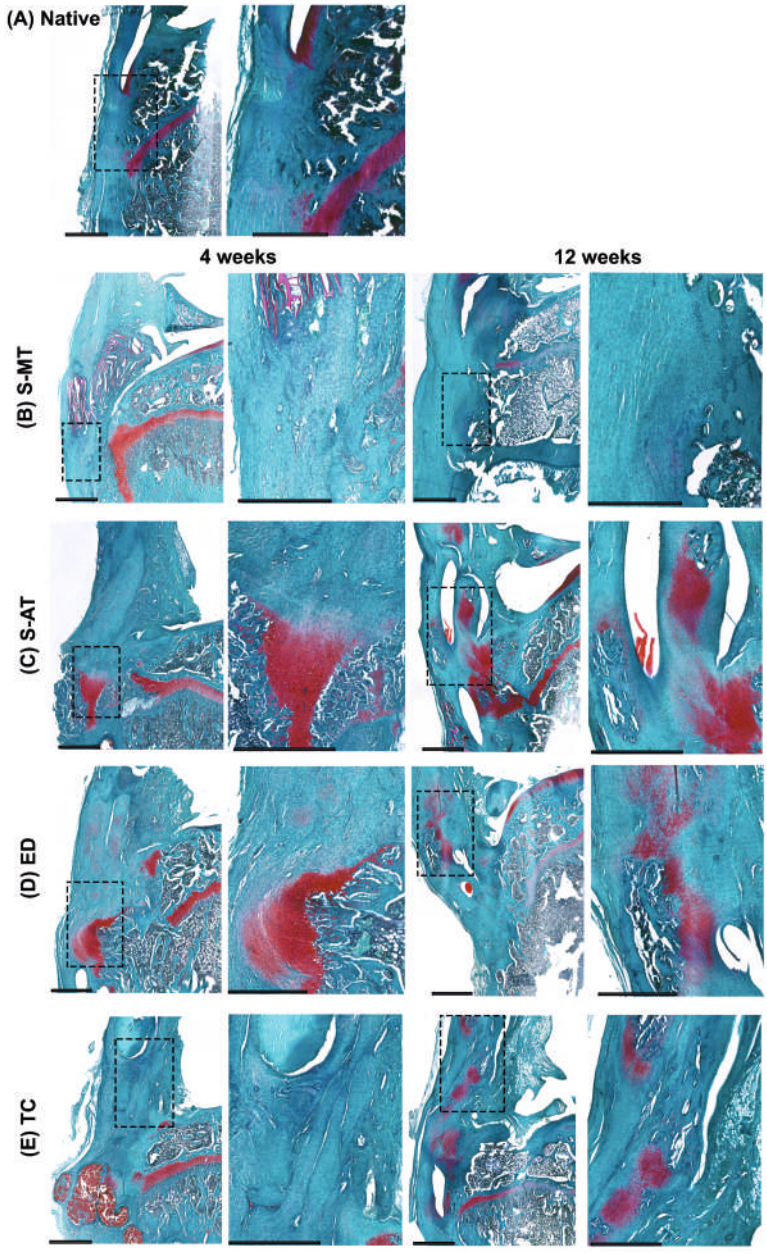


**Figure. 5.** Safranin O staining. Representative images of the histological analysis of enthesis defects at the patellar region at 4 (left pairs) and 12 weeks (right pairs) after surgery, in (**A**) native enthesis, (**B**) S-MT with mixed transition, (**C**) S-AT with abrupt transition, (**D**) empty defect, and (**E**) transversal cut at enthesis site. Proteoglycan-rich cartilage appears red (here the orange to red color indicates endochondral ossification), and background appears blue. Dashed squares in the left pairs indicate the locations of the magnified areas shown on the respective right. Scale bars = 800 μm.

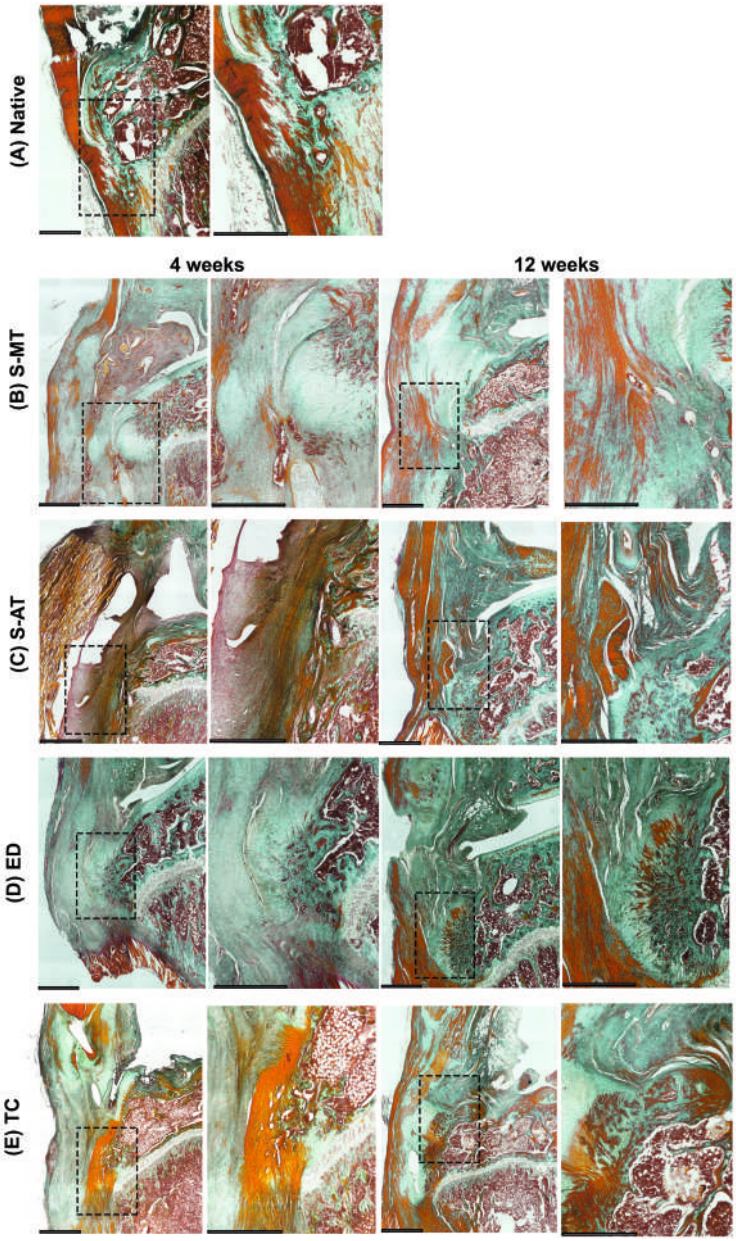


**Figure 6.** Masson–Goldner trichrome staining. Representative images of the histological analysis of enthesis defects at the patellar region at 4 (left pairs) and 12 weeks (right pairs) after surgery, in (**A**) native enthesis, (**B**) S-MT with mixed transition, (**C**) S-AT with abrupt transition, (**D**) empty defect, and (**E**) transversal cut at enthesis site. Dense collagen areas appear dark green, cartilage and newly formed collagen-rich tissue appears pale green. Muscle and cell cytoplasm are stained red. Dashed squares in the left pairs indicate the locations of the magnified areas shown on the respective right. Scale bars = 800 µm.

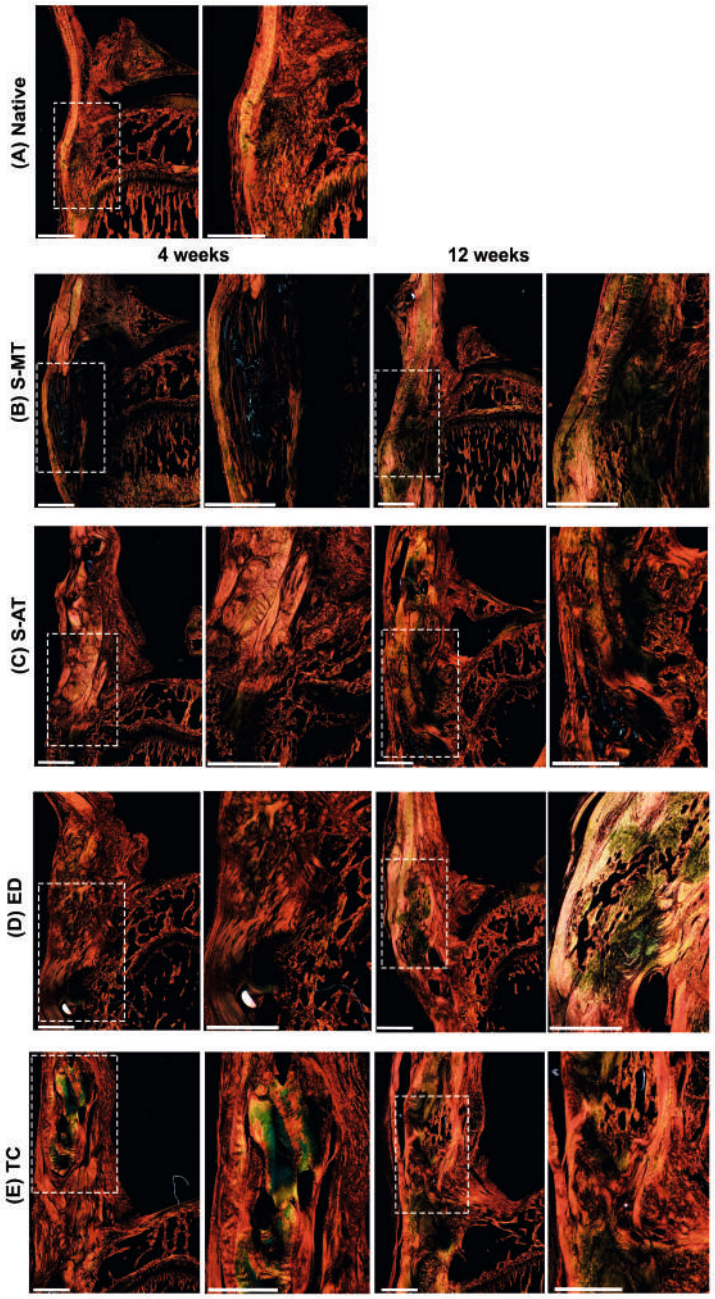


**Figure 7.** Picrosirius red staining. Representative images of the histological analysis of enthesis defects at the patellar region at 4 (left pairs) and 12 weeks (right pairs) after surgery, in (**A**) native enthesis, (**B**) S-MT with mixed transition, (**C**) S-AT with abrupt transition, (**D**) empty defect, and (**E**) transversal cut at enthesis site. Dashed squares in the left pairs indicate the locations of the magnified areas shown on the respective right. Scale bars = 800 μm.

### 3.5 Gene Expression; qPCR Array

The gene expression signature of 84 osteogenic and ECM-relevant genes was analyzed using RT-qPCR arrays. The fold regulation of the expression was determined with respect to the expression in the native tissue for genes with a Ct value ≤ 35. The cut-off for fold regulation was set at 2 fold. The top 10 upregulated and downregulated genes for each sample group are shown in Appendix A Tables A1 and A2, respectively. The heat map shows the genes that were downregulated for each group compared to the native tissue in green. Conversely, the heat map shows upregulated genes compared to the native tissue in red. Additionally, black indicates the same expression as native tissue and grey indicates undetected genes/no expression. The samples treated with the S-AT and S-MT scaffolds showed similar patterns of gene expression at 4 weeks after surgery (Fig. 8A, C). At this time point, key genes identified to play an important role in tissue remodeling, tendon, and cartilage formation, and extracellular matrix deposition (e.g., *Col1a1, Col2a1, Col3a1, Col5a1, Col6a1, Ctsk*, *Mmp2, Serpinh1* and *Spp1)* were upregulated by several folds in both scaffold-treated groups compared to native expression. On the contrary, the osteogenic markers *Bmp2, Bmp6,* and *Bmp7* were not expressed in the samples treated with the S-MT and S-AT scaffolds while *Bmp-4* was downregulated by 4.5 fold in the S-AT group and not expressed in the S-MT group. In addition, the osteogenic marker *Runx2* was downregulated or expressed at levels similar to native in both treatment groups at this time point: by 2.3 fold in the S-AT-treated group and by 1.9 fold in the S-MT group.

Interestingly, at 12 weeks after surgery, the gene expression pattern of the samples treated with the S-MT scaffold was substantially different from that of the S-AT group (Fig. 8B, D). At this time point, the samples treated with the S-MT scaffold showed a further increase in the upregulation of ECM-relevant genes (e.g., *Col1a1, Col2a1, Col3a1, Col5a1* and *Col6a1*) compared to the already high expression of those genes at week 4. Similarly, the expression of *Ctsk, Mmp2* and *Spp1* increased from week 4 to week 12 in magnitudes of 23.1, 7.9, and 110 fold, respectively. Additionally, at 12 weeks after surgery, the samples from the S-MT group showed the downregulation of many of the osteogenic genes included in the array (*Bglap*, *BMP2*, *BMP6* and *BMP7*).

In contrast, in the S-AT group, genes upregulated at 4 weeks (e.g., *Col1a1, Col2a1, Col3a1, Col5a1* and *Col6a1*) were strongly downregulated at 12 weeks after surgery. Moreover, the expression of *Ctsk*, *Mmp2* and *Spp1* was downregulated by 12.9, 10.2 and 28.3 fold, respectively, compared to at 4 weeks. Additionally, the expression of *Serpinh1* decreased in the S-AT-treated group to 1.7 fold but remained upregulated by 4.7 fold in the S-MT group at 12 weeks after surgery.

Both control groups exhibited a strong downregulation of the majority of the genes included in the array at 4 weeks after surgery. Of the 84 genes, 42 and 57 genes were not expressed in the ED and TC groups, respectively (Figure 8E,G). From genes detected within our set Ct cut-off value, of relevance was the upregulation of *Col2a1*, *Bgn*, and *Spp1* in the samples of both control groups, compared to native expression. Additionally, *Bmp1* was upregulated by 6.0 fold in the TC group while its expression remained low in the ED group at the same time point. Conversely, the expression of *Col1a1*, *Col3a1* and *Col5a1* was upregulated in the ED group at 4 weeks but downregulated in the TC group at the same time point. The overall gene expression of the TC group at 12 weeks after surgery was similar to that observed at 4 weeks, with a few of the non-expressed genes at 4 weeks showing a small upregulation at 12 weeks (Fig. 8H). The expression measured in the ED group showed a pattern of expression close to that observed in the native tissue (black boxes in the heatmap), lacking values of (extreme) down- or upregulation that are typically observed in regenerating tissue. However, some osteogenic genes such as *BMP1*, *BMPr1a*, *Bglap* and *Runx2* were among the few upregulated genes in the ED group at 12 weeks after surgery.

**Figure 8 (next page).** Gene expression in explanted samples at 4 weeks (left column) and 12 weeks (right column) after implantation (n = 8). (Top table) Plate layout with 84 genes investigated. Heat maps represent fold regulation of the gene expression compared to native tissue. Green indicates downregulation, red indicates upregulation, grey* indicates undetected expression and black indicates native levels of expression (= no regulation compared to native tissue). (**A**,**B**) S-MT, silk scaffold with mixed transition; (**C**,**D**) S-AT, silk scaffold with abrupt transition; (**E**,**F**) ED, empty defect; (**G**,**H**) TC, transversal cut.

| Layout | 01 | 02 | 03 | 04 | 05 | 06 | 07 | 08 | 09 | 10 | 11 | 12 |
|---|---|---|---|---|---|---|---|---|---|---|---|---|
| A | Acvr1 | Ahsg | Alpl | Anxa5 | Bglap | Bgn | BMP 1 | BMP 2 | BMP 3 | BMP 4 | BMP 5 | BMP 6 |
| B | BMP 7 | BMPr1a | BMPr1b | BMPr2 | Cd36 | Cdh11 | Cdhrd | Col10a1 | Col14a1 | Col1a1 | Col1a2 | Col2a1 |
| C | Col3a1 | Col4a1 | Col5a1 | Col6a1 | Comp | Cfs1 | Cfs2 | Cfs3 | Ctsk | Dlx5 | Egf | Fgf1 |
| D | Fgf2 | Fgfr1 | Fgfr2 | Flt1 | Fn1 | Gdf10 | Gli1 | Icam1 | Igf1 | Igf1r | Ihh | Itga2 |
| E | Itga3 | Itgam | Itgav | Itgb1 | Mmp10 | Mmp2 | Mmp8 | Mmp9 | Nfkb1 | Nog | Pdgfa | Phex |
| F | Runx2 | Serpinh1 | Smad1 | Smad2 | Smad3 | Smad4 | Smad5 | Sost | Sox9 | Sp7 | Spp1 | Tgfb1 |
| G | Tgfb2 | Tgfb3 | Tgfbr1 | Tgfbr2 | Tgfbr3 | Tnf | Tnfsf11 | Twist1 | Vcam1 | Vdr | Vegfa | Vegfb |

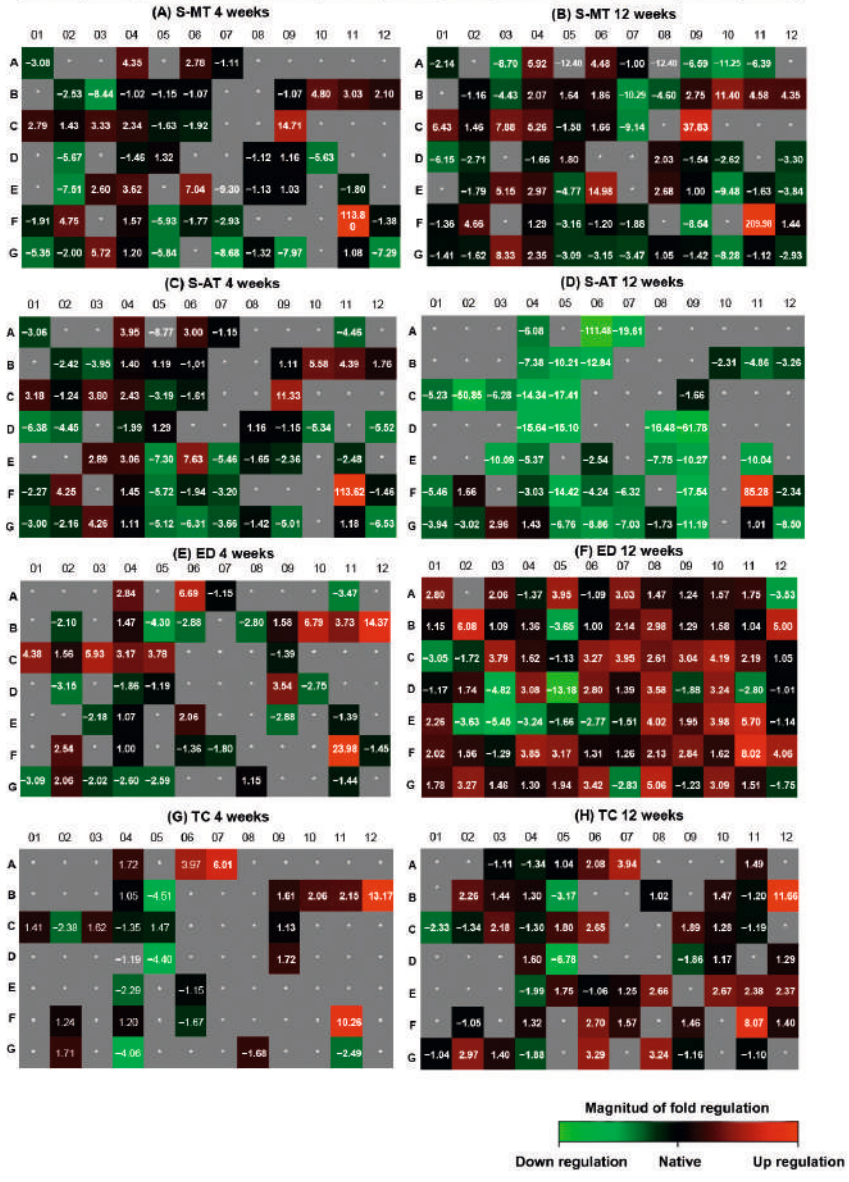

## 4 DISCUSSION

Interphase tissues, such as the enthesis, have a high incidence of injuries due to their anatomic role [8, 17, 49]. The reconstruction of such a complex tissue remains among the major current orthopedic challenges [3, 8, 48]. Among the many different approaches followed by tissue engineers to address enthesis regeneration, the utilization of biomimetic constructs to treat enthesopathies has shown promising results in many in vitro studies [20, 23, 26, 50]. In a previous study, we investigated the impact of the morphology of the transition zone of a biphasic silk fib]roin scaffold on cell proliferation and gene expression in vitro [23]. Following a similar approach but different techniques and materials, others have confirmed our previous observations that a biphasic construct presenting an aligned arrangement of fibers towards one end of the construct (tendon-like), and a disorganized pattern of fibers towards the opposite end (bone-like) can effectively promote cell alignment and organization, and gene expression in vitro, that mimics the tissue-specific gene expression and cell distribution and orientation observed in the healthy enthesis [51, 52].

However, evidence of the potential application of these constructs in vivo is still scarce. For example, Spalazzi and collaborators investigated their developed multiphasic scaffold in vivo concerning the improvement of the healing of interphase tissues [19]. Although this in vivo study demonstrated the effectiveness of their construct's design in stimulating matrix heterogeneity and fibrocartilage formation, it was conducted in an ectopic, subcutaneous athymic rat model, rather than in an orthotopic, injured enthesis model. The lack of in vivo studies exclusively addressing the use of biomimetic constructs to heal injured enthesis has been acknowledged as a challenge still to overcome [3, 53]. We have tried to fill in part of that gap in the present study.

Here, we have demonstrated that the morphology of the transition zone of a biphasic scaffold plays a significant role in promoting and directing the enthesis regeneration in vivo. Our research demonstrates that the treatment of an enthesis defect with our S-MT scaffold improved enthesis regeneration, allowing the injured tissue to develop mechanical properties and histological features that resembled that of the native enthesis at 12 weeks after surgery. We have also made evident that the conventional suture method used to treat the ED group fails to regenerate a native-like enthesis tissue. The histological assessment of these samples clearly demonstrated that reattaching directly the tendon to the bone leads to endochondral ossification and the native, microscopic structure is not restored (Figures 3–5).

Moreover, the analysis of the gene expression of the scaffold-treated groups revealed that, while both scaffolds were able to promote the expression of relevant entheses markers at 4 weeks after surgery, only the samples from the S-MT group sustained this upregulation at 12 weeks (Fig. 8). Relevant genes for tendon and enthesis regeneration, such as *Col1a1*, *Col1a2*, *Col3a1*, *Col5a1*, *Col6a1*, *Bgn*, *Fn1*, *Serphinh1* and *Mmp2*, were upregulated several folds in the samples of the S-MT scaffold group compared to native and to the ED group (Fig. 7). Additionally, the performed array included osteogenic genes such as *Bglap*, *Bmp2*, *Bmp6* and *Bmp7*, all of which were strongly downregulated in the S-MT group compared to the ED group, which is a wanted feature. This could well indicate lower osteogenic activity at the enthesis area in the S-MT group compared to the ED, which may favor the regeneration of the cartilaginous transition at the tendon-to-bone insertion site retaining low chances of endochondral ossification at the enthesis or tendon sites.



Collagens type 1, type 2, type 3, and type 10 are the most abundant collagens at the enthesis and they are responsible for the mechanical features of this tissue [54]. Our gene expression study revealed that the expression of many of these collagens was sustained for longer in the samples treated with the S-MT scaffold than in the samples from the S-AT group and the control groups. Additionally, *Col5a1, Col6a1* and *Bgn* were also upregulated at both time points of observation in the S-MT-treated groups. These ECM markers play a pivotal role during tendon healing by stabilizing the fibril structure of collagen type 1 in healing tendons [55, 56]. Likewise, the S-MT group exhibited sustained upregulation of other ECM-relevant genes for at least 12 weeks after surgery. This includes the procollagen-specific chaperone *Serpinh1*, which plays a key role in the assembly of triple-helical procollagen molecules [57], as well as *Mmp2* and *Tgfbr1*, which are known to be essential for ECM remodeling and the tendon healing process of acute injury [58-60]. In contrast, a strong downregulation of ECM-relevant genes was observed in the S-AT group at 12 weeks. Together with the lower tangent modulus measured for the explanted samples of this group, these data might indicate that the abrupt transition between the two phases of the S-AT scaffold failed to stimulate the levels of gene expression required to achieve effective enthesis repair and native-like mechanical properties in vivo.

The very good performance of our S-MT scaffold was also demonstrated by the significantly lower presence of ossification at the insertion site of the tendon compared to the S-AT-treated group and the control groups (Fig. 3). According to the µCT scans, the ED group also showed lower ectopic ossification than the S-AT in the tendon area. Nevertheless, ossification was still present. We should point out, however, that we observed high variability between bone volume formations within the same tested group. This variability is most likely associated

with the set region of interest (ROI) that delimited the defect area. The ROI was set by excluding the patella and tibia and including only the area of the enthesis defect. To ensure that all samples were treated similarly, and to avoid biased ROI selection, the same ROI was applied to all the samples analyzed. This comes with the limitation where the boundaries of the ROI, in some instances, failed to exclude the totality of the patella and/or tibia due to minor differences in sample size, sample orientation, and/or shape of the defect. Although differences were minor, this managed to increase the variability in the calculation of bone volume. We acknowledge this as a limitation of the utilized method to measure bone volume, but we believe that a more accurate measurement in such samples was not practically feasible.

The histological assessment of the ED group showed that ossification in this group occurred ectopically, and such ossification was not visible in the histological assessment of the S-MT samples. Heterotopic bone formation and mineralization are detrimental phenomena during tendon and enthesis healing [10, 46-48], for which no effective treatment has been yet developed [47]. In our study, ossification at the enthesis, as well as isolated mineralization spots in the tendon region, was observed in the histological assessment of the samples from the S-AT groups and the ED and TC control groups. In line with these observations, we identified an upregulation of *Bgn* and *Bmp1* in the samples of those groups at 4 weeks after surgery. In particular, the samples of the TC control group, which developed the largest amount of mineralization in the tendon region of the enthesis, showed sustained upregulation of *Bgn* and *Bmp1* at 4 and 12 weeks after surgery. In addition to the role in the tendon response to injury previously described, it has been observed that *Bgn* plays a crucial role in matrix mineralization and bone formation, possibly by regulating BMP-signaling [61, 62]. Moreover, BMP1, also known as the procollagen C-proteinase, is a proteolytic activator of TGFβ-1 that plays an important role in fibrosis and bone formation [63]. Previous studies have shown a link between the ossification of the tendon and the upregulation of osteogenic markers such as *Bmp2*, *Bmp4,* and *Bmp7* [46]. Interestingly, we did not observe a significant upregulation of these genes in either our treatment or control groups at 12 weeks. However, we did observe a several-fold downregulation of the osteogenic genes *Bglap*, *Bmp2*, *Bmp6,* and *Bmp7* in the S-MT-treated group compared to the ED control group.

The analyses presented here (biomechanics, histology, μCT scans, and gene expression signatures) of injured and treated entheses in vivo provide much-needed insight into the role of the transition zone of multiphasic scaffolds in the effective regeneration of the tendon-to-bone enthesis. Future studies might combine the optimized S-MT morphology of the transition zone in multiphasic scaffolds with different biomaterials and the use of coating agents (e.g., bioactive

growth factors [36]) to further improve the regeneration potential of these constructs.

The strategy described in the present study to improve the healing of an injured tendon-to-bone patellar enthesis supports our initial hypothesis about the potential role of the interphase morphology of a construct to stimulate the regeneration of such an interphase tissue in vivo. The results described here show that silk fibroin may be a suitable material to produce multiphasic constructs to be used for enthesis regeneration applications in vivo. Additionally, we have demonstrated the potential of tailored tissue engineering strategies to treat entheses defects as a complement to the conventional surgical-repair approaches. Nevertheless, in order to improve our strategy even further, we recommend fine-tuning the process of the design and fabrication of biomimetic constructs to specifically meet the morphological and biomechanical properties of the many different interphase tissues in the body.



## 5 ACKNOWLEDGMENT

C.H.E.'s research is partly funded by the John and Posy Krehbiel Professorship in Orthopedics. This work was supported by the Province of Limburg, Limburg Invests in its Knowledge Economy (LINK). The authors are also grateful to Hang Nguyen for the extensive revision of written English.

# 6 APPENDIX A

**Table A1.** Fold regulation of the expression of the top 10 upregulated genes for each group and time point of observation.

| 4 weeks | | | | 12 weeks | | | |
|---|---|---|---|---|---|---|---|
| S-MT scaffold treated group | | S-AT scaffold treated group | | S-MT scaffold treated group | | S-AT scaffold treated group | |
| Gene Symbol | Fold regulation | Gene Symbol | Fold regulation | Gene Symbol | Fold regulation | Gene Symbol | Fold regulation |
| Ssp1 | 113.8 | Spp1 | 113.6 | Ssp1 | 209.98 | Spp1 | 85.28 |
| Ctsk | 14.71 | Ctsk | 11.3 | Ctsk | 37.83 | Tgfbr1 | 2.96 |
| Mmp2 | 7.04 | Mmp2 | 7.63 | Mmp2 | 14.98 | Serpinh1 | 1.66 |
| Col1a1 | 4.8 | Col1a1 | 5.58 | Col1a1 | 11.4 | | |
| Serpinh1 | 4.75 | Bgn | 4.48 | Col5a1 | 7.88 | | |
| Anxa 5 | 4.35 | Col1a2 | 4.39 | Col3a1 | 6.43 | | |
| Col5a1 | 3.33 | Anxa 5 | 3.95 | Col6a1 | 5.26 | | |
| Col1a2 | 3.03 | Col5a1 | 3.8 | Col1a2 | 4.58 | | |
| Col3a1 | 2.79 | Col3a1 | 3.18 | Bgn | 4.48 | | |
| Bgn | 2.78 | Smad1 | 2.89 | Col2a1 | 4.35 | | |
| 4 weeks | | | | 12 weeks | | | |
| ED Control group | | TC Control Group | | ED Control group | | TC Control Group | |
| Gene Symbol | Fold regulation | Gene Symbol | Fold regulation | Gene Symbol | Fold regulation | Gene Symbol | Fold regulation |
| Ssp1 | 23.98 | Col2 | 13.17 | Ssp1 | 8.02 | Col2a1 | 11.66 |
| Col2a1 | 14.37 | Spp1 | 10.26 | Col2a1 | 6.08 | Spp1 | 8.07 |
| Col1a1 | 6.79 | Bmp1 | 6.01 | Pdgfa | 5.7 | Bmp1 | 3.94 |
| Bgn | 6.69 | Bgn | 3.97 | Twist1 | 5.06 | Tnf | 3.29 |
| Col5a1 | 5.93 | Col1a2 | 2.15 | Col2a1 | 5.00 | Twist1 | 3.24 |
| Col3a1 | 4.38 | Col1a1 | 2.06 | Dlx5 | 4.19 | Tgfb3 | 2.97 |
| Comp | 3.78 | Anax5 | 1.72 | Tgfb1 | 4.06 | Smad4 | 2.7 |
| Col1a2 | 3.73 | Tgfb2 | 1.71 | Nog | 3.98 | Nog | 2.67 |
| Igf1 | 3.54 | Col5a1 | 1.62 | Bglap | 3.95 | Mmp9 | 2.66 |
| Col6a1 | 3.17 | Ctsk | 1.61 | Cfs2 | 3.95 | Cfs1 | 2.65 |

**Table A2.** Fold regulation of the expression of the top 10 downregulated genes for each group and time point of observation.

| 4 weeks | | | | 12 weeks | | | |
|---|---|---|---|---|---|---|---|
| S-MT scaffold treated group | | S-AT scaffold treated group | | S-MT scaffold treated group | | S-AT scaffold treated group | |
| Gene Symbol | Fold regulation | Gene Symbol | Fold regulation | Gene Symbol | Fold regulation | Gene Symbol | Fold regulation |
| Tnfsf11 | -8.68 | Mmp10 | -7.30 | Bmp4 | -11.25 | Bgn | -111.4 |
| Bmpr1 | -8.44 | Vgefb | -6.53 | Cdhrd | -10.29 | Col4a1 | -50.85 |
| Vcam1 | -7.97 | Fgf2 | -6.38 | Nog | -9.48 | Igf1 | -61.78 |
| Itgam | -7.51 | Tnf | -6.31 | Cfs2 | -9.14 | Bmp1 | -19.61 |
| Vegfb | -7.29 | Smad4 | -5.72 | Alpl | -8.70 | Sox9 | -17.54 |
| Smad3 | -5.93 | Itga2 | -5.52 | Vdr | -8.28 | Comp | -17.41 |
| Tgfbr3 | -5.84 | Mmp8 | -5.46 | Bmp3 | -6.59 | Icam1 | -16.48 |
| Fgfr1 | -5.67 | Igf1r | -5.34 | Bmp5 | -6.39 | Flt1 | -15.64 |
| Igf1r | -5.63 | Tgfbr3 | -5.12 | Fgf2 | -6.15 | Smad3 | -14.42 |
| Tgfb2 | -5.35 | Vcam1 | -5.01 | Col10a1 | -4.60 | Col6a1 | -14.34 |
| 4 weeks | | | | 12 weeks | | | |
| ED Control group | | TC Control Group | | ED Control group | | TC Control Group | |
| Gene Symbol | Fold regulation | Gene Symbol | Fold regulation | Gene Symbol | Fold regulation | Gene Symbol | Fold regulation |
| Cd36 | -4.30 | Cd36 | -4.51 | Fn1 | -13.18 | Fn1 | -6.78 |
| Bmp5 | -3.47 | Fn1 | -4.40 | Itgav | -5.45 | Cd36 | -3.17 |
| Fgfr1 | -3.15 | Tgfbr2 | -4.06 | Fgfr2 | -4.82 | Col3a1 | -2.33 |
| Tgfb2 | -3.09 | Vegfa | -2.49 | Cd36 | -3.65 | Itgb1 | -1.99 |
| Nfkb1 | -2.88 | Col4a1 | -2.38 | Itgam | -3.63 | Tgbr2 | -1.88 |
| Cdh11 | -2.88 | Itgb1 | -2.29 | Bmp6 | -3.53 | Igf1 | -1.86 |
| Col10a1 | -2.80 | Twist1 | -1.68 | Itgb1 | -3.24 | Col4a1 | -1.34 |
| Igf1r | -2.75 | Smad4 | -1.67 | Col3a1 | -3.05 | Anxa5 | -1.34 |
| Tgfbr2 | -2.60 | Col6a1 | -1.35 | Tnfsf11 | -2.83 | Vcam1 | -1.16 |
| Tgfbr3 | -2.59 | Mmp2 | -1.15 | Ihh | -2.80 | Vegfa | -1.10 |

## 7 REFERENCES


1. Rossetti, L., et al., The microstructure and micromechanics of the tendon-bone insertion. Nat Mater, 2017. 16(6): p. 664-670.
2. Font Tellado, S., E.R. Balmayor, and M. Van Griensven, Strategies to engineer tendon/ligament-to-bone interface: Biomaterials, cells and growth factors. Adv Drug Deliv Rev, 2015. 94: p. 126-40.
3. Derwin, K.A., et al., Enthesis Repair: Challenges and Opportunities for Effective Tendon-to-Bone Healing. The Journal of bone and joint surgery. American volume, 2018. 100(16): p. e109-e109.
4. Lu, H.H. and S. Thomopoulos, Functional Attachment of Soft Tissues to Bone: Development, Healing, and Tissue Engineering. Annual Review of Biomedical Engineering, 2013. 15(1): p. 201-226.
5. Nawata, K., et al., Development of the attachment zones in the rat anterior cruciate ligament: changes in the distributions of proliferating cells and fibrillar collagens during postnatal growth. 2002(0736-0266 (Print)).
6. Bunker, D.L., et al., Tendon to bone healing and its implications for surgery. Muscles Ligaments Tendons J, 2014(2240-4554 (Print)): p. 343-50.
7. Klinger, H.M., et al., Biomechanical evaluation of rotator cuff repairs in a sheep model: suture anchors using arthroscopic Mason-Allen stitches compared with transosseous sutures using traditional modified Mason-Allen stitches. 2008(0268-0033 (Print)).
8. Moffat, K.L., et al., Orthopedic Interface Tissue Engineering for the Biological Fixation of Soft Tissue Grafts. Clinics in Sports Medicine, 2009. 28(1): p. 157-176.
9. Bonnin, M., S. Lustig, and D. Huten, Extensor tendon ruptures after total knee arthroplasty. Orthopaedics & Traumatology: Surgery & Research, 2016. 102(1, Supplement): p. S21-S31.
10. O'Brien, E.J., et al., Heterotopic mineralization (ossification or calcification) in tendinopathy or following surgical tendon trauma. Int J Exp Pathol., 2012(1365-2613 (Electronic)): p. 319-331.
11. Zhang, K., et al., Tendon mineralization is progressive and associated with deterioration of tendon biomechanical properties, and requires BMP-Smad signaling in the mouse Achilles tendon injury model. Matrix Biol., 2016(1569-1802 (Electronic)): p. Matrix Biol.
12. Hayashi, K., et al., Repair process after fibrocartilaginous enthesis drilling: histological study in a rabbit model. Journal of Orthopaedic Science, 2009. 14(1): p. 76-84.
13. Majewski, M., et al., Improved tendon healing using bFGF, BMP-12 and TGFβ1 in a rat model. European cells & materials, 2018. 35: p. 318-334.
14. Ateschrang, A., K. Gratzer C Fau - Weise, and K. Weise, Incidence and effect of calcifications after open-augmented Achilles tendon repair. Arch Orthop Trauma Surg, 2008(1434-3916 (Electronic)): p. 1087-92.
15. Järvelä, T., et al., Ultrasonographic and power Doppler evaluation of the patellar tendon ten years after harvesting its central third for reconstruction of the anterior cruciate ligament: comparison of patients without or with anterior knee pain. Am J Sports Med., 2004. 32(1)(0363-5465 (Print)): p. 39-46.
16. Su, W., et al., Promoting tendon to bone integration using graphene oxide-doped electrospun poly(lactic-co-glycolic acid) nanofibrous membrane. International journal of nanomedicine, 2019. 14: p. 1835-1847.

17. Patel, S., et al., Integrating soft and hard tissues via interface tissue engineering. J Orthop Res, 2018. 36(4)(1554-527X (Electronic)): p. 1069-1077.
18. Teh, T.K., J.C.H. Toh Sl Fau - Goh, and J.C. Goh, Aligned hybrid silk scaffold for enhanced differentiation of mesenchymal stem cells into ligament fibroblasts. 2011(1937-3392 (Electronic)).
19. Spalazzi, J.P., et al., In vivo evaluation of a multiphased scaffold designed for orthopaedic interface tissue engineering and soft tissue-to-bone integration. 2008(1552-4965 (Electronic)).
20. Spalazzi, J.P., et al., Mechanoactive scaffold induces tendon remodeling and expression of fibrocartilage markers. Clin Orthop Relat Res, 2008. 466(8)(1528-1132 (Electronic)): p. 1938-48.
21. Jeon, O., et al., Enhancement of ectopic bone formation by bone morphogenetic protein-2 released from a heparin-conjugated poly(L-lactic-co-glycolic acid) scaffold. Biomaterials, 2007. 28(17): p. 2763-71.
22. Patterson, J., et al., Hyaluronic acid hydrogels with controlled degradation properties for oriented bone regeneration. Biomaterials, 2010. 31(26): p. 6772-81.
23. Font Tellado, S., et al., Fabrication and Characterization of Biphasic Silk Fibroin Scaffolds for Tendon/Ligament-to-Bone Tissue Engineering. Tissue Eng Part A, 2017. 23(1937-335X (Electronic)): p. 859-872.
24. Spalazzi, J.P., et al., Development of controlled matrix heterogeneity on a triphasic scaffold for orthopedic interface tissue engineering. 2006(1076-3279 (Print)).
25. Caliari, S.R. and B.A. Harley, Structural and biochemical modification of a collagen scaffold to selectively enhance MSC tenogenic, chondrogenic, and osteogenic differentiation. Adv Healthc Mater, 2014. 3(7): p. 1086-96.
26. Qu, D., et al., Engineering complex orthopaedic tissues via strategic biomimicry. Ann Biomed Eng, 2015. 43(3): p. 697-717.
27. Criscenti, G., et al., Triphasic scaffolds for the regeneration of the bone–ligament interface. Biofabrication, 2016. 8(1): p. 015009.
28. Li, T., et al., Fabrication, mechanical property and in vitro evaluation of poly (L-lactic acid-co-ε-caprolactone) core-shell nanofiber scaffold for tissue engineering. Journal of the Mechanical Behavior of Biomedical Materials, 2019. 98: p. 48-57.
29. Cao, Y., et al., Three-dimensional printed multiphasic scaffolds with stratified cell-laden gelatin methacrylate hydrogels for biomimetic tendon-to-bone interface engineering. Journal of Orthopaedic Translation, 2020. 23: p. 89-100.
30. Sensini, A. and L. Cristofolini, Biofabrication of Electrospun Scaffolds for the Regeneration of Tendons and Ligaments. Materials (Basel, Switzerland), 2018. 11(10): p. 1963.
31. Chainani, A., et al., Multilayered electrospun scaffolds for tendon tissue engineering. Tissue engineering. Part A, 2013. 19(23-24): p. 2594-2604.
32. Fotticchia, A., et al., Anisotropic cytocompatible electrospun scaffold for tendon tissue engineering elicits limited inflammatory response in vitro. Journal of Biomaterials Applications, 2018. 33(1): p. 127-139.
33. Nerurkar, N.L., et al., Dynamic culture enhances stem cell infiltration and modulates extracellular matrix production on aligned electrospun nanofibrous scaffolds. Acta Biomaterialia, 2011. 7(2): p. 485-491.
34. Lipner, J., et al., In Vivo Evaluation of Adipose-Derived Stromal Cells Delivered with a Nanofiber Scaffold for Tendon-to-Bone Repair. Tissue engineering. Part A, 2015. 21(21-22): p. 2766-2774.

35. Pugliese, E. and D. Zeugolis, Design Of Multilayer Collagen-Based Scaffolds For The Tendon To Bone Integration. Orthopaedic Proceedings, 2020. 102-B(SUPP_11): p. 34-34.
36. Font Tellado, S., et al., Heparin functionalization increases retention of TGF-β2 and GDF5 on biphasic silk fibroin scaffolds for tendon/ligament-to-bone tissue engineering. Acta Biomaterialia, 2018. 72: p. 150-166.
37. Li, G., et al., In vitro and in vivo study of additive manufactured porous Ti6Al4V scaffolds for repairing bone defects. Scientific Reports, 2016. 6(1): p. 34072.
38. Pugliese, E., S. Korntner, and D.I. Zeugolis, Multilayer Collagen-Based Scaffold As Delivery Vehicles Of Bioactive Molecules For The Bone-To-Tendon Interface Regeneration. Orthopaedic Proceedings, 2018. 100-B(SUPP_14): p. 97-97.
39. Zheng, C., et al., Autologous Freeze-Dried, Platelet-Rich Plasma Carrying Icariin Enhances Bone-Tendon Healing in a Rabbit Model. The American Journal of Sports Medicine, 2019. 47(8): p. 1964-1974.
40. Farokhi, M., et al., Silk fibroin scaffolds for common cartilage injuries: Possibilities for future clinical applications. European Polymer Journal, 2019. 115: p. 251-267.
41. Kasoju, N. and U. Bora, Silk Fibroin in Tissue Engineering. Advanced Healthcare Materials, 2012. 1(4): p. 393-412.
42. Mozdzen, L.C., et al., The Effect of Gradations in Mineral Content, Matrix Alignment, and Applied Strain on Human Mesenchymal Stem Cell Morphology within Collagen Biomaterials. Adv Healthc Mater, 2016. 5(14): p. 1731-9.
43. Mandal, B.B., et al., Multilayered silk scaffolds for meniscus tissue engineering. 2011(1878-5905 (Electronic)).
44. Quirk, N.P., et al., Effects of freeze-thaw on the biomechanical and structural properties of the rat Achilles tendon. Journal of Biomechanics, 2018. 81: p. 52-57.
45. Wieloch, P., et al., A cryo-jaw designed for in vitro tensile testing of the healing Achilles tendons in rats. Journal of Biomechanics, 2004. 37(11): p. 1719-1722.
46. Yee Lui, P.P., et al., Expression of chondro-osteogenic BMPs in ossified failed tendon healing model of tendinopathy. Journal of Orthopaedic Research, 2011. 29(6): p. 816-821.
47. Zhang, Q., et al., Heterotopic ossification of tendon and ligament. Journal of Cellular and Molecular Medicine, 2020. 24(10): p. 5428-5437.
48. Holwein, C., et al., No healing improvement after rotator cuff reconstruction augmented with an autologous periosteal flap. Knee Surgery, Sports Traumatology, Arthroscopy, 2019. 27(10): p. 3212-3221.
49. Sensini, A., et al., Tissue Engineering for the Insertions of Tendons and Ligaments: An Overview of Electrospun Biomaterials and Structures. Frontiers in Bioengineering and Biotechnology, 2021. 9: p. 98.
50. Ratcliffe, A., et al., Scaffolds for tendon and ligament repair and regeneration. Annals of biomedical engineering, 2015. 43(3): p. 819-831.
51. Xie, J., et al., "Aligned-to-random" nanofiber scaffolds for mimicking the structure of the tendon-to-bone insertion site. Nanoscale, 2010. 2(6): p. 923-926.
52. Nowlin, J., et al., Engineering the hard-soft tissue interface with random-to-aligned nanofiber scaffolds. Nanobiomedicine, 2018. 5: p. 1849543518803538-1849543518803538.
53. Calejo, I., et al., Enthesis Tissue Engineering: Biological Requirements Meet at the Interface. Tissue Engineering Part B: Reviews, 2019. 25(4): p. 330-356.
54. Apostolakos, J., et al., The enthesis: a review of the tendon-to-bone insertion. Muscles, ligaments and tendons journal, 2014. 4(3): p. 333-342.

55. Peffers, M.J., et al., Proteomic Analysis Reveals Age-related Changes in Tendon Matrix Composition, with Age- and Injury-specific Matrix Fragmentation*. Journal of Biological Chemistry, 2014. 289(37): p. 25867-25878.
56. Snedeker, J.G. and J. Foolen, Tendon injury and repair – A perspective on the basic mechanisms of tendon disease and future clinical therapy. Acta Biomaterialia, 2017. 63: p. 18-36.
57. Widmer, C., et al., Molecular basis for the action of the collagen-specific chaperone Hsp47/SERPINH1 and its structure-specific client recognition. Proceedings of the National Academy of Sciences, 2012. 109(33): p. 13243.
58. Oshiro, W., et al., Flexor tendon healing in the rat: a histologic and gene expression study. J Hand Surg Am, 2003(0363-5023 (Print)): p. 814-23.
59. Del Buono, A., et al., Metalloproteases and tendinopathy. Muscles, ligaments and tendons journal, 2013. 3(1): p. 51-57.
60. Juneja, S.C., et al., Cellular and Molecular Factors in Flexor Tendon Repair and Adhesions: A Histological and Gene Expression Analysis. Connective Tissue Research, 2013. 54(3): p. 218-226.
61. Berendsen, A.D., et al., Biglycan modulates angiogenesis and bone formation during fracture healing. Matrix biology: journal of the International Society for Matrix Biology, 2014. 35: p. 223-231.
62. Kram, V., et al., Biglycan in the Skeleton. Journal of Histochemistry & Cytochemistry, 2020: p. 0022155420937371.
63. S., C., C. A., and B. A.K., Role of BMP1/Tolloid like Proteases in Bone Morphogenesis and Tissue Remodeling, in Proteases in Physiology and Pathology, D.N. Chakraborti S., Editor. 2017, Springer, Singapore.

CHAPTER 5

# MiRNAs as Potential Regulators of Enthesis Healing: Findings in a Rodent Injury Model

C. J. Peniche Silva, R. E. De La Vega, J. Panos, V. Joris,
C. H. Evans, E. R. Balmayor, M. van Griensven

*International Journal of Molecular Science, Vol. 24, 2023*

## ABSTRACT

MicroRNAs (miRNAs) are short non-coding RNA sequences with the ability to inhibit the expression of a target mRNA at the post-transcriptional level, acting as modulators of both the degenerative and regenerative processes. Therefore, these molecules constitute a potential source of novel therapeutic tools. In this study, we investigated the miRNA expression profile that presented in enthesis tissue upon injury. For this, a rodent enthesis injury model was developed by creating a defect at a rat's patellar enthesis. Following injury, explants were collected on days 1 ($n$ = 10) and 10 ($n$ = 10). Contra lateral samples ($n$ = 10) were harvested to be used for normalization. The expression of miRNAs was investigated using a "Fibrosis" pathway-focused miScript qPCR array. Later, target prediction for the aberrantly expressed miRNAs was performed by means of the Ingenuity Pathway Analysis, and the expression of mRNA targets relevant for enthesis healing was confirmed using qPCRs. Additionally, the protein expression levels of collagens I, II, III, and X were investigated using Western blotting. The mRNA expression pattern of *Egr1*, *Col2a1*, *Runx2*, *Smad1*, and *Smad3* in the injured samples indicated their possible regulation by their respective targeting miRNA, which included miR-16, -17, -100, -124, -133a, -155 and -182. Furthermore, the protein levels of collagens I and II were reduced directly after the injury (i.e., day 1) and increased 10 days post-injury, while collagens III and X showed the opposite pattern of expression.

## 1 INTRODUCTION

The enthesis is a complex interphase tissue, connecting tendons and ligaments to bones. It presents the opposite gradients of cellular composition, collagen alignment, and mineralization that are necessary for stress dissipation at the tendon-to-bone attachment site [1–3]. However, the complexity of the tissue makes the enthesis a highly challenging subject of study for tissue engineers.

Due to the physiology of the enthesis, this tissue is susceptible to sport-related injuries, overuse, and degeneration [4–7]. Upon injury, the healing process that is triggered at the enthesis usually yields scar tissue that resembles neither the morphology nor the mechanical properties of the native enthesis, increasing the risk of recurrent injury [1,8–10]. Hence, the development of effective tissue-engineering strategies to aid the regeneration and healing of injured entheses constitutes an unmet need [4].

To address this challenge, we aimed to characterize the early stages of healing in a rat's injured patellar enthesis by focusing on the expression patterns of a set of fibrosis-related microRNAs (miRNAs).



MiRNAs are a highly interesting class of molecules. They are short, non-coding RNA sequences, usually 21–25 nucleotides in length and possessing the ability to target specific mRNA molecules [11–13]. MiRNAs are generally complementary to the 3'-UTR region of their mRNA target, where they bind, terminating translation, and thus repress protein synthesis [12]. MiRNAs exhibit diverse expression patterns, intervening in many developmental and physiological processes [13]. Additionally, an individual miRNA can have several mRNA targets, while one mRNA target can be regulated by several miRNAs [14]. Hence, a single miRNA can participate in the regulation of several biological processes.

Since the first miRNA, lin-4, was described in 1993, over two thousand new miRNAs have been identified [15,16]. In 2016, 60% of all human protein-coding genes were estimated to be post-transcriptionally regulated by miRNAs [16]. Furthermore, several miRNAs have been identified to play key roles in cancer, liver, heart, and musculoskeletal diseases, among other conditions [14,17–20].

More recently, the inhibitory effect of miRNAs on their mRNA targets has inspired the use of miRNA mimics and inhibitors to specifically tailor their regulatory effects to different pathways. In the field of cancer research, miRNA replacement therapy aims to increase or restore the expression of tumor-suppressing miRNAs that might be downregulated or deleted in cancer cells, while miRNA reduction therapy aims to decrease or inhibit the expression of oncogenic miRNAs [21–23].

A similar strategy is being followed to fight alcohol-associated liver disease, fatty liver, and drug-induced liver injury using miRNA mimics or inhibitors, depending on the desired effect over the expressing miRNA [24,25].

In the field of musculoskeletal research, recent reports indicate that miRNAs can also be used as epigenetic regulators to improve the process of healing injured tendons and cartilage, as well as to aid in the process of bone healing and remodeling upon fracture [19,26–29]. Among other roles, miR-29a has been reported to regulate the in vitro expression of collagen III in fibroblasts from patients with systemic sclerosis [30]. Consequently, the treatment of injured tendons in a horse model with a miR-29a mimic showed improved early tendon healing by reducing collagen III transcript levels without affecting the expression levels of collagen I [28]. In an osteoarthritic cartilage model, in vitro transfection of chondrocytes with a miR-148a precursor decreased the expression of collagen X while increasing the expression of collagen II, which indicated the potential therapeutic use of this miRNA to modulate hypertrophic differentiation within these cells [29]. Additionally, in patients with traumatic brain injury and concomitant fractures, injection of miR-26a mimics at the fracture site led to increased bone formation, possibly through regulation of the phosphatase and tensin homolog deleted on chromosome 10 (*PTEN*) [31].

The occurrence of fibrosis, scar formation, and tendon adhesion during the healing of injured tendon has been previously linked to the overexpression or inhibition of specific miRNAs [32]. Especially relevant for fibrosis and tendon adhesion are those miRNAs capable of regulating the TGFβ signaling pathway in tenocytes and fibroblasts [32,33]. The TGFβ pathway is key for tendon development. However, the overactivation of such pathway leads to fibrosis and tendon adhesion [33]. Two well-known examples of miRNAs that regulate the TGFβ signaling pathway are miR-21-5p and miR-29b. While miR-21-5p activates the TGFβ-1 pathway by inhibiting *SMAD7* in tenocytes and fibroblasts, miR-29b inhibits the same pathway by targeting *SMAD3* [34,35]. Yet, in the context of the tendon-to-bone enthesis, little is known about the role of fibrosis-related miRNAs during either the healing process or scar formation after injury.

By investigating the pattern expression of fibrosis-related miRNAs upon injury in an enthesis animal model, we aimed to identify miRNAs with therapeutic potential that might aid the process of enthesis regeneration and healing.

## 2 MATERIALS AND METHODS

### 2.1 Rat Patellar Model

A partial enthesis injury animal model was developed for the purpose of this study. All animal procedures were approved by the Mayo Clinic Institutional Animal Care and Use Committee (protocol #A00006605-22).

Twenty male Fischer 344 rats (Charles River Laboratories, Wilmington, MA, USA) at 16 weeks of age were used. Animals were anesthetized with isoflurane (Piramal Critical Care, Talangana, India) in an induction chamber and had the fur on their right hindlimb shaved and cleaned with povidone iodine (Professional Disposables Internationals, Orangeburg, NY, USA) and 70% ethanol. All animals received a single dose of subcutaneous cefazolin (50 mg/kg; antibiotic (Pharmaceuticals, Columbus, OH, USA) and slow-release buprenorphine (1 mg/kg; for analgesia (Zoopharma, Laramie, WY, USA) prior to surgery. Animals were then placed on the surgical table in the dorsal recumbency position and the right hindlimb was left exposed using a sterile fenestrated drape. All rats received a unilateral, partial patellar enthesis injury in their right limb, and their left patellar enthesis was used as native control. A 5 mm medial parapatellar incision was swiftly created on the right knee, using a #15 scalpel blade. The patellar enthesis was exposed and a 2 mm injury was created on the medial aspect using a #11 scalpel blade in the axial plane. The skin was then closed using one 9 mm wound clip and the animal was transferred to a heated recovery chamber, set at 32°C. Once the animal recovered from anesthesia, it was transferred to its cage where it was allowed to bear weight and access to food and water ad libitum.



At the day 1 and day 10 (n = 10 respectively) time points, the animals were euthanized using an automated $CO_2$ delivery system. The injured and contralateral patellar enthesis were then harvested for analysis. The knee joint was accessed above the patella and the anterior cruciate ligament tendon was then cut, allowing for anterior displacement of the tibia. A coronal cut was created on the tibial plateau, posterior to the enthesis, and an axial cut on the metaphysis, distal to the tibial tuberosity using a rotary saw blade. Samples undergoing histological analysis were immediately processed. Samples undergoing PCR analysis were placed in 5 mL of RNAlater (Invitrogen, Waltham, MA, USA) and subsequently trimmed closer to the enthesis.

### 2.2 Sample Preparation and RNA Extraction

Samples from the injured patellar entheses tissue from both time points of observation (n = 5 per time point), in addition to the contralateral/native tissues (n = 5), were recovered from RNAlater, snap-frozen in liquid nitrogen, and homogenized with steel beads in the presence of TRIzol (SigmaAldrich,

Saint Louis, MO, USA) using a TissueLyser II set to cycles of 3 min at 30 Hz (Qiagen GmbH, Hilden, Germany). The isolation of the total RNA was performed following the well-established phenol-chloroform extraction protocol. The concentration and purity of the extracted RNA were measured using a NanoDrop spectrophotometer (NanoDrop Tech. Inc., Greenville, SC, USA). In every case, the ratios 260/230 and 260/280 were found to be ≥1.8.

### 2.3 cDNA Synthesis and PCR Array for miRNA Expression

The extracted total RNA was the starting material for the cDNA synthesis reactions. Then, cDNA synthesis was performed using the miScript II RT Kit (Qiagen GmbH, Hilden, Germany) in a C1000 Touch Thermal Cycler (Eppendorf AG, Hamburg, Germany) following the instructions from the manufacturer. To ensure the PCR quantification of mature miRNAs only, the cDNA synthesis mix was prepared using the miScript HiSpec buffer. Afterwards, cDNA samples from native tissue taken from both time points were pooled and used as the template for the qPCR array. The qPCR array was performed in a CFX 96 Real-Time System thermocycler (Bio-Rad, Hercules, CA, USA) utilizing a Fibrosis-Pathway focused miScript qPCR array (MIRN-117Z) and the miScript SYBER® Green PCR (Qiagen GmbH, Hilden, Germany).

Following Qiagen's instructions, the obtained Ct values from the qPCR array were exported to an Excel file and uploaded to Qiagen's data analysis web portal http://www.qiagen.com/geneglobe, accessed on 13 July 2022. Samples were assigned to both control (native tissue) and test groups (injury 1 day, injury 10 days). The Ct values were normalized against the arithmetic mean of the Ct values from the reference genes included in the array (i.e., Snord61, Snord68, Snord72, Snord95, Snord96A, Rnu6-6p). For each time point of observation, the fold regulation (FR) of each miRNA was calculated with respect to the native tissue, following the $2^{(-\Delta\Delta Ct)}$ method for fold change. Treated data have been displayed as fold regulation (FR), as this facilitates the interpretation of the results. FR is the same as fold change (FC) when FC ≥ 1, and FR is the inverse negative of the FC when FC < 1.

Additionally, qPCR was performed on the individual enthesis samples for the relevant miRNAs that were shown to be dysregulated by the qPCR array. For this, the SYBR® Green-based PCR miScript Primer assay for each respective miRNA to validate was used (Qiagen GmbH, Hilden, Germany) and the expression was normalized against the reference miRNA Snord68.

### 2.4 cDNA Synthesis and PCR for mRNA Expression

Total RNA was used as starting material for the cDNA synthesis reaction using the iScriptTM cDNA synthesis kit (Bio-Rad, Hercules, CA, USA) and the C1000 Touch Thermal Cycler. The qPCR reaction mix was prepared with the iQTM SYBR®

Green supermix (Bio-Rad, Hercules, CA, USA) following the manufacturer's instructions. A list of the primers used can be found in Table 2. Gene expression was normalized against the reference gene β-tubulin, and the fold regulation of the expression was calculated in the same manner as previously described.

**Table 2.** Primers used for the qPCR reactions for the mRNA targets.

| Targets | Forward 5′→3′ | Reverse 5′→3′ |
|---|---|---|
| *COL1A1* | TTTCCCCCAACCCTGGAAAC | CAGTGGGCAGAAAGGGACTT |
| *COL2A1* | CACGCCTTCCCATTGTTGAC | AGATAGTTCCTGTCTCCGCCT |
| *COL3A1* | TGCAATGTGGGACCTGGTTT | GGGCAGTCTAGTGGCTCATC |
| *MKX* | GACGACGGCTGAAGAACACTG | CCTCTTCGTTCATGTGAGTTCTTGG |
| *RUNX2* | CAAGGAGGCCCTGGTGTTTA | AAGAGGCTGTTTGACGCCAT |
| *SMAD1* | CAATAGAGGAGATGTTCAAGCAGT | CAGACCGTGGTGGGATGAAA |
| *SMAD3* | CTGGTGCTGGGGTTAGGTCA | GGCCATCCAGGGACTCAAAC |
| *EGR1* | GCACCCACCTTTCCTACTCC | GTGTAAGCTCATCCGAGCGA |
| *ANKH* | CTGGTGGGATGTGCCTCAAT | GACCGTGTTGTTCGTGTTGG |
| *TUBB* | GAGGGCGAGGACGAGGCTTA | TCTAACAGAGGCAAAACTGAGCACC |

## 2.5 Ingenuity Pathway Analysis

The identities of those miRNAs dysregulated by more than twofold in the injured samples (compared to the native tissue) were uploaded to the Ingenuity Pathway Analysis software v012004 (IPA, Qiagen GmbH, Hilden, Germany). Then, the miRNA target filter tool was employed to select miRNAs with mRNA targets either known or predicted to be associated with diseases and/or functions relevant to enthesis healing or injury. The filter parameters used were (i) species/tissue: rat/tendon or rat/cartilage, (ii) cell type: tenocyte, chondrocyte, or osteoblast, (iii) confidence: experimentally observed or highly predicted, and (iv) diseases and functions: tendon tissue or cartilage tissue.

In addition to the target prediction from the IPA software v012004, we performed extensive literature research to identify targets that were not yet included in the IPA knowledge database.

## 2.6 Protein Purification and Western Blots

After total RNA extraction with the TRIzol reagent, the fraction of total protein was isolated and solubilized following a standard chloroform/isopropanol/guanidine hydrochloride extraction protocol [71]. RNA and DNA were swiftly extracted, and isopropanol (SigmaAldrich, Saint Louis, MO, USA) was added to the sample to precipitate the proteins. After centrifugation, the pellet was washed in guanidine hydrochloride 0.3 M (SigmaAldrich, Saint Louis, MO,

USA), followed by a final wash with ethanol. After air-drying, the pellet was resuspended in SDS 1% (SigmaAldrich, Saint Louis, MO, USA ). For Western blotting, the total protein content was quantified using the bicinchoninic acid (BCA) method, utilizing the PierceTM BCA kit (Thermo Fisher, Waltham, MA, USA), and 15 µg were loaded in each well of 8% bis-acrylamide gel. Electrophoresis was performed in a running buffer (Tris, SDS, Glycine) for 60 min at 120 V. After separation, proteins were transferred on a nitrocellulose membrane using transfer buffer (Tris-base, glycine, SDS, methanol) under 350 mA for 90 min. Ponceau S staining (SigmaAldrich, Saint Louis, MO, USA ) was performed and membranes were then blocked for 60 min at room temperature in a solution of 5% non-fat dry milk (Merck KGaA, Darmstadt, Germany), diluted in Tris Buffer Saline supplemented with 0.1% Tween20 (TBST (Merck KGaA, Darmstadt, Germany)). Primary antibodies used for immunodetection were incubated overnight at 4°C: collagen I (1/1000; ab270993), collagen II (1/2000; ab34712), collagen III (1/1000; ab6310), and collagen X (1/500; 2031501005). Primary antibodies for collagen I, collagen II, and collagen III were purchased from Abcam (Cambridge, UK), and anti-collagen X was purchased from Quartett (Berlin, Germany). After rinsing, the membranes were incubated with horseradish peroxidase (HRP)-conjugated secondary antibodies (1/3000) at room temperature for 60 min. All antibodies were diluted in TBST/milk 5%. The protein signal was developed using a Clarity Western ECL substrate (Bio-Rad, Hercules, CA, USA) and chemiluminescence was detected using Chemidoc technology (Bio-Rad, Hercules, CA, USA). The intensity of the band was then quantified using ImageJ software 1.53t (NIH, Bethesda, MD, USA) and normalized to total proteins (Ponceau S).

### 2.7 Histology

The histological characterization included safranin O, alcian blue, and Masson trichrome staining. Additionally, immunohistochemical staining (IHC) for collagen I and collagen II was performed.

The samples used for histology ($n$ = 5 per group) were fixed for 48 h using 4% paraformaldehyde (SigmaAldrich, St. Louis, MO, USA). Subsequently, the samples were rinsed with PBS (Thermo Fisher Scientific, Landsmeer, the Netherlands), and decalcified for 30 days using 10% buffered EDTA solution (SigmaAldrich, Saint Louis, MO, USA) with regular buffer exchange every two to three days. The endpoint of the decalcification was determined by X-ray.

After the decalcification, the samples were dehydrated in an increasingly concentrated ethanol series and embedded in paraffin. Samples were sectioned to 7 microns using a Leica RM 2165 microtome (Leica Biosystems, Nussloch, Germany).

Before each staining, the samples were rehydrated in descending strength ethanol series in combination with distilled water, after two changes of NeoClear-xylene substitute (Merck KGaA, Darmstadt, Germany).

For the safranin O staining, the rehydrated samples were incubated for 10 min with hematoxylin solution (Carl Roth GmbH, Karlsruhe, Germany), followed by 5 min staining with 0.1% fast green solution (SigmaAldrich, Saint Louis, MO, USA). Afterward, the samples were rinsed with 0.1% acetic acid, and further stained with 0.1% safranin O solution for 10 min (SigmaAldrich, Saint Louis, MO, USA). Thereafter, the samples were dehydrated in ascending ethanol series, cleared with NeoClear-xylene substitute, and mounted with UltraKit mounting media (Thermo Fisher Scientific, Landsmeer, The Netherlands). The Alcian blue staining was performed by incubating the rehydrated slides in a working solution of alcian blue at pH 2.5 (SigmaAldrich, Saint Louis, MO, USA) for 10 min, followed by three washes with distilled water. Subsequently, samples were rehydrated, cleared, and mounted as described above.

For the Masson trichrome staining, the Trichrome Stain (Masson) kit was purchased from SigmaAldrich (Saint Louis, MO, USA). The staining was performed following the indications from the manufacturer. Briefly, the samples were incubated for 15 min in preheated Bouin's Solution at 56°C. Later, the slides were washed in tap water to remove the yellow color from the section. Consequently, the slides were stained for 5 min in hematoxylin solution (Carl Roth GmbH, Karlsruhe, Germany), washed in running tap water for 5 min, stained in Biebrich scarlet-acid fuchsin for 5 min, and rinsed with deionized water. Finally, the slides were placed in a working phosphotungstic/phosphomolybdic acid solution for 5 min, followed by a 5 min incubation in aniline blue solution, and a 2 min incubation with 1% acetic acid. Once the protocol was completed, the samples were rehydrated, cleared, and mounted as described above.

For the IHC staining, the primary and secondary antibodies (Table 3) and DAPI counterstaining were purchased from Abcam (Cambridge, UK).

**Table 3.** List of antibodies and working dilutions used in IHC.

| Name | Abcam ID | Working dilution |
|---|---|---|
| Anti-collagen type I | ab270993 | 1:250 |
| Anti-collagen type II | ab34712 | 1:50 |
| Rabbit IgG isotype control | ab172730 | 1:50 |
| Alexa Fluor 647 Goat anti Rabbit | ab190565 | 1:500 |

Antigen retrieval was conducted using 10 mM citrate buffer (pH 6 (Abcam, Cambridge, UK) for 10 min at 95°C. Subsequently, blocking was carried out by incubating the samples with blocking solution (0.1% Triton, 1% BSA, 5% goat serum) (SigmaAldrich, Saint Louis, MO, USA) for 1 h at room temperature. Afterward, the slides were placed in a humidity chamber and incubated overnight at 4°C, with the primary antibody diluted in blocking solution without goat serum. This was followed by incubation with the secondary antibody for 2 h at room temperature. Finally, counterstaining with DAPI was performed and the slides were mounted with Dako fluorescent mounting media (Agilent Technology, Santa Clara, CA, USA).

The stained slides were visualized using a Nikon DS-Ri2 camera mounted on a Nikon Ti Slide Scanner Microscope (Nikon Instruments Europe BV, Amsterdam, The Netherlands).

Histology images of the native tissue and the injured tissue corresponding to time point 10 days were uploaded to Image J v1.53p (NIH, Bethesda, MD, USA) The width of the tendon was measured in the samples using the measurement tool of Image J. The measurements were imported into GraphPad Prism 8.0 (GraphPad Software, San Diego, CA, USA). Statistically significant differences were determined by an unpaired *t*-test with Welch's correction $p < 0.05$.

### 2.8 *In situ* Hybridization

For the *in situ* hybridization (ISH) experiments, the double-DIG miRCURRY LNA detection probe, miRCURRY ISH Buffer, and control probes were purchased from Qiagen (Qiagen GmbH, Hilden, Germany). The sheep anti-DIG-AP, sheep serum, NBT/BCIP ready-to-use tablets, levamisole hydrochloride, and the 30% BSA solution were purchased from Sigma-Aldrich (Saint Louis, MO, USA) and the ultrapure SSC 20× buffer was purchased from Thermo Fisher Scientific (Thermo Fisher Scientific Inc., Waltham, MA, USA). The hybridization protocol was conducted as recommended by Qiagen. All steps of the ISH experiments were conducted in RNase-free conditions, following the manufacturer's recommendations.

Briefly, the samples were deparaffinized and rehydrated in NeoClear-xylene substitute, descending serial dilutions of ethanol, and RNase-free distilled water (Qiagen GmbH, Hilden, Germany). Subsequently, proteinase K (SigmaAldrich, Saint Louis, MO, USA) was added to the slides, and the samples were incubated for 10 min at 37°C using a Dako hybridizer (DAKO Colorado, Inc., Fort Collins, CO, USA). Afterward, the slides were washed twice with sterile PBS (Thermo Fisher Scientific Inc., Waltham, MA, USA) and incubated with the hybridization mix containing the detection probes or controls, respectively, for 60 min at 55°C in the Dako hybridizer. The hybridization probes were used the recommended

concentrations of 1 nM for the LNA U6 snRNA detection probe and 40 nM for the double-DIG miRNA and the scramble detection probes.

This hybridization step was followed by stringent washes with 5×, 1×, and 0.2× SSC buffer at 55°C. Blocking was performed for 15 min at room temperature before a 1 h incubation with the anti-DIG (dilution 1:800). The slides were then washed with PBS, and a freshly prepared AP substrate was added to the samples, which were then incubated for 2 h at 30°C in a humidity chamber. The AP reaction was stopped by incubating the samples two times for 5 min each with KTBT buffer (50 mM TrisHCl, 150 mM NaCl, 10 mM KCl). Subsequently, the samples were counterstained with fast green solution (Carl Roth GmbH, Karlsruhe, Germany) for 4 min, washed for 10 s with a 1% solution of acetic acid and water. Finally, the samples were dehydrated in an increasingly concentrated ethanol series before mounting with UltraKit mounting media (J.T. Baker, Leicestershire, UK). Images were taken with a Nikon DS-Ri2 camera, mounted on a Nikon Ti Slide Scanner Microscope (Nikon Europe B.V., Amstelveen, The Netherlands).



## 3 RESULTS

All the animals used in the study survived the surgical creation of the patellar injury and remained otherwise healthy until the collection of the explants.

### 3.1 miRNA Expression

The miRNA expression in samples harvested at days 1 and 10 after injury was assessed using a qPCR array. We observed that 1 day after the creation of the injury, 28 miRNAs were dysregulated over twofold more in comparison to their expression in the native tissue (Fig. 1). Of this total, six miRNAs were upregulated, and 22 miRNAs downregulated. Furthermore, at 10 days after enthesis injury, 52 miRNAs resulted in dysregulation beyond the twofold cut-off. Of these, only seven miRNAs were downregulated while 45 miRNAs were upregulated.

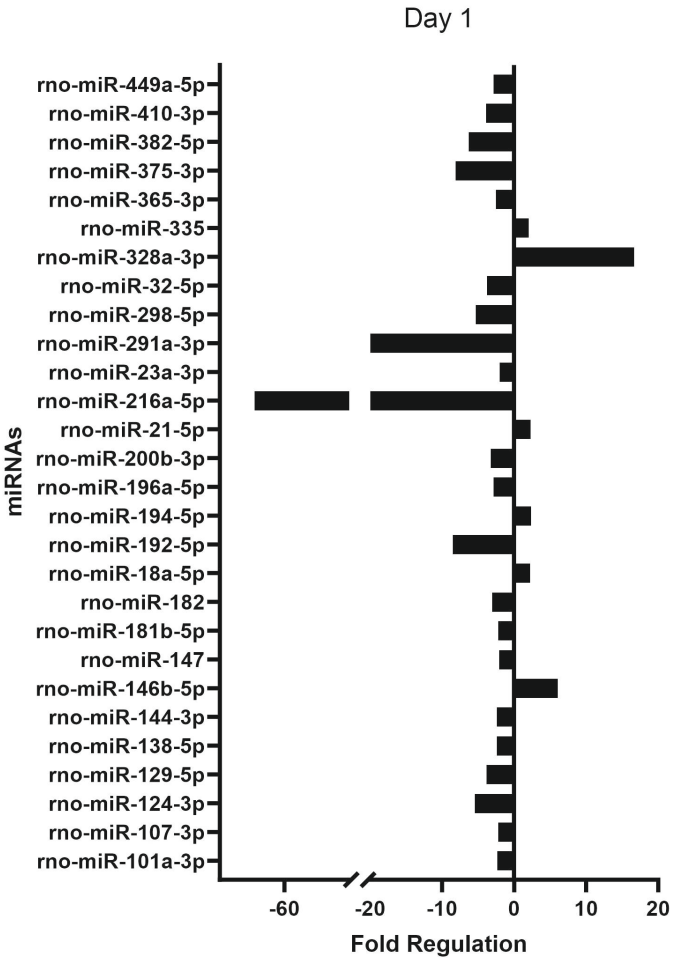
Day 1
rno-miR-449a-5p
rno-miR-410-3p
rno-miR-382-5p
rno-miR-375-3p
rno-miR-365-3p
rno-miR-335
rno-miR-328a-3p
rno-miR-32-5p
rno-miR-298-5p
rno-miR-291a-3p
rno-miR-23a-3p
rno-miR-216a-5p
rno-miR-21-5p
rno-miR-200b-3p
rno-miR-196a-5p
rno-miR-194-5p
rno-miR-192-5p
rno-miR-18a-5p
rno-miR-182
rno-miR-181b-5p
rno-miR-147
rno-miR-146b-5p
rno-miR-144-3p
rno-miR-138-5p
rno-miR-129-5p
rno-miR-124-3p
rno-miR-107-3p
rno-miR-101a-3p
miRNAs
-60
-20
-10
0
10
20
Fold Regulation

(a)

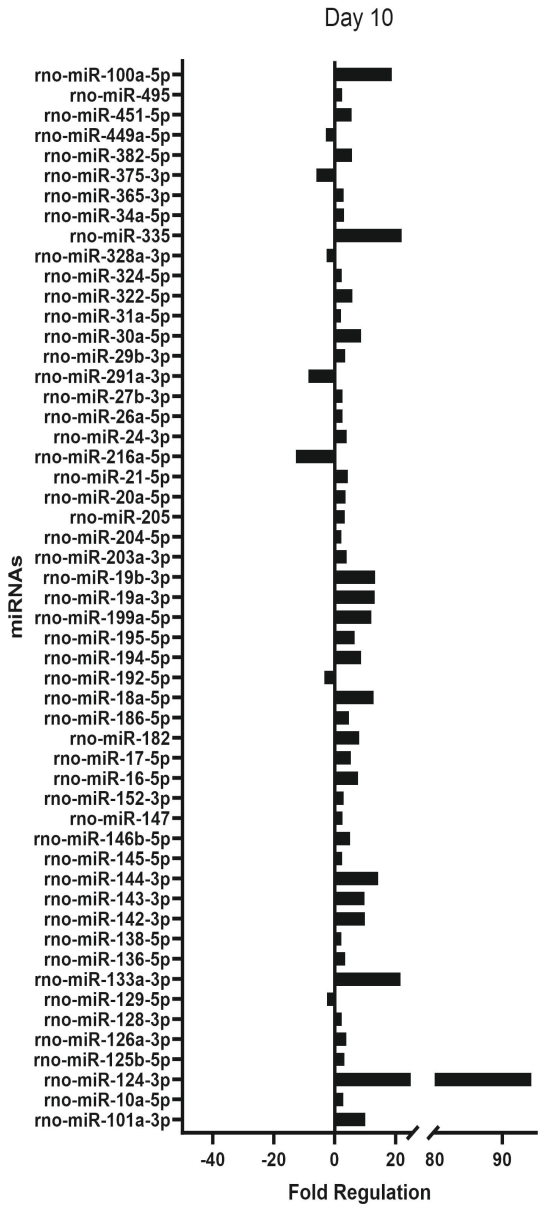


(**b**)

**Figure 1.** Dysregulated miRNAs following injury at (a) day 1, and (b) day 10, with respect to the expression in the native tissue.

The identities of all miRNAs found to be aberrantly regulated were uploaded to the Ingenuity Pathway Analysis (IPA) software v012004. Target prediction was conducted according to those gene networks of significance to enthesis-

associated pathways. Those miRNAs and respective mRNA targets that were associated with cartilage and tendon pathways were identified using the IPA software v012004, and are summarized in Fig. 2. In addition, we included in our analysis the interactions between miRNAs and mRNA targets that had been reported in the literature to be relevant for the regulation of tendon or cartilage pathways but which were not predicted by the IPA. These interactions between the miRNAs and respective mRNA targets are indicated in Fig. 2 with an asterisk (*). Given their importance in the context of enthesis injury and to subsequent healing, we have investigated the mRNA expression in the injured samples, as well as with the IPA-predicted mRNA targets.

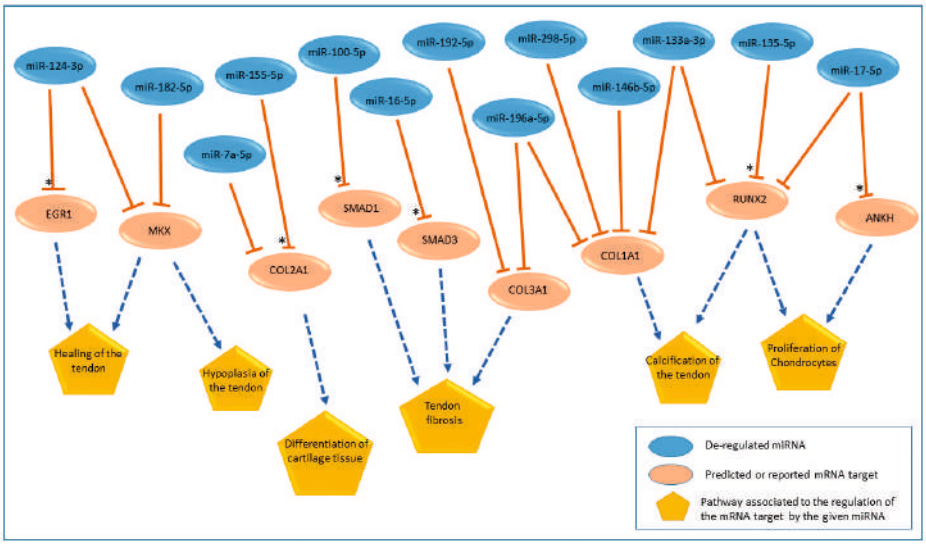


**Figure 2.** Schematic representation of the interactions between the aberrantly regulated miRNAs at early stages of healing on an enthesis injury in the rats' patella. The predicted and/or reported mRNA targets in the context of tendon- and cartilage-relevant pathways are indicated. The asterisk symbol (*) indicates interactions between the deregulated miRNAs and mRNA target genes found therein that had not been predicted by the IPA, but which have been reported in the literature as targets of the respective miRNA [36–40].

Results obtained by the miScript qPCR array were validated with qPCR in each individual sample, and for each investigated time of observation (Fig. 3). Of note, only aberrantly regulated miRNAs that were deemed relevant to enthesis injury according to the IPA analysis were selected for validation.

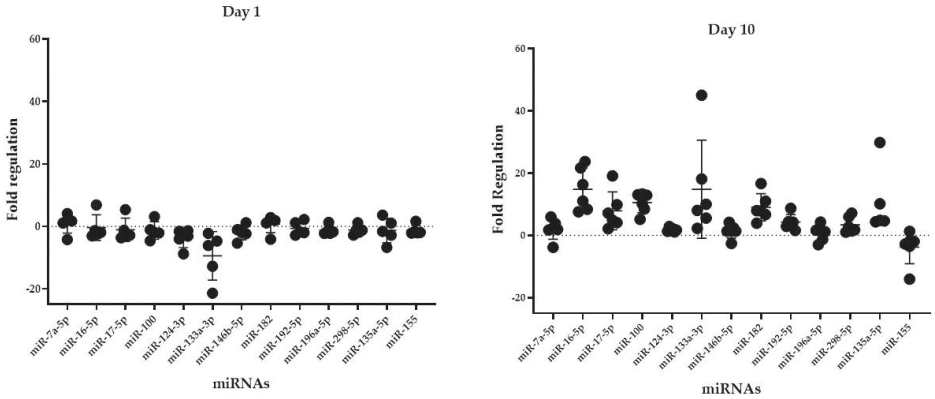


**Figure 3.** Fold regulation (Mean ± SD) of the expression of the deregulated miRNAs in the injured samples, with respect to the native tissue.

### 3.2 mRNA Expression

To investigate the potential effect of the dysregulated miRNAs in the injured samples, the expression levels of their enthesis-relevant mRNA targets were evaluated using qPCR in each sample at both time points after the injury (Fig. 4).

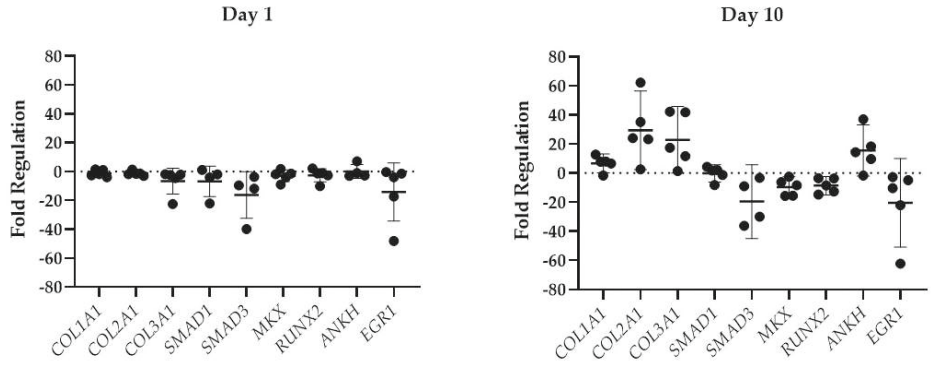


**Figure 4.** Fold regulation (Mean ± SD) of the expression of the targets mRNA in the injured samples with respect to the native tissue.

A downregulation was observed in the mRNA levels of *COL3A1*, *SMAD1*, *SMAD3*, *RUNX2*, *MKX*, and *EGR1* for the samples harvested 1 day following the enthesis injury. At day 10 following the injury, *RUNX2*, *MKX*, *SMAD3*, and *EGR1* remained downregulated beyond the two fold cut-off mark, while *COL1A1*, *COL2A1*, *COL3A1*, and *ANKH* showed increased levels of mRNA expression.

### 3.3 Western Blot

The protein expression levels of collagen I, collagen II, collagen III, and collagen X were investigated using the Western blot procedure. The results were normalized against total protein content and are depicted in Fig. 5. A decrease was observed in the presence of collagen I and collagen II, as was an increase in the protein-content of collagen III and collagen X immediately after enthesis injury (i.e., day 1). Interestingly, 10 days after enthesis injury, the opposite pattern of collagen content was observed, showing an increase in the amount of collagen I and collagen II, and a strong decrease in the amount of collagen III and collagen X (Fig. 6).

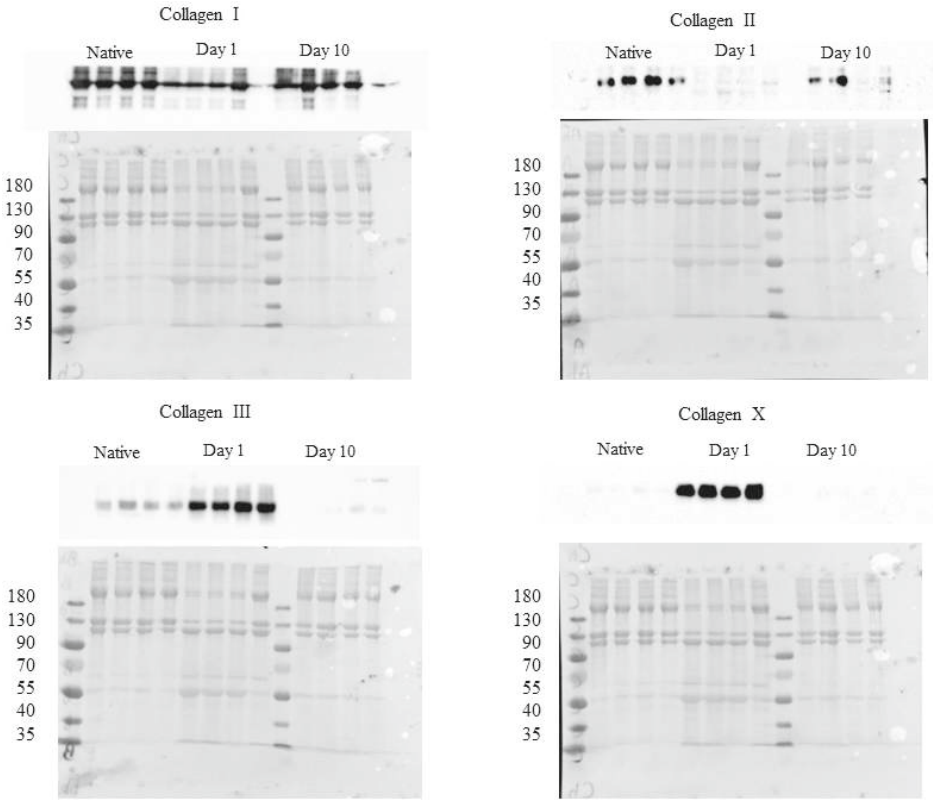


**Figure 5.** Western blot for proteins of the native tissue samples, with both injured tissue at 1 day and at 10 days following injury. Each lane corresponds to an individual sample. Normalized against total protein content.

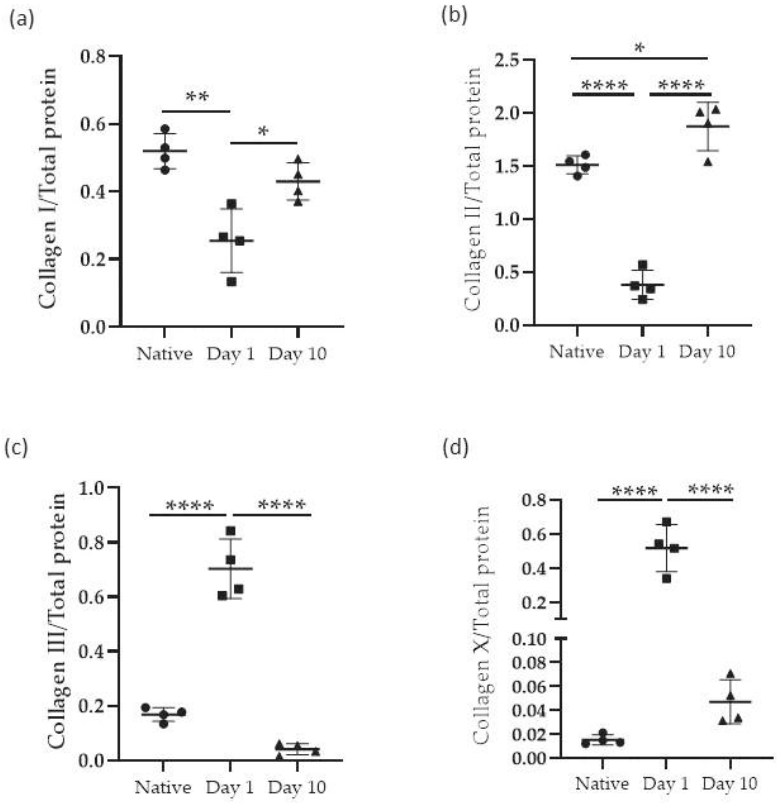


**Figure 6.** Protein expression of collagen I (a), collagen II (b), collagen III (c) and collagen X (d) normalized against total protein content. Results are illustrated for both the native and injured tissue samples at each time point of observation (Mean ± SD). Statistical significance is indicated by * $p < 0.05$, ** $p < 0.01$, and **** $p < 0.0001$.

## 3.4 Histology

### *3.4.1 Safranin O, Alcian Blue and Masson Trichrome Staining*

Samples from both the native tissue and the injured tissue were stained with safranin O, alcian blue, and Masson trichrome (Fig. 7). The intensity of the safranin O staining was proportional to the proteoglycan content of the cartilage tissue. In addition to proteoglycans, alcian blue also stains for mucopolysaccharides and glycoproteins. Masson trichrome stains collagen fibers and muscle. The staining of the samples harvested 1 day after the enthesis injury allowed us to visualize the extent of the injury at the enthesis site, while the observation of the stained samples harvested 10 days after the injury provided a great deal of information on the healing process of the enthesis, the occurrence of fibrosis, and the eventual ectopic ossification.

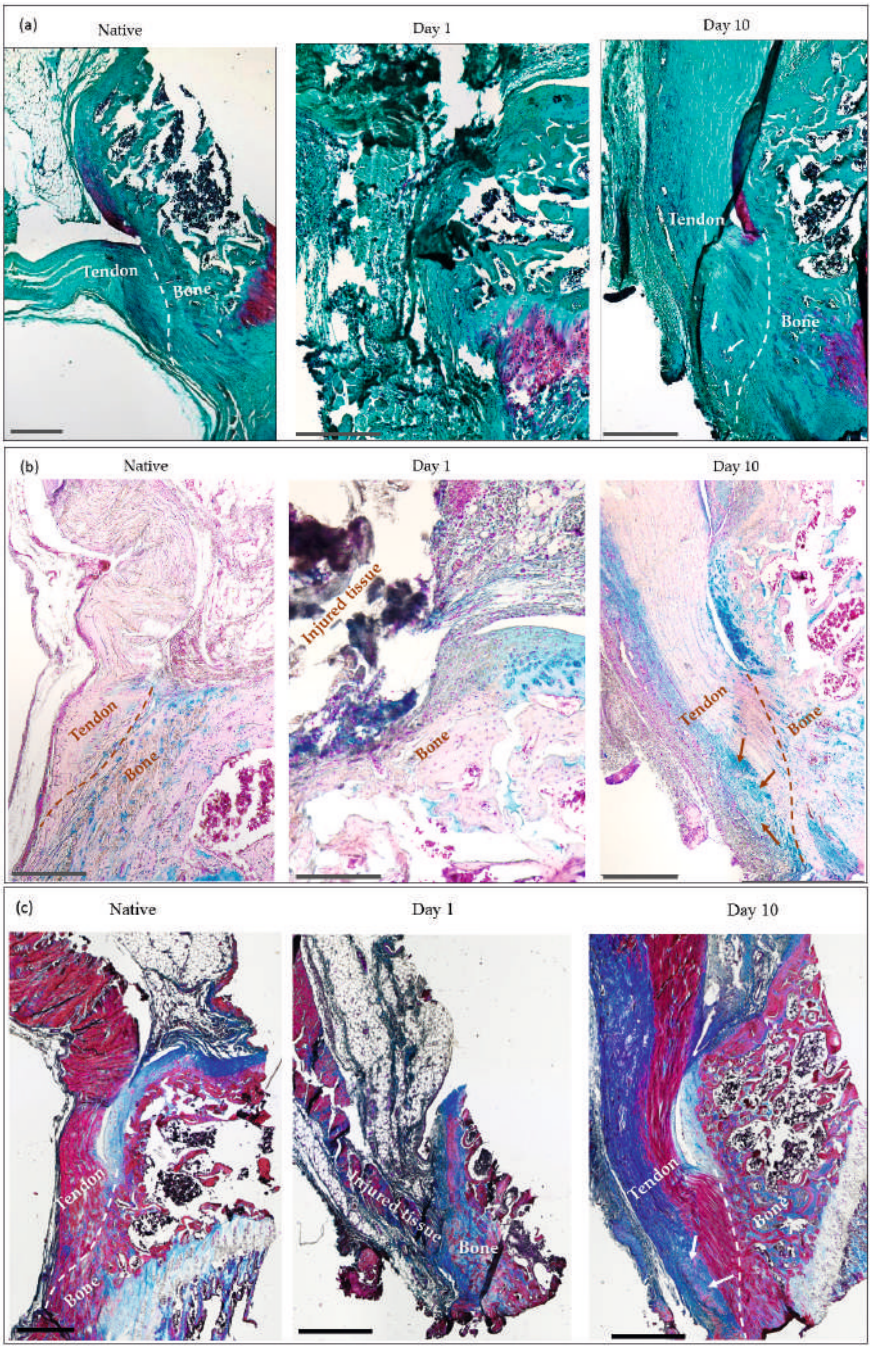


**Figure 7.** Safranin O (**a**), alcian blue (**b**) and Masson trichrome staining (**c**) of both native and injured samples (1 day and 10 days after the injury). Dashed lines indicate the tendon-to-bone interphase or enthesis. Arrows indicate ossification in the tendon side of the enthesis. Scale bar = 500 μm.

The safranin O staining of the samples harvested at 10 days after the injury revealed an enlarged tendon, with a clear distinction between a native-like tendon towards the medial part of the tendon and a fibrotic portion towards the lateral part of the tendon, which was positively stained for proteoglycans. In the fibrotic area, the collagen fibers showed poor alignment compared to the alignment present in the uninjured tissue (Fig. 7a). Proteoglycan was not observed in the native tendon tissue. Additionally, in the same group of samples (i.e., 10 days after enthesis injury) a dense area of extracellular matrix (ECM) was visible that resembled cartilage at the tendon side of the enthesis, whereas, in the native tissue, this area contained no cartilage but instead comprised the parallel aligned collagen fibers characteristic of the tendon tissue.

Similarly, the alcian blue and Masson trichrome staining of the samples harvested 10 days after the injury showed positive blue staining in the fibrotic portion of the injured tendon that was absent in the native, healthy tissue. This staining highlighted the area of disorganized collagen fibers which were rich in glycoproteins and noticeably different from the native tendon morphology (Fig. 7b). Additionally, Masson trichrome stained sections allowed us to confirm the occurrence of ectopic bone formation in the tendon side of the enthesis (Fig. 7c).



Measurements of the tendon width revealed that the samples corresponding to the injured tissue at 10 days suffered from a significant enlargement ($p < 0.05$) of the tendon when compared to the native tissue (Table 1). The measurement of the tendon width was not possible in the samples from 1 day after the injury due to the recent creation of the defect, which made a reproducible measurement of the tendon unfeasible.

**Table 1.** Tendon width (Mean + SD) of the native tissue and the injured tissue harvested at 10 days after enthesis injury.

| Samples | Tendon Width (μm) |
|---|---|
| Native tissue | 341.0 ± 78.4 |
| Injured tissue (time point: 10 days) | 807.6 ± 31.8 |

### *3.4.2 Immunohistochemistry*

Samples from the native and injured tissues were stained for collagen I and collagen II, which are two of the main structural collagens present at the tendon-to-bone enthesis. The native tissue samples showed a strong presence of collagen I at both the tendon and bony sides of the enthesis. The presence of collagen II in the healthy tendon was not verified by the corresponding staining at the tendon side of the enthesis, but rather only at the fibrocartilaginous portion of the enthesis (Fig. 8).

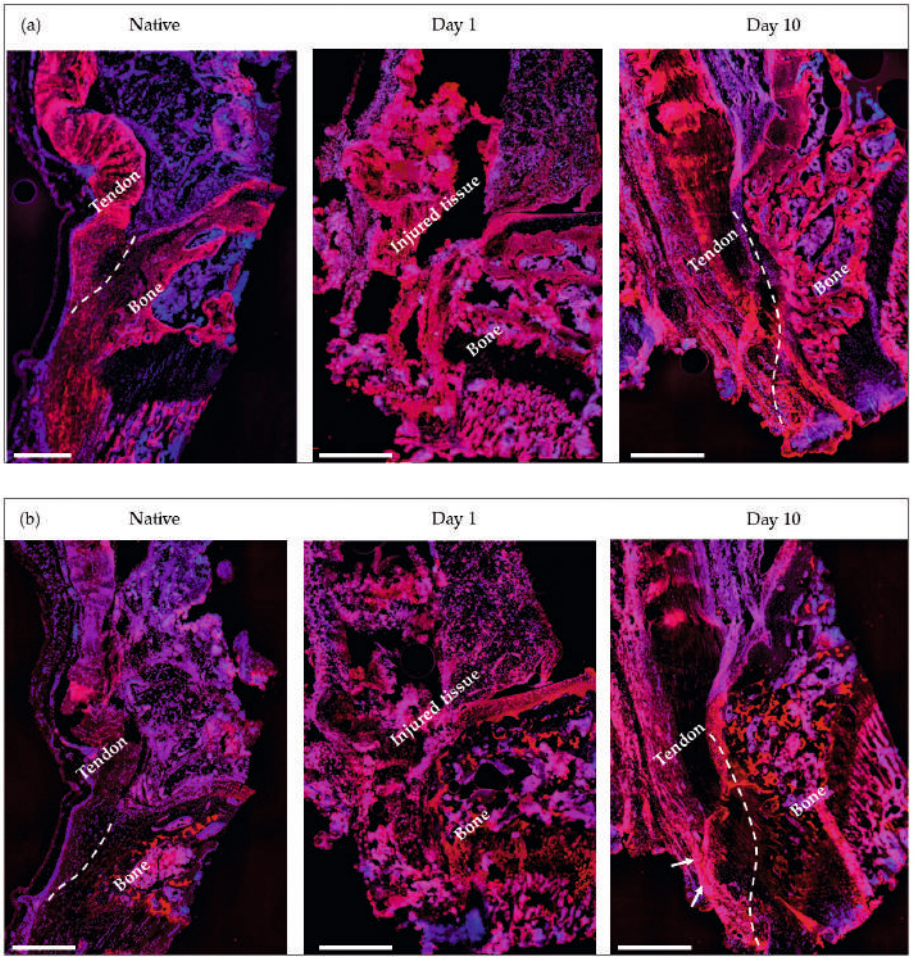


**Figure 8.** Collagen I (**a**) and collagen II (**b**) staining of native and injured tissue samples (1 day and 10 days after enthesis injury). Dashed lines indicate the tendon-to-bone interphase. Red = collagen, blue = DAPI. Arrows indicate ossification in the tendon side of the enthesis. Scale bar = 500 μm.

Injured samples harvested at day 1 after enthesis injury showed a similar pattern of collagen deposition to that described for the healthy tissue. However, there was a significant presence of recently damaged tissue in the tendon and tendon-to-bone interphase areas that made the identification of the histological features of these samples difficult. This was not the case in the injured samples harvested 10 days after enthesis injury; there, the distribution of collagen I was similar to that observed in the native tissue (that is, a strong presence of collagen I at both sides of the enthesis). Remarkably, intense collagen II staining was observed along the fibrotic portion of the tendon, as well as in the surroundings of the

abnormal bony structure previously identified in the tendon portion of the enthesis with the prior safranin O and Masson trichrome staining.

### 3.5 *In situ* Hybridization

*In situ* hybridization (ISH) was performed to visualize the tissue localization of previously identified miRNAs that were dysregulated in the injured enthesis samples. As recommended by the manufacturer, the ISH protocol was optimized using the U6 positive control probe, with a scrambled miRNA probe for a negative control. The use of a scrambled miRNA probe allowed us to confirm that no nonspecific interactions were present in our ISH experiments that could hinder the interpretation of our results.

Two relevant miRNAs were investigated (miR-16-5p and miR-133a-3p) in the native tissue samples, as well as in the sample harvested 10 days after the injury. In the native tissue, the expression of miR-16-5p could not be verified by the *in situ* hybridization. This was not the case for miR-133a-3p, which was localized mainly in the chondrocytes present at the growth plate of the tibia, while the expression in the tendon portion was barely noticeable except for some scattered positive cells in the tendon portion around 500 µm from the enthesis area. Conversely, in the samples from the injured tissue (10 days post-injury), the expression of both miRNAs was abundant in both the fibrotic portions of the tendon and the surroundings of the ectopic ossification area on the tendon side of the enthesis. The expression patterns in the injured samples of both miR-16-5p and miR-133a-3p highlighted a well-defined boundary that divided the tendon longitudinally in two halves along different morphologies and miRNA expression (Fig. 9).

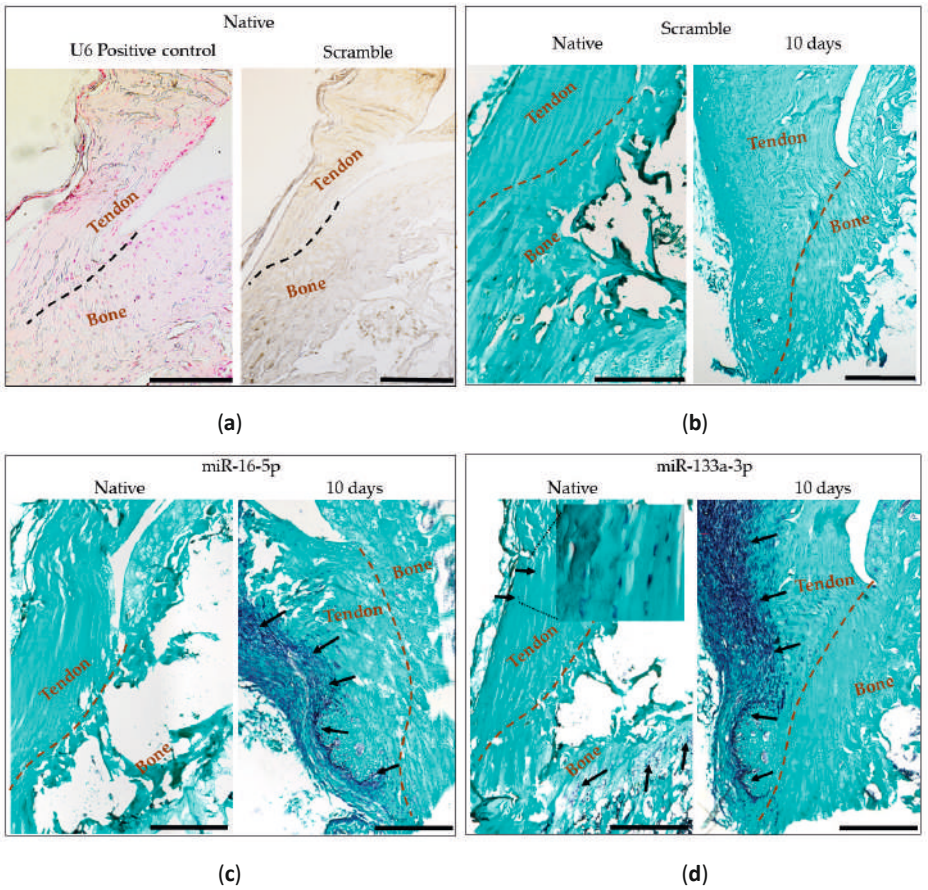


**Figure 9.** *In situ* hybridization. U6 positive control and scramble negative control in native tissue (**a**); Scramble negative control in native and injured tissue 10 days after injury (**b**); and miR-16-5p (**c**) and miR-133a-3p (**d**) in both native and injured tissue 10 days after the injury. Dashed lines indicate the tendon-to-bone interphase. Arrows indicate the presence of the corresponding miRNA: dark blue = miRNA expression, and light green = counterstaining with fast green. Scale bar = 500μm.

## 4 DISCUSSION

The tendon-to-bone enthesis is a frequent site of injury. It has been estimated that 30% of all musculoskeletal consultations are due to a form of tendon or enthesis injury [41,42]. Most tendon or enthesis injuries can heal without the need for clinical intervention. However, non-surgical treatment is usually followed by surgery, due to improper healing of the injured tendon or tendon-to-bone enthesis [43,44]. Hence, the need for current efforts to elucidate the underlying mechanisms of enthesis healing.

In a recently published review, Chartier *et al*. summarized the three overlapping steps involved in tendon healing: inflammation, proliferation, and remodeling [45]. These three steps take place while mediated by a balance of extrinsic and intrinsic mechanisms [46,47]. Extrinsic mechanisms are active in the early stages of healing. They involve the infiltration of inflammatory cells and fibroblasts from the surrounding tissue (e.g., synovium, tendon sheath, and paratenon), and are usually associated with an increase in collagen disorganization, high levels of glycosaminoglycans, and increased tendon diameter. The timeline for the intrinsic mechanism is usually delayed by a few days when compared to the extrinsic mechanism, comprising the migration of tenoblasts and tenocytes from within the tendon (mostly from the epitenon and endotenon) toward the wound site [45]. Collagen production by tenocytes and by the cells populating the epitenon usually yields more mature and larger collagen molecules than those produced by the cells migrating from the synovial sheath or the paratenon [48]. Thus, several authors have focused on the comparison between both mechanisms, aiming to answer the question of whether or not one of these two healing patterns might be enough for the adequate restoration of the healthy morphology and biomechanics of the tendon [48–50].



With our injury model, we were able to follow the progression of enthesis healing for up to 10 days after the injury. The observed enlargement of the tendon, the collagen disorganization, and the proteoglycan-positive staining in the fibrotic portion at 10 days are in line with the aforementioned characteristics of the extrinsic healing mechanism, which seemed to be predominant in this early stage of healing in our injury model [45,49,50]. Additionally, we observed that as a result of such a healing response, an area suffering from ectopic ossification was present in the tendon portion of the enthesis of the injured samples after 10 days. Both the positive collagen II staining and the presence of chondroid metaplasia surrounding the ossification area indicated that such ossification has an endochondral, rather than intramembranous, origin. These observations support the consensus that most of the ectopic ossification of tendons and tendon-to-bone occur by endochondral ossification [10,51,52].

The occurrence of ectopic ossification in both the tendon and the tendon-to-bone enthesis upon injury has been observed in human and animal models as an undesired effect of the failed regeneration of the native tissue structure [10,53]. Tendon ossification is associated with severe pain and an increased risk of rupture, and although it is commonly seen in clinics, it has been poorly characterized [52]. Some authors have associated the formation of ectopic ossification with the extrinsic migration of inflammatory cells (possibly those derived from bone marrow) to the site of the injury, although the precise mechanisms of ectopic ossification of the tendon and enthesis are far from understood [52,54].

In an attempt to shed light on the intricate mechanisms responsible for the occurrence of fibrosis and ectopic ossification of injured tendon-to-bone entheses, we investigated the expression profile of fibrosis-related miRNAs in the early stages of patellar enthesis healing. MiRNAs have drawn significant attention in recent years as being potential therapeutic targets, signaling mediators, and even biomarkers, due to their ability to regulate a multitude of pathways through their suppressing of expression of their target mRNAs [19,55,56]. Several reports indicate that among the most relevant miRNAs associated with early tendinopathy are the members of the miR-29 family [57–59]. It has been demonstrated that the members of this family act as post-transcriptional regulators of collagen, and that they are typically dysregulated upon tendon injury [57]. However, in our enthesis injury model, we only observed dysregulation of one member of this family, the miR-29b-3p, which showed a 3.4-fold increase at 10 days, whereas the expression of miR-29a-3p and miR-29c-3p was similar to that of the native tissue. In addition, miR-29b-3p has been reported to play a role in chondrocyte homeostasis and in repressing *SMAD3* signaling. In this regard, we observed that *SMAD3* was downregulated in the injured samples at both time points of observation. However, the suppression of this gene was strongest at 10 days, when the expression of the miR-29b-3p was the highest. This observation is also in line with the strong upregulation of the miR-16-5p at the same time point, which (similarly to miR-29b-3p) is known to target *SMAD3* in chondrocytes, one of the signature cell populations in the patellar enthesis [36,60]

Another set of interesting miRNAs that resulted in upregulated at 10 days but not at one day in our injured samples include miR-17-5p, miR-133a-3p, and miR-182. Both miR-17-5p and miR-133a-3p were predicted by our IPA analysis to target and inhibit *RUNX2*, which we found to be downregulated several-fold at 10 days. This prediction had been confirmed previously using luciferase reporter assays [40,61]. Moreover, a regulatory role for miR-17-5p in ectopic bone formation in ligaments has been described in patients of ankylosing spondylitis, wherein it targets and suppresses the ankylosis protein homolog (*ANKH*) and enhances the expression of *COL1A1* [40]. Furthermore, the stimulatory effect of miR-17-5p over the expression of *COL1A1* was also described in patients with non-traumatic osteonecrosis, as a consequence of the inhibition of *SMAD7* [62]. Interestingly, *ANKH* and *COL1A1* were upregulated in the day 10 samples in comparison to expression levels in the native tissue, while the protein expression level of collagen I at the later time point was similar to that of the native tissue, but significantly higher than the expression level observed one day after the injury.

When upregulated 10 days after the injury, miRNA-182 was predicted to target *MKX*, and resulted in downregulation in our samples of this timeframe. Different regulatory roles have been described for the miR-182, including cell growth,

cancer progression, lymphocyte expansion, and even positive regulation of osteoclastogenesis via the miR-182-PKR-IFN-β pathway [63]. However, to the extent of our knowledge, there is no published experimental evidence for the regulation of *MKX* through miR-182 targeting. Our observations might well serve as a possible indication of such interaction in an in vivo setting, worthy of further investigation.

Of all the miRNAs investigated using our injury model, miR-16-5p and miR-133-3p were two of the most dysregulated, showing downregulation immediately after the injury and strong upregulation at 10 days. These two miRNAs are highly interesting, and especially relevant for our injury model since both of them have been proven to act as anti-fibrotic regulators by inhibiting myofibroblast activation [64,65]. The origin of myofibroblasts during wound healing is unclear [66]. However, they play a critical role in matrix remodeling during healing and have been reported to be involved in the maintenance of scar tissue, whether by actively producing fibrotic ECM or by inhibiting the migration of other cell types [67]. The observed upregulation of these miRNAs (and the strong downregulation at the same time point) in the collagen III protein could well indicate that, after 10 days, the healing process of the injured enthesis has been redirected against fibrosis. This would also be in line with the observed downregulation of the miR-155, known to be a major profibrotic regulator in multiple tissues and pathologies, seen at the same time point [68,69].



Our *in situ* hybridization experiments revealed that the overexpression of both miR-16-5p and miR-133a-3p was specifically localized in the fibrotic portion of the injured tissue and in the area surrounding the site of ectopic ossification. This finding is particularly relevant when studying such a complex interphase tissue as the tendon-to-bone enthesis since it allows us to pinpoint the exact localization of the cell population responsible for the overexpression of such miRNAs. Our observations did not necessarily address the direct molecular consequences of the dysregulation of miR-16-5p and miR-133a-3p in the early healing response of the injured enthesis. However, the highly specific localization of the overexpression of these miRNAs did highlight a potential antifibrotic role in injured enthesis that has not been previously described. Additionally, such findings could serve as a stepping stone toward the development of potential therapeutic strategies, especially those that might rely on either the enhancement or the fine-tuning of the timing and duration of the overexpression of these antifibrotic miRNAs upon injury, owing to the fibrosis that we found to be strongly present in the injured tissue, based on its morphological appearance after 10 days.

With our study, we aimed to characterize a rat-based patellar injury model during the early stages of healing, paying special attention to the local miRNA expression profile. The enlargement of the tendon at the 10-day time point was

in line with the rapid increase in collagen III production immediately after the injury, followed by the later increase in collagen I and collagen II. The regulation of extracellular matrix production is a complex mechanism with multiple players, which include some of the miRNAs that we have investigated in our study [70]. The observed downregulation of miRNAs associated with the inhibition of collagen production (e.g., miR-124-3p and miR-133a-3p) immediately following injury could be connected with the increase in ECM deposition at the earlier recorded time points. Similarly, the upregulation of antifibrotic miRNAs at 10 days (e.g., miR-133a-3p and miR-16-5p), in addition to the normalization of the production of collagen I and collagen III, could mark the beginning of the remodeling phase of the enthesis healing process. However, a more in-depth study would be necessary to establish the precise roles of these microRNA in the process of enthesis healing.

Although the knowledge gained paves the way toward deeper insights into the healing mechanisms of the enthesis, our study is not exempt from limitations. We limited our time points of observation to 1 and 10 days after the injury. Adding a later time point could have been beneficial, to assess the evolution of the fibrosis and the ectopic ossification upon the upregulation of the antifibrotic miRNAs observed at the 10-day time point. Nonetheless, in a previous study, we investigated the healing of the enthesis after 4 and 12 weeks from creating a patellar defect [10]. The nontreated controls showed at both time points clear signs of fibrosis and ectopic bone formation in the tendon and enthesis area. This is evidence that scar formation and tendon ossification were neither effectively avoided nor reverted by the native mechanism of enthesis healing, including the overexpression of antifibrotic miRNAs observed in this study after 10 days. Another constraint is the limited selection of mRNA targets for the enthesis-relevant dysregulated miRNAs whose expression had been validated using qPCR in the injured samples. However, by using IPA analysis, we attempted to cover the most fibrotic-relevant predicted targets for our pool of dysregulated miRNAs. Future studies could focus on investigating the expression of other members of the multitude of potential mRNA targets of dysregulated miRNAs upon enthesis injury, in addition to investigating the validation of the miRNA–mRNA interactions.

## 5 CONCLUSIONS

Tendon and enthesis injuries are debilitating conditions that affect a growing number of people worldwide. Here, we have characterized the early healing response of an injured patellar enthesis in a rodent model. We described the occurrence of fibrotic scar tissue 10 days after the creation of the injury, in addition to the occurrence of ectopic ossification at the tendon-to-bone enthesis. Moreover, we reported the dysregulated expression of at least 13 enthesis-relevant miRNAs both 1 day and 10 days after the injury, whose predicted mRNA targets are known to play relevant roles in the process of enthesis healing and regeneration. Additionally, we were able to localize the expression of miR-16-5p and miR-133a-3p in the fibrotic portion of the injured tissue, which indicates a direct relationship between the overexpression of such miRNAs and the healing of the tendon-to-bone enthesis. We believe that the results described in the present manuscript could stimulate future studies to explore the therapeutic potential of such miRNAs by their ability to tune the expression of their mRNA targets, and thereby improve the regeneration of injured entheses.



## 6 ACKNOWLEDGMENTS

C.H.E.'s research is partly funded by the John and Posy Krehbiel Professorship in Orthopedics. The project 20-105 was supported by a grant from the ON Foundation, Switzerland. This work was supported by the Province of Limburg's Limburg Invests in its Knowledge Economy (LINK) program.

## 7 REFERENCES


1. Watad, A.; Cuthbert, R.J.; Amital, H.; McGonagle, D. Enthesitis: Much More Than Focal Insertion Point Inflammation. Curr. Rheumatol. Rep. 2018, 20, 41–41. https://doi.org/10.1007/s11926-018-0751-3.
2. Apostolakos, J.; Durant, T.J.; Dwyer, C.R.; Russell, R.P.; Weinreb, J.H.; Alaee, F.; Beitzel, K.; McCarthy, M.B.; Cote, M.P.; Mazzocca, A.D. The enthesis: A review of the tendon-to-bone insertion. Muscles Ligaments Tendons J. 2014, 4, 333–342.
3. Rossetti, L.; Kuntz, L.A.; Kunold, E.; Schock, J.; Muller, K.W.; Grabmayr, H.; Stolberg-Stolberg, J.; Pfeiffer, F.; Sieber, S.A.; Burgkart, R.; et al. The microstructure and micromechanics of the tendon-bone insertion. Nat. Mater. 2017, 16, 664–670. https://doi.org/10.1038/nmat4863.
4. Derwin, K.A.; Galatz, L.M.; Ratcliffe, A.; Thomopoulos, S. Enthesis Repair: Challenges and Opportunities for Effective Tendon-to-Bone Healing. J. Bone Jt. Surg. Am. 2018, 100, e109. https://doi.org/10.2106/JBJS.18.00200.
5. Mattap, S.; Aitken, D.; Wills, K.; Halliday, A.; Ding, C.; Han, W.; Cicuttini, F.; Jones, G.; Laslett, L. Patellar tendon enthesis abnormalities and their association with knee pain and structural abnormalities in older adults. Osteoarthr. Cartil. 2018, 26, S412-S413. https://doi.org/10.1016/j.joca.2018.02.796.
6. Calejo, I.; Costa-Almeida, R.; Reis, R.L.; Gomes, M.E. Enthesis Tissue Engineering: Biological Requirements Meet at the Interface. Tissue Eng. Part B Rev. 2019, 25, 330–356. https://doi.org/10.1089/ten.teb.2018.0383.
7. Baraliakos, X.; Sewerin, P.; de Miguel, E.; Pournara, E.; Kleinmond, C.; Wiedon, A.; Behrens, F. Achilles tendon enthesitis evaluated by MRI assessments in patients with axial spondyloarthritis and psoriatic arthritis: A report of the methodology of the ACHILLES trial. BMC Musculoskelet. Disord. 2020, 21, 767. https://doi.org/10.1186/s12891-020-03775-4.
8. Fan, L.; Xu, B.; Liu, N.; Wang, L. Histopathological changes in patellar tendon enthesis of rabbit induced by electrical stimulation intensity. J. Orthop. Sci. 2020, 25, 344–348. https://doi.org/10.1016/j.jos.2019.04.007.
9. Holwein, C.; von Bibra, B.; Jungmann, P.M.; Karampinos, D.C.; Wörtler, K.; Scheibel, M.; Imhoff, A.B.; Buchmann, S. No healing improvement after rotator cuff reconstruction augmented with an autologous periosteal flap. Knee Surg. Sport. Traumatol. Arthrosc. 2019, 27, 3212–3221. https://doi.org/10.1007/s00167-019-05384-8.
10. Peniche Silva, C.J.; Müller, S.A.; Quirk, N.; Poh, P.S.P.; Mayer, C.; Motta, A.; Migliaresi, C.; Coenen, M.J.; Evans, C.H.; Balmayor, E.R.; et al. Enthesis Healing Is Dependent on Scaffold Interphase Morphology-Results from a Rodent Patellar Model. Cells 2022, 11, 1752. https://doi.org/10.3390/cells11111752.
11. He, L.; Hannon, G.J. MicroRNAs: Small RNAs with a big role in gene regulation. Nat. Rev. Genet. 2004, 5, 522–531. https://doi.org/10.1038/nrg1379.
12. Cannell, I.G.; Kong, Y.W.; Bushell, M. How do microRNAs regulate gene expression? Biochem. Soc. Trans. 2008, 36, 1224–1231. https://doi.org/10.1042/BST0361224.
13. Bushati, N.; Cohen, S.M. microRNA Functions. Annu. Rev. Cell Dev. Biol. 2007, 23, 175–205. https://doi.org/10.1146/annurev.cellbio.23.090506.123406.

14. Hashimoto, Y.; Akiyama, Y.; Yuasa, Y. Multiple-to-multiple relationships between microRNAs and target genes in gastric cancer. PLoS ONE 2013, 8, e62589-e62589. https://doi.org/10.1371/journal.pone.0062589.
15. Bhaskaran, M.; Mohan, M. MicroRNAs: History, biogenesis, and their evolving role in animal development and disease. Vet. Pathol. 2014, 51, 759–774. https://doi.org/10.1177/0300985813502820.
16. Catalanotto, C.; Cogoni, C.; Zardo, G. MicroRNA in Control of Gene Expression: An Overview of Nuclear Functions. Int. J. Mol. Sci. 2016, 17, 1712. https://doi.org/10.3390/ijms17101712.
17. Peng, Y.; Croce, C.M. The role of MicroRNAs in human cancer. Signal Transduct. Target 2016, 1, 15004–15004. https://doi.org/10.1038/sigtrans.2015.4.
18. Schueller, F.; Roy, S.; Vucur, M.; Trautwein, C.; Luedde, T.; Roderburg, C. The Role of miRNAs in the Pathophysiology of Liver Diseases and Toxicity. Int. J. Mol. Sci. 2018, 19, 261. https://doi.org/10.3390/ijms19010261.
19. Groven, R.V.M.; van Koll, J.; Poeze, M.; Blokhuis, T.J.; van Griensven, M. miRNAs Related to Different Processes of Fracture Healing: An Integrative Overview. Front. Surg. 2021, 8, 584.
20. Kelch, S.; Balmayor, E.R.; Seeliger, C.; Vester, H.; Kirschke, J.S.; van Griensven, M. miRNAs in bone tissue correlate to bone mineral density and circulating miRNAs are gender independent in osteoporotic patients. Sci. Rep. 2017, 7, 15861–15861. https://doi.org/10.1038/s41598-017-16113-x.
21. Mollaei, H.; Safaralizadeh, R.; Rostami, Z. MicroRNA replacement therapy in cancer. J. Cell Physiol. 2019, 234, 12369–12384. https://doi.org/10.1002/jcp.28058.
22. Garofalo, M.; Leva, D.G.; Croce, M.C. microRNAs as Anti-Cancer Therapy. Curr. Pharm. Des. 2014, 20, 5328–5335. https://doi.org/10.2174/1381612820666140128211346.
23. Bader, A. miR-34—a microRNA replacement therapy is headed to the clinic. Front. Genet. 2012, 3, 120
24. Wang, X.; He, Y.; Mackowiak, B.; Gao, B. MicroRNAs as regulators, biomarkers and therapeutic targets in liver diseases. Gut 2021, 70, 784. https://doi.org/10.1136/gutjnl-2020-322526.
25. Ye, D.; Zhang, T.; Lou, G.; Liu, Y. Role of miR-223 in the pathophysiology of liver diseases. Exp. Mol. Med. 2018, 50, 1–12. https://doi.org/10.1038/s12276-018-0153-7.
26. Wu, J.; Kuang, L.; Chen, C.; Yang, J.; Zeng, W.-N.; Li, T.; Chen, H.; Huang, S.; Fu, Z.; Li, J.; et al. miR-100-5p-abundant exosomes derived from infrapatellar fat pad MSCs protect articular cartilage and ameliorate gait abnormalities via inhibition of mTOR in osteoarthritis. Biomaterials 2019, 206, 87–100. https://doi.org/10.1016/j.biomaterials.2019.03.022.
27. Geng, Y.; Zhao, X.; Xu, J.; Zhang, X.; Hu, G.; Fu, S.-C.; Dai, K.; Chen, X.; Patrick, Y.s.-h.; Zhang, X. Overexpression of mechanical sensitive miR-337-3p alleviates ectopic ossification in rat tendinopathy model via targeting IRS1 and Nox4 of tendon-derived stem cells. J. Mol. Cell Biol. 2019, 12, 305–317. https://doi.org/10.1093/jmcb/mjz030.
28. Watts, A.E.; Millar, N.L.; Platt, J.; Kitson, S.M.; Akbar, M.; Rech, R.; Griffin, J.; Pool, R.; Hughes, T.; McInnes, I.B.; et al. MicroRNA29a Treatment Improves Early Tendon Injury. Mol. Ther. 2017, 25, 2415–2426. https://doi.org/10.1016/j.ymthe.2017.07.015.

29. Vonk, L.A.; Kragten, A.H.M.; Dhert, W.J.A.; Saris, D.B.F.; Creemers, L.B. Overexpression of hsa-miR-148a promotes cartilage production and inhibits cartilage degradation by osteoarthritic chondrocytes. Osteoarthr. Cartil. 2014, 22, 145–153. https://doi.org/10.1016/j.joca.2013.11.006.
30. Maurer, B.; Stanczyk, J.; Jüngel, A.; Akhmetshina, A.; Trenkmann, M.; Brock, M.; Kowal-Bielecka, O.; Gay, R.E.; Michel, B.A.; Distler, J.H.W.; et al. MicroRNA-29, a key regulator of collagen expression in systemic sclerosis. Arthritis Rheum. 2010, 62, 1733–1743. https://doi.org/10.1002/art.27443.
31. Xiong, Y.; Cao, F.; Hu, L.; Yan, C.; Chen, L.; Panayi, A.C.; Sun, Y.; Zhou, W.; Zhang, P.; Wu, Q.; et al. miRNA-26a-5p Accelerates Healing via Downregulation of PTEN in Fracture Patients with Traumatic Brain Injury. Mol. Ther.-Nucleic Acids 2019, 17, 223–234. https://doi.org/10.1016/j.omtn.2019.06.001.
32. Liu, Q.; Zhu, Y.; Zhu, W.; Zhang, G.; Yang, Y.P.; Zhao, C. The role of MicroRNAs in tendon injury, repair, and related tissue engineering. Biomaterials 2021, 277, 121083. https://doi.org/10.1016/j.biomaterials.2021.121083.
33. Shen, L.; Qinglin, K.; Rui, Z.; Yanhao, L.; Rong, B. Tendon Adhesion and Novel Solutions. In Tendons; Nahum, R., Ed.; IntechOpen: Rijeka, Croatia, 2022; Chapter 3.
34. Chen, Q.; Lu, H.; Yang, H. Chitosan inhibits fibroblasts growth in Achilles tendon via TGF-β1/Smad3 pathway by miR-29b. Int. J. Clin. Exp. Pathol. 2014, 7, 8462.
35. Cui, H.; He, Y.; Chen, S.; Zhang, D.; Yu, Y.; Fan, C. Macrophage-Derived miRNA-Containing Exosomes Induce Peritendinous Fibrosis after Tendon Injury through the miR-21-5p/Smad7 Pathway. Mol. Ther.-Nucleic Acids 2019, 14, 114–130. https://doi.org/10.1016/j.omtn.2018.11.006.
36. Li, L.; Jia, J.; Liu, X.; Yang, S.; Ye, S.; Yang, W.; Zhang, Y. MicroRNA-16-5p controls development of osteoarthritis by targeting SMAD3 in chondrocytes. Curr. Pharm. Des. 2015, 21, 5160–5167.
37. Zhang, Y.; Li, S.; Jin, P.; Shang, T.; Sun, R.; Lu, L.; Guo, K.; Liu, J.; Tong, Y.; Wang, J.; et al. Dual functions of microRNA-17 in maintaining cartilage homeostasis and protection against osteoarthritis. Nat. Commun. 2022, 13, 2447. https://doi.org/10.1038/s41467-022-30119-8.
38. Wang, B.; Guo, J.; Feng, L.; Suen, C.W.; Fu, W.M.; Zhang, J.F.; Li, G. MiR124 suppresses collagen formation of human tendon derived stem cells through targeting egr1. Exp. Cell Res. 2016, 347, 360–366. https://doi.org/10.1016/j.yexcr.2016.08.018.
39. Fu, H.L.; Pan, H.X.; Zhao, B.; Dong, B.C.; Shao, L.; Fu, G.S.; Wang, Q.; Li, M. MicroRNA-100 inhibits bone morphogenetic protein-induced osteoblast differentiation by targeting Smad1. Eur. Rev. Med. Pharm. Sci. 2016, 20, 3911–3919.
40. Qin, X.; Zhu, B.; Jiang, T.; Tan, J.; Wu, Z.; Yuan, Z.; Zheng, L.; Zhao, J. miR-17-5p Regulates Heterotopic Ossification by Targeting ANKH in Ankylosing Spondylitis. Mol. Ther.-Nucleic Acids 2019, 18, 696–707. https://doi.org/10.1016/j.omtn.2019.10.003.
41. Jordan, K.P.; Jöud, A.; Bergknut, C.; Croft, P.; Edwards, J.J.; Peat, G.; Petersson, I.F.; Turkiewicz, A.; Wilkie, R.; Englund, M. International comparisons of the consultation prevalence of musculoskeletal conditions using population-based healthcare data from England and Sweden. Ann. Rheum. Dis. 2014, 73, 212. https://doi.org/10.1136/annrheumdis-2012-202634.
42. Andarawis-Puri, N.; Flatow, E.L.; Soslowsky, L.J. Tendon basic science: Development, repair, regeneration, and healing. J. Orthop. Res. 2015, 33, 780–784. https://doi.org/10.1002/jor.22869.

43. Zafar, M.S.; Mahmood, A.; Maffulli, N. Basic science and clinical aspects of achilles tendinopathy. Sport. Med. Arthrosc. Rev. 2009, 17, 190–197.
44. Wu, F.; Nerlich, M.; Docheva, D. Tendon injuries: Basic science and new repair proposals. EFORT Open Rev. 2017, 2, 332. https://doi.org/10.1302/2058-5241.2.160075.
45. Chartier, C.; ElHawary, H.; Baradaran, A.; Vorstenbosch, J.; Xu, L.; Efanov, J.I. Tendon: Principles of Healing and Repair. Semin. Plast. Surg. 2021, 35, 211–215.
46. Beredjiklian, P.K. Biologic Aspects of Flexor Tendon Laceration and Repair. JBJS 2003, 85, 539–550.
47. Sharma, P.M.N. Biology of tendon injury: Healing, modeling and remodeling. J. Musculoskelet. Neuronal. Interact. 2006, 6, 181–190.
48. Cadby, J.A.; Buehler, E.; Godbout, C.; Van Weeren, P.R.; Snedeker, J.G. Differences between the Cell Populations from the Peritenon and the Tendon Core with Regard to Their Potential Implication in Tendon Repair. PLoS ONE 2014, 9, e92474. https://doi.org/10.1371/journal.pone.0092474.
49. Carpenter, J.E.; Flanagan, C.L.; Thomopoulos, S.; Yian, E.H.; Soslowsky, L.J. The effects of overuse combined with intrinsic or extrinsic alterations in an animal model of rotator cuff tendinosis. Am. J. Sport. Med. 1998, 26, 801–807.
50. Thomopoulos, S.; Parks, W.C.; Rifkin, D.B.; Derwin, K.A. Mechanisms of tendon injury and repair. J. Orthop. Res. 2015, 33, 832–839. https://doi.org/10.1002/jor.22806.
51. Wang, X.; Li, F.; Xie, L.; Crane, J.; Zhen, G.; Mishina, Y.; Deng, R.; Gao, B.; Chen, H.; Liu, S. Inhibition of overactive TGF-β attenuates progression of heterotopic ossification in mice. Nat. Commun. 2018, 9, 1–13.
52. Zhang, Q.; Zhou, D.; Wang, H.; Tan, J. Heterotopic ossification of tendon and ligament. J. Cell. Mol. Med. 2020, 24, 5428–5437. https://doi.org/10.1111/jcmm.15240.
53. Louwerens, J.; Alkaduhimi, H.; van den Bekerom, M. Association between rotator cuff tears and calcific tendinopathy. Arthroscopy 2020, 36, 625–626.
54. O'Brien, E.J.; Frank, C.B.; Shrive, N.G.; Hallgrímsson, B.; Hart, D.A. Heterotopic mineralization (ossification or calcification) in tendinopathy or following surgical tendon trauma. Int. J. Exp. Pathol. 2012, 93, 319–331.
55. Ding, L.; Wang, M.; Qin, S.; Xu, L. The Roles of MicroRNAs in Tendon Healing and Regeneration. Front. Cell Dev. Biol. 2021, 9, 687117. https://doi.org/10.3389/fcell.2021.687117.
56. McGill, M.R.; Jaeschke, H. MicroRNAs as signaling mediators and biomarkers of drug-and chemical-induced liver injury. J. Clin. Med. 2015, 4, 1063–1078.
57. Millar, N.L.; Gilchrist, D.S.; Akbar, M.; Reilly, J.H.; Kerr, S.C.; Campbell, A.L.; Murrell, G.A.C.; Liew, F.Y.; Kurowska-Stolarska, M.; McInnes, I.B. MicroRNA29a regulates IL-33-mediated tissue remodelling in tendon disease. Nat. Commun. 2015, 6, 6774–6774. https://doi.org/10.1038/ncomms7774.
58. Hall, K.E.; Sarkissian, E.J.; Sharpe, O.; Robinson, W.H.; Abrams, G.D. Identification of differentially expressed micro-RNA in rotator cuff tendinopathy. Muscles Ligaments Tendons J. (MLTJ) 2018, 8, 8–14.
59. Plachel, F.; Heuberer, P.; Gehwolf, R.; Frank, J.; Tempfer, H.; Lehner, C.; Weissenbacher, N.; Wagner, A.; Weigl, M.; Moroder, P. MicroRNA profiling reveals distinct signatures in degenerative rotator cuff pathologies. J. Orthop. Res.® 2020, 38, 202–211.

60. Peniche Silva, C.J.; Müller, S.A.; Quirk, N.; De la Vega, R.E.; Coenen, M.J.; Evans, C.H.; Balmayor, E.R.; van Griensven, M. Enthesis: Not the same in each localisation—a molecular, histological and biomechanical study. Eur. Cell Mater. 2022, 44, 43–55. https://doi.org/10.22203/eCM.v044a03.
61. Liao, X.-B.; Yuan, K.; Liu, Y.; Feng, X.; Cui, R.-R.; Hu, Y.-R.; Yuan, Z.-S.; Gu, L.; Li, S.-J.; Mao, D.-A.; et al. MiR-133a Modulates Osteogenic Differentiation of Vascular Smooth Muscle Cells. Endocrinology 2013, 154. https://doi.org/10.1210/en.2012-2236.
62. Jia, J.; Feng, X.; Xu, W.; Yang, S.; Zhang, Q.; Liu, X.; Feng, Y.; Dai, Z. MiR-17-5p modulates osteoblastic differentiation and cell proliferation by targeting SMAD7 in non-traumatic osteonecrosis. Exp. Mol. Med. 2014, 46, e107-e107. https://doi.org/10.1038/emm.2014.43.
63. Inoue, K.; Deng, Z.; Chen, Y.; Giannopoulou, E.; Xu, R.; Gong, S.; Greenblatt, M.B.; Mangala, L.S.; Lopez-Berestein, G.; Kirsch, D.G.; et al. Bone protection by inhibition of microRNA-182. Nat. Commun. 2018, 9, 4108.
64. Yao, Q.; Xing, Y.; Wang, Z.; Liang, J.; Lin, Q.; Huang, M.; Chen, Y.; Lin, B.; Xu, X.; Chen, W. MiR-16-5p suppresses myofibroblast activation in systemic sclerosis by inhibiting NOTCH signaling. Aging 2020, 13, 2640–2654.
65. Wei, P.; Xie, Y.; Abel, P.W.; Huang, Y.; Ma, Q.; Li, L.; Hao, J.; Wolff, D.W.; Wei, T.; Tu, Y. Transforming growth factor (TGF)-β1-induced miR-133a inhibits myofibroblast differentiation and pulmonary fibrosis. Cell Death Dis. 2019, 10, 670.
66. Nichols, A.E.C.; Best, K.T.; Loiselle, A.E. The cellular basis of fibrotic tendon healing: Challenges and opportunities. Transl Res 2019, 209, 156–168.
67. Williams, I.; Heaton, A.; McCullagh, K. Cell morphology and collagen types in equine tendon scar. Res. Vet. Sci. 1980, 28, 302–310.
68. Eissa, M.G.; Artlett, C.M. The MicroRNA miR-155 Is Essential in Fibrosis. Non-coding RNA 2019, 5, 23.
69. Pashangzadeh, S.; Motallebnezhad, M.; Vafashoar, F.; Khalvandi, A.; Mojtabavi, N. Implications the Role of miR-155 in the Pathogenesis of Autoimmune Diseases. Front. Immunol. 2021, 12, 669382. https://doi.org/10.3389/fimmu.2021.669382.
70. Papalia, G.F.; Franceschetti, E.; Giurazza, G.; Parisi, F.R.; Gregori, P.; Zampogna, B.; Longo, U.G.; Papalia, R. MicroRNA expression changes in the development of rotator cuff tendon injuries. JSES Rev. Rep. Tech. 2023, in press. https://doi.org/10.1016/j.xrrt.2023.03.006.
71. Hummon, A.B.; Lim, S.R.; Difilippantonio, M.J.; Ried, T. Isolation and solubilization of proteins after TRIzol extraction of RNA and DNA from patient material following prolonged storage. Biotechniques 2007, 42, 467–472. https://doi.org/10.2144/000112401.

CHAPTER 6

# Synergistic Effect of miRNA Modulation and Tendon Mimetic Microenvironment Enhancing Tenogenesis of Adipose Tissue-Derived Stem Cells

C. J. Peniche Silva, R. Dominguez, S. M. Bakht, A. Pardo, V. Joris, A. I. Gonçalves, S. P. B. Texeira, E. R. Balmayor, M. E. Gomes, M. van Griensven

## ABSTRACT

Tendons and tendon-to-bone entheses heal poorly after injury, and the scar tissue that is typically formed fails to regenerate the native morphology of the healthy tissue. We have previously described a magnetically-assisted 3D-bioprinting technique to obtain tendon-mimetic hydrogels with an anisotropic morphology capable of inducing the tenogenic commitment of the encapsulated adipose-derived stem cells (hASCs). In this study, we have explored a novel approach for *in situ* transfection of the encapsulated hASCs with microRNA (miRNA) probes to further enhance their tenogenic commitment. miRNAs are short, non-coding sequences of RNA that act as post-transcriptional regulators of gene expression. Mimics or inhibitors of specific miRNAs have been used to restore lost functions at the cell level or improve healing at the tissue level. We found that miR-16-5p was upregulated in the fibrotic portion of injured tendons in a rat model. The published literature describes an antifibrotic role for miR-16-5p via targeting of *SMAD3*. Thus, we aimed to explore the effects of miRNA-16-5p mimics and inhibitors on the tenogenic differentiation of hASCs. For this, we have encapsulated hASCs in our gelatin-methacrylated(GelMa)-based magnetically-responsive bioink that incorporates miR-16-5p (mimics or inhibitors) to obtain tendon-mimetic miRNA-laden hydrogels. The obtained GelMA hydrogels retained the encapsulated miRNA probes, which permitted the *in situ* transfection of the hASC. Furthermore, we found that the *in situ* transfection with the miR-16-5p mimic led to a prolonged increase in the expression of the tenogenic markers *TNC*, *TNMD*, *DCN*, and others compared to the transfection with the inhibitors. Thus, indicating a potential tenogenic role for miR-16-5p.

## 1 INTRODUCTION

Injuries at tendon-to-bone entheses are problematic [1,2]. Partial or full-thickness tendon or enthesis ruptures often undergo poor healing, which in most cases yields scar tissue that fails to recapitulate the native morphology of the uninjured tissue [3,4]. In particular, the highly specialized extracellular matrix (ECM) of the tendon-to-bone enthesis presents gradients of mineralization and collagen alignment patterns that are not regenerated during the normal healing process after injury [5-7].

We have previously described the occurrence of fibrosis and ectopic ossification in the tendon side of a rat patellar enthesis as a result of the healing process upon injury [4]. Furthermore, we identified a group of fibrosis-related microRNAs (miRNAs) that were dysregulated in the injured samples during the early stages of healing. .

The interest in the therapeutic potential of miRNAs as post-transcriptional regulators of gene expression and thereby, protein production, has been growing steadily over the last two decades [8-11]. In the context of tendon healing, it has been shown that intralesional injection of miRN-29a improves early tendon healing in horses [12]. Similarly, the intralesional injection of miR-210 was reported to promote Achilles tendon healing in a rat model [13]. Furthermore, an inhibitory effect on collagen production and the tenogenic differentiation of tendon progenitor stem cells has been described *in vitro* for miR-124 [14].



Using a rodent patellar enthesis injury model, we recently identified miR-16-5p to be upregulated in the fibrotic portion of the injured tissue 10 days after the creation of the injury [4]. miR-16-5p has been proven to modulate the TGF-β/Smad pathway by inhibition of *SMAD2/3* in liver fibrosis, or *SMAD3* in skin and cardiac fibrosis [15]. More specifically, it has been observed that the overexpression of miR-16-5p in myofibroblasts results in the inhibition of the fibrotic and proliferative properties of these cells by inactivating the TGF-β pathway. In line with these reports, we described the downregulation of *SMAD3* in injured patellar enthesis samples where miR-16-5p was upregulated [4]. Moreover, the anti-fibrotic effects of miR-16-5p have also been linked to the inhibition of inflammatory cytokines and other pro-fibrotic mediators (e.g. IL-6, TNF-α, and IL-1β) and the secretion of the anti-inflammatory factor IL-10, reducing inflammation and the formation of fibrous scar tissue [16,17].

The published data support an anti-fibrotic role for miR-16-5p, which indicates a potential therapeutic use for such miRNA in the modulation or inhibition of fibrosis during tendon healing. Additionally, by regulating the TGF-β pathway via the inhibition of SMAD3, miR-16-5p could also influence the processes of

tenogenic differentiation and tendon healing. Interestingly, at least to the extent of our knowledge, this miRNA has not yet been investigated in the context of tendon healing and regeneration.

We have previously described the obtention of a cell-laden tendon-mimetic construct by magnetically-assisted 3D bioprinting capable of promoting the tenogenic commitment of adipose-derived stem cells (hASCs) [18]. For this, a cell-laden gelatin methacrylated (GelMa) magnetically responsive bioink was developed. The obtained bioink incorporates hASCs and magnetically responsive polycaprolactone (PCL) microfibers that would align longitudinally in response to the presence of an external magnetic field. Thus, creating an anisotropic, tendon-mimetic microenvirorment for the encapsulated cells. It was demonstrated that the tendon-mimetic microenvironment achievable by using this technique has the potential to elicit tenogenic differentiation of the encapsulated hASC. In the present study, we aimed to investigate the role of miR-16-5p beyond the potential inhibition of fibrosis, in the tenogenic commitment of hASCs when cultured in a 3D tendon-mimetic microenvirorment. For this, we have encapsulated miR-16-5p mimics or inhibitors in the cell-laden magnetically responsive GelMa bioink to obtain miRNA-laden, cell-laden tendon-mimetic hydrogels. We hypothesize that the modulatory effects of miR-16-5p on the TGFβ/Smad pathway could further enhance the tenogenic commitment of the hASCs -loaded hydrogel by preventing the overactivation of the TGF-β pathway.

## 2 MATERIALS AND METHODS

### 2.1 Cell culture

The hASCs used in this study were obtained from lipoaspirate samples of the abdominal region of patients undergoing liposuction surgery with the appropriate informed consent, and following the protocols established with Hospital da Prelada (Porto Portugal) and with the approval of the Hospital and University of Minho Ethics Committee (approval numbers 005/2019 and 014/2019). The isolation was performed following previously optimized protocols [19,20]. Cells were cultured and expanded in alpha-modified Eagle medium (α-MEM) supplemented with 10% v/v fetal bovine serum and 1% (v/v) penicillin (ThermoFisher, Waltham, MA, USA). The cells were not used beyond passage number six.

### 2.2 miRNA mimic/inhibitor loaded-hydrogel preparation

The hsa-miRNA-16-5p miCURY LNA mimic-FAM, hsa-miRNA-16-5p miCURY LNA inhibitor-FAM, miRNA mimic negative control-FAM, miRNA inhibitor negative control-FAM, and the HiPerfect Transfection Reagent were purchased from Qiagen (Qiagen GmbH, Hilden, Germany). Fish GelMa was dissolved in α-MEM cell culture media (20% w/v) for 1h at 60$^0$C with constant agitation. Afterward,

the GelMa solution was cooled down and kept at 37$^0$C until further use. The magnetically-responsive polycaprolactone microfibers (MRFs) were obtained as described before [18]. Briefly, magnetic nano-particles (~9 nm) were prepared through a process of thermal decomposition following previously reported procedures for the synthesis of iron oxide nanoparticles [18]. Later, PCL-MRFs were prepared by electrospinning, incorporating the previously obtained magnetic nanoparticles into the polymeric precursor solution (Sigma-Aldrich, Saint Louis, USA). Electrospun membranes were cut into 3 × 3 mm portions and embedded in OCT blocks (Sigma-Aldrich, Sint Luis, USA) that were frozen at -20$^0$C and micro-cut to produce MRFs of 25 µm in length. Finally, a solution of MRFs was prepared by dissolving 4.7 mg/ml of the obtained MRFs in cell culture media. Additionally, a LAP (lithium phenyl-2,4,6-trimethylbenzoylphosphinate; Sigma-Aldrich, Saint Louis, USA) solution was prepared at a concentration of 1.25% w/v in sterile PBS.

To incorporate the miRNA mimic or inhibitor probes into the GelMa hydrogels, miRNA mimics or inhibitors were mixed with the HiPerfect transfection reagent in the LAP solution to form transfection complexes following the recommendation of the manufacturer. miRNA probes and transfection reagent were mixed at adequate proportions to obtain a final amount of 15 pmol of miRNA mimic or 75 pmol in the case of the miRNA inhibitor per 150 ul of hydrogel. That is, ~6 pmol of miRNA mimic/$10^5$ cells and 30 pmol of miRNA inhibitor/$10^5$ cells.



The incorporation of the cells into the GelMa hydrogel was done by trypsinizing the hASCs and resuspending the cells in the MRFs solution. Later the MRFs cell-containing solution was mixed with the dissolved GelMA and the LAP solution containing the transfection complex. The proportions of each gel precursor solution were calculated to obtain gels of 150 µl with a final concentration of 7.5% w/v of GelMa, 0.25% w/v of LAP containing the transfection complexes, 2 mg/ml of MRFs, and a cell density of 1.5 × $10^6$ cells/ml. The gel precursor mix was pipetted onto an 8-well µ-slide IBIDI chamber (IBIDI, Gräfelfing, Germany) in the presence of an external magnetic field provided by an in-house fabricated system of two-pairs of parallel magnets and exposed to a 385 W cm$^{-2}$ UV light for 30s using an Omnicure S2000 Spot UV Curing System (Exelitas Technology, Waltham, USA). The intensity of the magnetic field and the effects of the microfiber length, magnetic nanoparticle content, and MRF concentration, were previously evaluated in a different study [18]. A total of three gels per condition and time points were cast. After UV cross-linking, the gels were removed from the IBIDI chambers and placed in 24-well non-treated tissue culture plates containing at least 500 µl of media. Media change was performed every three days. The alignment of the MRFs after crosslinking was assessed by optical microscopy and the encapsulated cells were imaged with confocal microscopy at days 7 and 14.

The transfection efficiency at timepoint 72h was assessed by flow cytometry. The gels were enzymatically digested with collagenase (2 mg/ml) for 60 min. Later, the product of digestion was centrifuged, the pellet was washed twice with PBS, and at least $10^5$ cells were resuspended in acquisition buffer (1% v/v formalin/PBS). A minimum of $2\times10^4$ hASCs were acquired and the fraction of cells that internalized the FAM-labeled miRNA probes was determined with a FACS-Calibur Flow Cytometer (BD Biosciences, New Jersey, USA) and analyzed with CellQuest software V3.3.

### 2.3 Analysis of miRNA probes retention by the GleMa hydrogels

GelMa hydrogels (50 µl) were loaded with the complex formed by the miRNA mimic negative control-FAM at a concentration of 200nM and the HiPerfect transfection reagent as described before. After cross-linking, the gels were incubated in 96 well plates containing 100 µl of PBS at $37^0$C in a humidified atmosphere of 5% $CO_2$ for up to 10 days. At every indicated time point, 80 µl of the releasates were collected for measurement and replaced with fresh PBS. The content of miRNA probe released to the PBS was quantified by measuring the fluorescent signal of the releasates at 518 nm with a Clariostar plate reader (BMG Labtech, Ortenberg, Germany). The cumulative release of the miRNA mimic negative control-FAM from the hydrogel was determined by interpolation with a standard curve previously obtained for this purpose.

### 2.4 RNA and protein extraction from GelMa hydrogels

RNA and proteins were extracted from at least three gels per condition and timepoint (4, 10, 14, and 21 days for RNA and 10 and 21 days for protein). For the RNA extraction, each gel was digested with collagenase (2 mg/ml for 45 min at $37^0$C), centrifuged and the pellet resuspended in Trizol Reagent (Sigma-Aldrich, Saint Louis, USA). The isolation of the total RNA was performed following the well-established phenol-chloroform extraction protocol. The concentration and purity of the extracted RNA were measured using a NanoDrop spectrophotometer (NanoDrop Tech. Inc., Greenville, USA). In every case, the ratios 260/230 and 260/280 were found to be ≥1.8. The extracted RNA was used for cDNA synthesis.

Protein isolation and solubilization was performed following a standard chloroform/isopropanol/guanidine hydrochloride extraction protocol [21]. After extraction, the protein pellet was resuspended in SDS 1%. For Western blotting, the total protein content was quantified using the bicinchoninic acid (BCA) method, utilizing the Pierce™ BCA kit (ThermoFisher, Waltham, USA), and 15 µg were loaded in each well of 8% bis-acrylamide gel. Electrophoresis was performed in a running buffer (Tris, SDS, Glycine) for 60 min at 120 V. After separation, proteins were transferred on a nitrocellulose membrane using transfer buffer (Tris-base, glycine, SDS, methanol) under 350 mA for 90 min.

Later, the membrane was incubated overnight at 4°C with a SMAD3 primary antibody (1/1000; #9513) for immunodetection of Smad3 protein and GAPDH as housekeeper control. The primary Smad3 antibody was purchased from Cell Signalling Technology (MA, USA) and GAPDH from Abcam (Cambridge, UK). After rinsing, the membrane was incubated with horseradish peroxidase (HRP)-conjugated secondary antibodies (1/3000) at room temperature for 60 min. All antibodies were diluted in tris-buffered saline with 0.1% Tween® 20 and milk 5%. The protein signal was developed using a Clarity Western ECL substrate (Bio-Rad, Hercules, USA) and chemiluminescence was detected using Chemidoc technology (Bio-Rad, Hercules, USA). The intensity of the band was then quantified using ImageJ software 1.53t (NIH, Bethesda, USA) and normalized to GAPDH.

### 2.5 cDNA synthesis and qPCR

The total RNA extracted from the gels was used as the starting material for the cDNA synthesis reactions. cDNA was synthesized from the mRNA fraction of the total RNA using the iScript™ cDNA synthesis kit (Bio-Rad, Hercules, USA). The cDNA synthesis reactions were conducted in a C1000 Touch Thermal Cycler following the cDNA synthesis kit instructions from the manufacturer.

The qPCR reaction mix for the analysis of the gene expression was prepared with the iQ™ SYBR® Green supermix (Bio-Rad, Hercules, USA) following the manufacturer's instructions. A list of the primers used can be found in Table 1. Gene expression was normalized against the reference gene β-tubulin, and the fold regulation of each gene was calculated with respect to the corresponding mimic or inhibitor control sample group, following the $2^{(-\Delta\Delta Ct)}$ method for fold change. Treated data have been displayed as fold regulation (FR), as this facilitates the interpretation of the results. FR is the same as fold change (FC) when FC ≥ 1, and FR is the inverse negative of the FC when FC < 1.

Additionally, the expression of miRNA-16-5p was investigated in the cells extracted from the gels loaded with the miR-16-5p inhibitor probe after 4 days of culture. For this, the cDNA was synthesized from the miRNA fraction of the total RNA using the miScript RT II cDNA synthesis kit (Qiagen GmbH, Hilden, Germany). The qPCR reaction mix for the expression of miR-16-5p was prepared using the miRScript SYBER® Green PCR mix and normalized against the expression of Snord68.

**Table 1:** List of primers used for qPCRs

| Targets | Forward 5'→3' | Reverse 5'→3' |
|---|---|---|
| *COL3a1* | GCTGGCTACTTCTCGCTCTG | GTTGGCATGGTTCTGGCTTCC |
| *MKX* | TGTTAAGGCCATAGCTGCGT | TCGCACAGACACCTGGAAAA |
| *SCX* | CGAGAACACCCAGCCCAAAC | CTCCGAATCGCAGTCTTTCTGTC |
| *SMAD3* | AAACCAGTGACCACCAGATGA | TAGGAGATGGAGCACCAGAAG |
| *TNMD* | CCGCGTCTGTGAACCTTTAC | CACCCACCAGTTACAAGGCA |
| *DCN* | CAGCATTCCTCAAGGTCTTCCT | GAGAGCCATTGTCAACAGCA |
| *TUBB* | GAGGGCGAGGACGAGGCTTA | TCTAACAGAGGCAAAACTGAGCAC |

# 3 RESULTS

## 3.1 GelMA hydrogels enable effective miRNA transfection of the encapsulated cells

The obtained GelMa hydrogels showed a retention of about 80% of the encapsulated miRNA probes by day 10, with a burst of rapid release of approximately 15% of the miRNA probes during the first 24 hours (Fig. 1A). Moreover, by time point 72h, approximately 65% of the encapsulated cells were detected as FAM-labeled by flow cytometry (Figure 1B). The internalization of the FAM-labeled miRNA probes by the encapsulated cells was also observable by confocal microscopy (Fig. 1C). Furthermore, qPCRs for miR-16-5p showed that the cells from the miRNA inhibitor-laden GelMa hydrogel exhibited a down-regulation of miRNA-16-5p of approximately eight-fold after four days of culture when compared to untransfected cells (Fig. 1D).

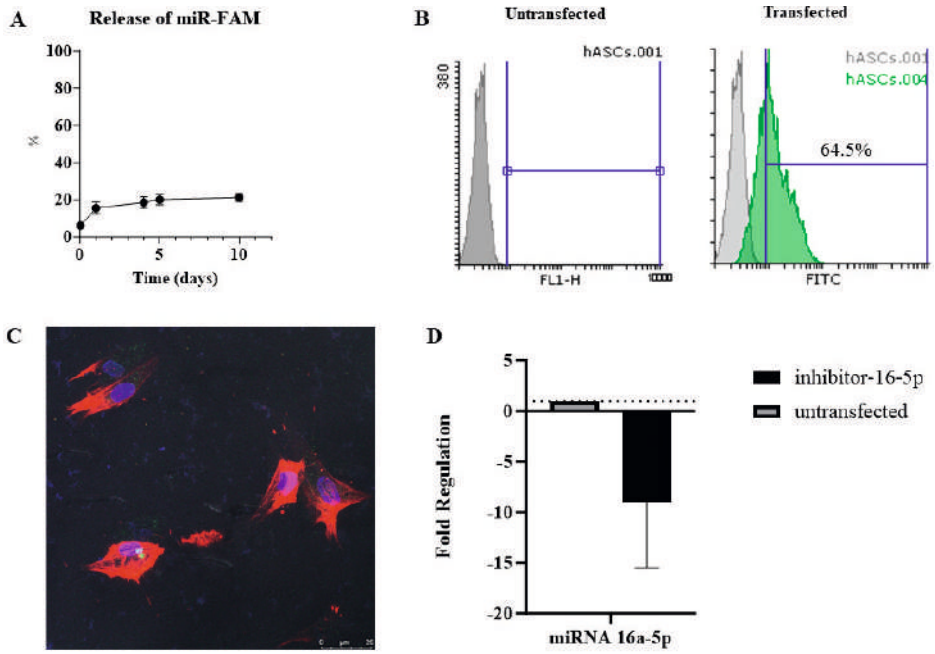


**Figure 1:** (A) Release profile of the encapsulated FAM-labeled miRNA. (B) Flow cytometric analysis showing untransfected cells (left) and the *in situ* transfected cells (right). (C) Confocal image of the *in situ* transfected hASCs after 7 days of culture showing the miRNA complexes in the cytoplasms of the transfected cells. Blue=dapi, red=phalloidin; green=FAM-labeled miRNA probe. Scale bar = 25 µm. (D) Fold regulation (Mean ± SD) of miR-16-5p in the GelMa-encapsulated hASCs after four days of culture in the presence of miR-16-5p inhibitor.



### 3.2 3D-transfection with miRNA-16-5p mimic or inhibitors induces regulation of the target SMAD3 at the gene and protein level

qPCR was conducted for the miR-16-5p target *SMAD3* (Fig. 2A). On the one hand, the expression pattern of *SMAD3* in the cells transfected with the miR-16-5p mimics showed a stable downregulation of about 2-fold in magnitude that lasted from day 4 to day 14 of culture. On the other hand, the transfection with the miR-16-5p inhibitor yielded an increase in the *SMAD3* expression of similar magnitude for the same period. However, at the time point of 21 days, the gene expression of *SMAD3* for both groups was not different from that of the cells transfected with either mimics or inhibitor control probes.

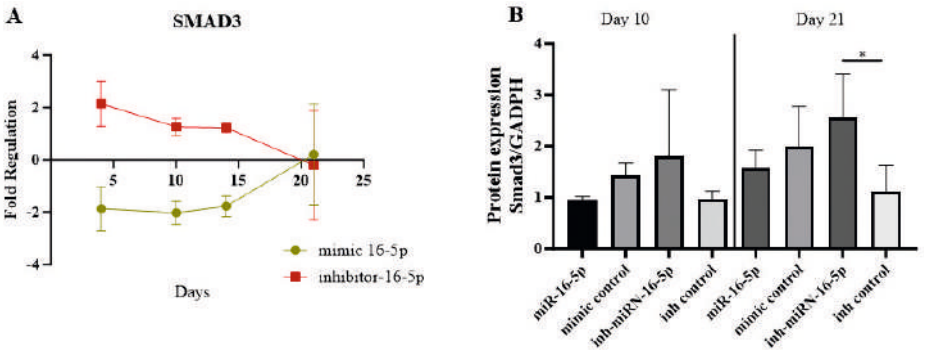


**Figure 2:** (A) Fold regulation (Mean ± SD) of *SMAD3* expression in the samples transfected with the miR-16-5p mimic and inhibitors normalized to the expression in the mimic control and inhibitor control samples respectively. (B) Protein production of SMAD3 with respect to GAPDH at time points day 10 and day 21 after encapsulation represented as mean with SEM. * indicates p > 0.5

The SMAD3 protein production of the encapsulated cells was investigated by western blotting (Figure 2B). The cells transfected with the miR-16-5p mimic showed lower SMAD3 protein production than that of the mimic control at both 10 and 21-day time points, although without statistical significance. Additionally, the SMAD3 production in the samples transfected with the miR-16-5p inhibitor was the highest at both time points, reaching statistical significance at day 21 compared to the inhibitor control sample group.

### 3.3 Overexpression of miRNA-16-5p favors the tenogenic commitment of hASCs in a tendon-mimetic construct.

The expression of several tenogenic markers was investigated in the encapsulated cells by qPCRs. It was observed that transfection with miR-16-5p mimic, led to an increase in the expression of the tendon markers tenomodulin (*TNMD)* and tenascin-C (*TNC*) from time point 10 days onwards, reaching the highest expression level at day 21. Interstingly, both tendon markers also appear to be upregulated at time point 10 days in the cells transfected with the miR-16-5p inhibitor. However, such upregulation was followed by a strong downregulation at day 14 in the case of the *TNMD* and day 21 for *TNC* (Fig. 3).

The expression of the proteoglycan decorin (*DCN*) was upregulated in the miR-16-5p mimic group after time point 10 days, and remained upregulated at least until time point 21 days. This pattern was not observed in the miR-16-5p inhibitor group, where *DCN* was strongly downregulated by day 10, followed by an increase of the expression on day 14 and a downregulation to levels of expression similar to the control group on day 21.

Interestingly, in the gels loaded with miR-16-5p mimics, the transcription factor Mohawk (*MKX*) was either similar to the control groups or slightly down-regulated until day 14, after which the expression increased about two-folds compared to the control group. By contrast, *MKX* was upregulated 2-fold at time point 4 days in the gels loaded with miRNA-16-5p inhibitor. However, such upregulation was immediately followed by a decrease in the expression to levels similar to the control groups from day 10 onwards.

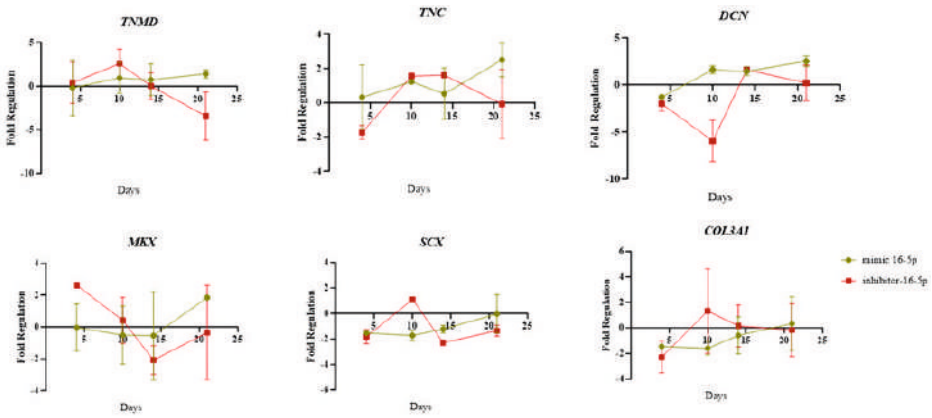


**Figure 3:** Fold regulation (Mean ± SD) of tenogenic markers that resulted dysregulated by either mimics or inhibitors of miR-16-5p. (Green=transfection with 16-5p mimic; Red= Transfection with 16-5p inhibitor)

It was also observed that the expression of scleraxis (*SCX*) remained downregulated for both groups (i.e., miR-16-5p mimic and inhibitor) except for a transient 2-fold upregulation observed by day 10 in the miR-16-5p inhibitor group. A surprisingly similar pattern of expression was observed for *COL3A1*, which was overall down-regulated except for a short-lived increase in the expression by day 10 in the miR-16-5p inhibitor group.

## 4 DISCUSSION

The use of tendon-mimetic constructs represents a promising tissue-engineering strategy to achieve integrative tendon and/or enthesis tissue repair [22]. The fact that specific morphological cues can significantly impact cell proliferation and differentiation *in vitro* as well as tissue growth *in vivo* has been well-documented in the scientific literature [23-27]. Additionally, the functionality of the anisotropic GelMA hydrogel used in the present study was extensively characterized and discussed before [18]. Moreover, the enhancing effects of the anisotropic morphology of our GelMa hydrogels on the tenogenic commitment of the encapsulated cells are in line with several other reports, where a tendon mimetic

morphology is used to promote tenogenic differentiation of mesenchymal stem cells (MSCs) [24,26,28-30].

GelMA is a very attractive and inexpensive material for tissue engineering applications [31]. One important advantage of working with GelMA based-hydrogels is that the porosity and stiffness of GelMa hydrogels are easily tunable by varying the concentration of GelMA in the hydrogel. Furthermore, they exhibit great injectability and UV-cross-linked properties, which makes GelMa a suitable material as bio-ink for 3D bioprinting applications [32-34]. For our study, however, we aimed to explore another advantageous property of GelMA-based hydrogels, which is the ability to encapsulate not only cells but also bioactive molecules, such as the microRNA mimics and inhibitors herein used.

Hydrogel-based delivery of miRNA has been effectively used to achieve *in situ* miRNA transfection of MSC. Carthew *et al*. used a gelatin-PEG hydrogel for *in situ* transfection of the hydrogel-encapsulated MSCs with the osteogenic miRNAs miR-100-5p and miR-143-3p [35]. They reported an enhancement of the MSC osteogenic potential, characterized by increased mineralization and increased osteogenic gene expression. Similarly, Lolli *et al*. used a fibrin/hyaluronan (FB/HA) hydrogel to deliver a miR-221 inhibitor to MSCs and promote chondrogenesis. Moreover, the authors used the miR-221 inhibitor-loaded FB/HA hydrogel to fill defects in osteochondral biopsies that were implanted subcutaneously in mice, achieving the consequent enhancement of cartilage repair by endogenous cells *in vivo* [36].

Our GelMa-based hydrogel showed adequate retention of approximately 80% of the miRNA probes after 10 days of casting the hydrogels, which is comparable to the retention of encapsulated miRNA probes reported in FB/HA hydrogels [36]. This retention would allow for the *in situ* transfection of the encapsulated hASCs in a sustained manner. Moreover, we found that after the first 72h of culture, approximately 65 % of the cells were effectively transfected with our encapsulated miRNA probes according to the flow cytometric analysis. This is a comparable result to that reported by Cartwhew *et al*. using their gelatin-PEG hydrogels. The subsequent cell proliferation and the diffusion of the miRNA probes within the gels are expected to bring cells and miRNA probes in contact to achieve transfection at later time points. Moreover, the observed 65% transfection efficiency after 72 hours was enough to support the 2-fold dysregulation of *SMAD3* measured at timepoint 4 days in both miR-16-5p inhibitor and mimic groups.

The direct effects of miR-16-5p mimics or inhibitors over the expression of the mRNA target *SMAD3* were measurable in our samples at least for the first 14 days of culture. After 21 days of culture, however, the expression of *SMAD3*

was similar in both miRNA mimic and inhibitor groups as well as in the control groups. This could be partially attributed to the potential degradation of the miRNA probes by the timepoint 21 days. Another plausible explanation could be the high number of cells present in the gels at this later time point as a result of cell proliferation, which could lead to the depletion of miRNA mimic or inhibitor available for transfection.

*SMAD3* is a downstream effector of the canonical TGF-β pathway [37]. The TGF-β pathway regulates many aspects of tissue development and homeostasis. However, it is also involved in many pathophysiological mechanisms [37-39]. Several studies support the role of the TGF-β/Smads pathway in the tenogenic differentiation of MSCs [40,41]. Conversely, the overactivation of the TGF-β pathway in injured tendons has been reported to lead to pro-inflamatory and pro-fibrotic responses [42,43].

In our study, the hASCs from the hydrogels loaded with miR-16-5p mimics showed decreased levels of *SMAD3* and increased expression of *TNC*, *TNMD*, and *DCN* compared to the transfection with the miR-16-5p inhibitor. This could indicate a more progressive and controlled tenogenic commitment achieved upon the downregulation of *SMAD3*. Such observations are in line with previous reports of increased *TNMD* production and accelerated tenogenic differentiation of MSCs upon chemical inhibition of *SMAD3* [44]. Furthermore, it has been observed that, after *SMAD3* inhibition, TGF-β-induced tenogenesis occurs via alternative pathways, such as the PTEN/PI3K/AKT pathway [37,44]. Moreover, in line with the *SMAD3* downregulation, we observed a sustained downregulation of the *COL3A1* expression in the miR-16-5p mimic transfected cells, which could be an indication of a favorable tenogenic commitment instead of fibrogenesis. However, it is important to point out that, the downregulation of *SMAD3* in our miR-16-5p mimic transfected samples does not lead to a total inhibition of *SMAD3*. Thus, some *SMAD3* activity, which is as well necessary for tenogenic differentiation of ASCs, still persists.

Unfortunately, in our study, we did not explore the effect of the stimulation of the encapsulated cells with TGF-β in the presence of the miR-16-5p mimics or inhibitors. Future research may incorporate this variable for a more in-depth study on the tenogenic commitment of ASCs and the potential therapeutic role of miR-16-5p in the context of tendon or enthesis healing. An interesting addition could be the supplementation with different members of the TGF-β family since different isoforms have been described to intervene in different processes (e.g., TGF-β1 in fibrosis, -β2 in tenogenesis, and -β3 in chondrogenesis) [37,41,45]. Another variable to consider in the future would be the mechanostimulation of the cell-laden hydrogels. We have previously observed that the tendon

marker *TNMD*, recognized as a tension-modulating protein, is upregulated by mechanical stimuli [18]. This observation leads to the question as to whether the increase in the expression of *TNMD* observed in our miR-16-5p mimic-laden hydrogel could be further amplified by mechanical stimulation, theoretically enhancing tenogenesis.

## 5 CONCLUSIONS

With the work herein summarized, we have developed and tested an anisotropic miRNA-laden GelMa-hydrogel with enhanced tenogenic potential. We reported that contrary to what is observed in the presence of the miR-16-5p inhibitor, the encapsulation of miR-16-5p mimics within our tendon-mimetic GelMa hydrogels can lead to a stable increase in the expression of important tenogenic markers for a period of at least 21 days. Thus signifying a potential tenogenic role for miR-16-5p.

## 6 ACKNOWLEDGMENTS

This work was supported by the Province of Limburg, Limburg Invests in its Knowledge Economy (LINK), and the ESCI Mobility Grant 2022. The project 20-105 was supported by a grant from the ON Foundation, Switzerland.

## 7 REFERENCES


1. Chartier, C.; ElHawary, H.; Baradaran, A.; Vorstenbosch, J.; Xu, L.; Efanov, J.I. Tendon: Principles of Healing and Repair. In Proceedings of the Seminars in Plastic Surgery, 2021; pp. 211-215.
2. Derwin, K.A.; Galatz, L.M.; Ratcliffe, A.; Thomopoulos, S. Enthesis Repair: Challenges and Opportunities for Effective Tendon-to-Bone Healing. J Bone Joint Surg Am 2018, 100, e109-e109, doi:10.2106/JBJS.18.00200.
3. Thomopoulos, S.; Williams, G.R.; Soslowsky, L.J. Tendon to Bone Healing: Differences in Biomechanical, Structural, and Compositional Properties Due to a Range of Activity Levels. Journal of Biomechanical Engineering 2003, 125, 106-113, doi:10.1115/1.1536660.
4. Peniche Silva, C.J.; De La Vega, R.E.; Panos, J.; Joris, V.; Evans, C.H.; Balmayor, E.R.; van Griensven, M. MiRNAs as Potential Regulators of Enthesis Healing: Findings in a Rodent Injury Model. International Journal of Molecular Sciences 2023, 24, doi:10.3390/ijms24108556.
5. Williams, I.; Heaton, A.; McCullagh, K. Cell morphology and collagen types in equine tendon scar. Research in veterinary science 1980, 28, 302-310.
6. Oshiro, W.; Lou J Fau - Xing, X.; Xing X Fau - Tu, Y.; Tu Y Fau - Manske, P.R.; Manske, P.R. Flexor tendon healing in the rat: a histologic and gene expression study. J Hand Surg Am 2003, 814-823, doi:10.1016/s0363-5023(03)00366-6.
7. Lu, H.H.; Thomopoulos, S. Functional Attachment of Soft Tissues to Bone: Development, Healing, and Tissue Engineering. Annual Review of Biomedical Engineering 2013, 15, 201-226, doi:10.1146/annurev-bioeng-071910-124656.
8. Dharap, A.; Pokrzywa, C.; Murali, S.; Pandi, G.; Vemuganti, R. MicroRNA miR-324-3p Induces Promoter-Mediated Expression of RelA Gene. PLoS One 2013, 8, e79467, doi:10.1371/journal.pone.0079467.
9. Jia, J.; Feng, X.; Xu, W.; Yang, S.; Zhang, Q.; Liu, X.; Feng, Y.; Dai, Z. MiR-17-5p modulates osteoblastic differentiation and cell proliferation by targeting SMAD7 in non-traumatic osteonecrosis. Experimental & Molecular Medicine 2014, 46, e107-e107, doi:10.1038/emm.2014.43.
10. Ding, L.; Wang, M.; Qin, S.; Xu, L. The Roles of MicroRNAs in Tendon Healing and Regeneration. Frontiers in Cell and Developmental Biology 2021, 9, doi:10.3389/fcell.2021.687117.
11. Groven, R.V.M.; Peniche Silva, C.J.; Balmayor, E.R.; van der Horst, B.N.J.; Poeze, M.; Blokhuis, T.J.; van Griensven, M. Specific microRNAs are associated with fracture healing phases, patient age and multi-trauma. Journal of Orthopaedic Translation 2022, 37, 1-11, doi:https://doi.org/10.1016/j.jot.2022.07.002.
12. Watts, A.E.; Millar, N.L.; Platt, J.; Kitson, S.M.; Akbar, M.; Rech, R.; Griffin, J.; Pool, R.; Hughes, T.; McInnes, I.B.; et al. MicroRNA29a Treatment Improves Early Tendon Injury. Molecular Therapy 2017, 25, 2415-2426, doi:10.1016/j.ymthe.2017.07.015.
13. Usman, M.A.; Nakasa, T.; Shoji, T.; Kato, T.; Kawanishi, Y.; Hamanishi, M.; Kamei, N.; Ochi, M. The effect of administration of double stranded MicroRNA-210 on acceleration of Achilles tendon healing in a rat model. Journal of Orthopaedic Science 2015, 20, 538-546, doi:https://doi.org/10.1007/s00776-015-0709-5.
14. Wang, B.; Guo, J.; Feng, L.; Suen, C.W.; Fu, W.M.; Zhang, J.F.; Li, G. MiR124 suppresses collagen formation of human tendon derived stem cells through targeting egr1. Exp Cell Res 2016, 347, 360-366, doi:10.1016/j.yexcr.2016.08.018.

15. Wen, D.; Zhang, H.; Zhou, Y.; Wang, J. The Molecular Mechanisms and Function of miR-15a/16 Dysregulation in Fibrotic Diseases. International Journal of Molecular Sciences 2022, 23, doi:10.3390/ijms232416041.
16. Wang, M.; Li, J.; Cai, J.; Cheng, L.; Wang, X.; Xu, P.; Li, G.; Liang, X. Overexpression of MicroRNA-16 Alleviates Atherosclerosis by Inhibition of Inflammatory Pathways. BioMed Research International 2020, 2020, 8504238, doi:10.1155/2020/8504238.
17. Liang, X.; Xu, Z.; Yuan, M.; Zhang, Y.; Zhao, B.; Wang, J.; Zhang, A.; Li, G. MicroRNA-16 suppresses the activation of inflammatory macrophages in atherosclerosis by targeting PDCD4. Int J Mol Med 2016, 37, 967-975, doi:10.3892/ijmm.2016.2497.
18. Pardo, A.; Bakht, S.M.; Gomez-Florit, M.; Rial, R.; Monteiro, R.F.; Teixeira, S.P.B.; Taboada, P.; Reis, R.L.; Domingues, R.M.A.; Gomes, M.E. Magnetically-Assisted 3D Bioprinting of Anisotropic Tissue-Mimetic Constructs. Advanced Functional Materials 2022, 32, 2208940, doi:https://doi.org/10.1002/adfm.202208940.
19. Carvalho, P.P.; Wu, X.; Yu, G.; Dias, I.R.; Gomes, M.E.; Reis, R.L.; Gimble, J.M. The Effect of Storage Time on Adipose-Derived Stem Cell Recovery from Human Lipoaspirates. Cells Tissues Organs 2011, 194, 494-500, doi:10.1159/000324892.
20. Yu, G.; Floyd, Z.E.; Wu, X.; Halvorsen, Y.-D.C.; Gimble, J.M. Isolation of human adipose-derived stem cells from lipoaspirates. Methods Mol Biol 2011, 702, 17-27, doi:10.1007/978-1-61737-960-4_2.
21. Hummon, A.B.; Lim, S.R.; Difilippantonio, M.J.; Ried, T. Isolation and solubilization of proteins after TRIzol extraction of RNA and DNA from patient material following prolonged storage. Biotechniques 2007, 42, 467-470, 472, doi:10.2144/000112401.
22. Vasiliadis, A.V.; Katakalos, K. The Role of Scaffolds in Tendon Tissue Engineering. J Funct Biomater 2020, 11, doi:10.3390/jfb11040078.
23. Lee, Y.J.; Elosegui-Artola, A.; Le, K.H.T.; Kim, G.-M. Morphological Cues for Regulation of Cell Adhesion and Motility with Tailored Electrospun Scaffolds of PCL and PCL/PVP Blends. Cellular and Molecular Bioengineering 2013, 6, 482-495, doi:10.1007/s12195-013-0293-8.
24. Wu, S.; Peng, H.; Li, X.; Streubel, P.N.; Liu, Y.; Duan, B. Effect of scaffold morphology and cell co-culture on tenogenic differentiation of HADMSC on centrifugal melt electrospun poly (L-lactic acid) fibrous meshes. Biofabrication 2017, 9, 044106, doi:10.1088/1758-5090/aa8fb8.
25. Uebersax, L.; Hagenmüller, H.; Hofmann, S.; Gruenblatt, E.; Müller, R.; Vunjaknovakovic, G.; Kaplan, D.L.; Merkle, H.P.; Meinel, L. Effect of Scaffold Design on Bone Morphology In Vitro. Tissue Engineering 2006, 12, 3417-3429, doi:10.1089/ten.2006.12.3417.
26. Font Tellado, S.; Bonani, W.; Balmayor, E.R.; Foehr, P.; Motta, A.; Migliaresi, C.; van Griensven, M. Fabrication and Characterization of Biphasic Silk Fibroin Scaffolds for Tendon/Ligament-to-Bone Tissue Engineering. Tissue Eng Part A 2017, 23, 859-872, doi:10.1089/ten.TEA.2016.0460.
27. Peniche Silva, C.J.; Müller, S.A.; Quirk, N.; Poh, P.S.P.; Mayer, C.; Motta, A.; Migliaresi, C.; Coenen, M.J.; Evans, C.H.; Balmayor, E.R.; et al. Enthesis Healing Is Dependent on Scaffold Interphase Morphology-Results from a Rodent Patellar Model. Cells 2022, 11, doi:10.3390/cells11111752.
28. Baldwin, M.; Snelling, S.; Dakin, S.; Carr, A. Augmenting endogenous repair of soft tissues with nanofibre scaffolds. Journal of the Royal Society Interface 2018, 15, 20180019.

29. Graça, A.L.; Domingues, R.M.A.; Gomez-Florit, M.; Gomes, M.E. Platelet-Derived Extracellular Vesicles Promote Tenogenic Differentiation of Stem Cells on Bioengineered Living Fibers. Int J Mol Sci 2023, 24, doi:10.3390/ijms24043516.
30. Kishore, V.; Bullock, W.; Sun, X.; Van Dyke, W.S.; Akkus, O. Tenogenic differentiation of human MSCs induced by the topography of electrochemically aligned collagen threads. Biomaterials 2012, 33, 2137-2144.
31. Bupphathong, S.; Quiroz, C.; Huang, W.; Chung, P.F.; Tao, H.Y.; Lin, C.H. Gelatin Methacrylate Hydrogel for Tissue Engineering Applications-A Review on Material Modifications. Pharmaceuticals (Basel) 2022, 15, doi:10.3390/ph15020171.
32. Li, S.; Sun, J.; Yang, J.; Yang, Y.; Ding, H.; Yu, B.; Ma, K.; Chen, M. Gelatin methacryloyl (GelMA) loaded with concentrated hypoxic pretreated adipose-derived mesenchymal stem cells(ADSCs) conditioned medium promotes wound healing and vascular regeneration in aged skin. Biomaterials Research 2023, 27, 11, doi:10.1186/s40824-023-00352-3.
33. Galliger, Z.; Vogt, C.D.; Helms, H.R.; Panoskaltsis-Mortari, A. Extracellular Matrix Microparticles Improve GelMA Bioink Resolution for 3D Bioprinting at Ambient Temperature. Macromolecular Materials and Engineering 2022, 307, 2200196, doi:https://doi.org/10.1002/mame.202200196.
34. Albrecht, F.B.; Schmidt, F.F.; Volz, A.C.; Kluger, P.J. Bioprinting of 3D Adipose Tissue Models Using a GelMA-Bioink with Human Mature Adipocytes or Human Adipose-Derived Stem Cells. Gels 2022, 8, doi:10.3390/gels8100611.
35. Carthew, J.; Donderwinkel, I.; Shrestha, S.; Truong, V.X.; Forsythe, J.S.; Frith, J.E. In situ miRNA delivery from a hydrogel promotes osteogenesis of encapsulated mesenchymal stromal cells. Acta Biomaterialia 2020, 101, 249-261, doi:https://doi.org/10.1016/j.actbio.2019.11.016.
36. Lolli, A.; Sivasubramaniyan, K.; Vainieri, M.L.; Oieni, J.; Kops, N.; Yayon, A.; van Osch, G.J.V.M. Hydrogel-based delivery of antimiR-221 enhances cartilage regeneration by endogenous cells. Journal of Controlled Release 2019, 309, 220-230, doi:https://doi.org/10.1016/j.jconrel.2019.07.040.
37. Tzavlaki, K.; Moustakas, A. TGF-β Signaling. Biomolecules 2020, 10, doi:10.3390/biom10030487.
38. Berthet, E.; Chen, C.; Butcher, K.; Schneider, R.A.; Alliston, T.; Amirtharajah, M. Smad3 binds Scleraxis and Mohawk and regulates tendon matrix organization. J Orthop Res 2013, 31, 1475-1483, doi:10.1002/jor.22382.
39. Pan, Q.; Guo, C.-J.; Xu, Q.-Y.; Wang, J.-Z.; Li, H.; Fang, C.-H. miR-16 integrates signal pathways in myofibroblasts: determinant of cell fate necessary for fibrosis resolution. Cell Death & Disease 2020, 11, 639, doi:10.1038/s41419-020-02832-z.
40. Font Tellado, S.; Chiera, S.; Bonani, W.; Poh, P.S.P.; Migliaresi, C.; Motta, A.; Balmayor, E.R.; van Griensven, M. Heparin functionalization increases retention of TGF-β2 and GDF5 on biphasic silk fibroin scaffolds for tendon/ligament-to-bone tissue engineering. Acta Biomaterialia 2018, 72, 150-166, doi:https://doi.org/10.1016/j.actbio.2018.03.017.
41. Melzer, M.; Schubert, S.; Müller, S.F.; Geyer, J.; Hagen, A.; Niebert, S.; Burk, J. Rho/ROCK Inhibition Promotes TGF-β3-Induced Tenogenic Differentiation in Mesenchymal Stromal Cells. Stem Cells International 2021, 2021, 8284690, doi:10.1155/2021/8284690.

42. Maeda, T.; Sakabe, T.; Sunaga, A.; Sakai, K.; Rivera, A.L.; Keene, D.R.; Sasaki, T.; Stavnezer, E.; Iannotti, J.; Schweitzer, R. Conversion of mechanical force into TGF-β-mediated biochemical signals. Current Biology 2011, 21, 933-941.
43. Eissa, M.G.; Artlett, C.M. The MicroRNA miR-155 Is Essential in Fibrosis. Noncoding RNA 2019, 5.
44. Theodossiou, S.K.; Murray, J.B.; Hold, L.A.; Courtright, J.M.; Carper, A.M.; Schiele, N.R. Akt signaling is activated by TGFβ2 and impacts tenogenic induction of mesenchymal stem cells. Stem Cell Res Ther 2021, 12, 88, doi:10.1186/s13287-021-02167-2.
45. Dahlin, R.L.; Ni, M.; Meretoja, V.V.; Kasper, F.K.; Mikos, A.G. TGF-β3-induced chondrogenesis in co-cultures of chondrocytes and mesenchymal stem cells on biodegradable scaffolds. Biomaterials 2014, 35, 123-132, doi:10.1016/j.biomaterials.2013.09.086.

CHAPTER 7

# General Discussion

# 1 DISCUSSION

The tendon-to-bone enthesis remains a challenging site of injury due to its structural complexity, poor inherent healing capacity, and inefficient scar tissue formation upon injury. Addressing these challenges requires a comprehensive understanding of the biomechanics and biology of the tendon-to-bone enthesis, as well as the development of advanced therapeutic approaches that promote effective healing and tissue regeneration. The work presented in this thesis is aimed to advance the field of tendon and enthesis tissue-engineering as complement or even alternative to the currently available therapies. Hereafter, we will discuss the most significant aspects dealt with in the different chapters of this thesis, including the selection of our animal model, the use of biomimetic biomaterials, and the potential use of miRNAs as therapeutic tools for tendon and enthesis tissue-engineering. Finally, we will explore future directions towards a more efficient healing of this intrincate interphase tissue.

## 1.1 Selection of an animal model for enthesis regeneration studies

Interphase tissues are remarkably difficult to study. Such difficulty arises from many angles, and one of the most overlooked ones has to do with the delimitation of the tissue per se. By attaching tendons to bones, the enthesis exhibits both tendon and bony zones. However, the term "enthesis" is generally used to refer to the continuous structural gradient between both. Although such a definition is broadly accepted, it fails to clearly define the beginning and end of the enthesis. Similarly, the delimitation between the four zones for the fibrocartilaginous entheses or the three zones in the fibrous entheses is, in many cases, just an approximation.

The lack of precise boundaries for the enthesis and its zones is a limitation that could potentially affect the reproducibility and interpretation of results, especially when working with small animal models such as mice or rats. However, rodent models are cheaper and easier to handle than their larger counterparts [1]. Furthermore, mice and rats have been used as animal models extensively, and they continue to be widely employed and studied [2]. These are important practical advantages compared to larger animal models like sheep or horses. Hence, we opted for rats as an animal model for our enthesis studies. However, to ensure the optimal selection of our rodent enthesis model, we proceeded to characterize the three most relevant sites of enthesis injury (i.e. Supraspinatus enthesis, Achilles tendon enthesis, and patellar tendon enthesis) in these animals. This characterization is described in detail in chapter 3 [3]. There, we standardized the limits of the enthesis tissue for each localization ensuring that, when isolating the entheses, equal portions of the tendon and bony zones would be included in the explant together with the interphase tissue. We then investigated

mechanical and physical properties, histological features, and gene expression, which allowed for the assessment of the similarities and differences between the three entheses. Finally, we selected the patellar tendon enthesis as our model for enthesis regeneration studies, in particular, due to the larger cross-sectional area of the tendon-to-bone insertion site, the strong mechanical properties, and the easier access to this localization.

Such comparative characterizations between different anatomical localizations are very useful as they allow for pinpointing specific features for each site. In a similar study, Lee *et al*. compared the hierarchical organization of three different tendons using a rat model for tendinopathies [4]. They investigated the rat's tail tendon, the plantaris tendon, and the Achilles tendon. As a result, they described distinct features for each tendon related to their localization and mechanical function, and proposed that each tendon could be used to answer specific research questions. Similarly, Prodinger *et al*. characterized the biomechanical behavior and radiological characteristics of the humerus, the tibia, and the femur in rats [5]. This comparison allowed the authors to determine that the rat's femur offers the most accurate and consistent biomechanical results, thus, offering the best mechanical features for the three-point bending experiments used in many rat fracture models.

By performing the comparative characterization between three clinically relevant sites of enthesis injury described in Chapter 3, we attempted to maximize the reproducibility of our future work and facilitate the translation of pre-clinical investigation for specific enthesis injury sites. Furthermore, we established an enthesis injury model that was successfully used in chapters 4 and 5 to investigate enthesis regeneration and healing.



### 1.2 Biomimetic scaffolds for enthesis regeneration

The use of biomimetic scaffolds to recapitulate native morphological features for the treatment of injured tissues has a direct and positive effect on cell proliferation, differentiation, ECM deposition, and tissue growth [6-9]. The search for efficient designs of enthesis-biomimetic constructs capable of enhancing the regeneration of the continuous tendon-to-bone interphase has led to a wide range of promising findings in the last couple of decades [10-13]. In this context, most of the biomimetic strategies aim to develop multilayer scaffolds consisting of two to three different phases imitating the morphological and mechanical properties of each one of the zones of the tendon-to-bone interphase.

Most published data advocate for the compartmentalization of the enthesis zones in the scaffold design to ensure the correct cell differentiation and ECM deposition at each one of the enthesis zones. However, in Chapter 4 we

investigated and discussed the positive impact on enthesis regeneration for the interphase between the two phases of a biphasic silk-fibroin enthesis scaffold that was designed and produced to exhibit a tendon zone, a bony zone, and an interconnected transition between the two [14]. Thus, demonstrating that the interconnection between the phases was not only important but also desired to achieve efficient tissue integration.

In the same way, other authors reported comparable positive outcomes regarding enthesis healing when similarly designed constructs were developed for enthesis tissue engineering applications [15-17]. Thus, we believe that, at least for the foreseeable future, the design of scaffolds/constructs for enthesis regeneration will follow the same basic principle, which is to mimic not only the morphology of the tendon, fibrocartilage, and bony phases but also the interconnection between these phases. Moreover, advances in 3D printing, electrospinning, and nanotechnology will allow for better and more precise design of biomimetic constructs, capable of a more accurate recapitulation of the native enthesis morphology.

However, when it comes to the selection of the biomaterial for the development of such constructs, a plethora of options are available, and new ones are being developed every day [18]. In Chapter 2, we discussed the applications and potential of silk biomaterials in tendon and enthesis tissue engineering applications. Silk is a highly attractive biomaterial as it exhibits great biocompatibility and a wide range of mechanical properties and tunable physical structures [19]. Hence, it can be used as a base material for tissue engineering applications for both soft and hard tissues [20,21]. Which makes it an ideal candidate for tissue engineering of soft-to-hard tissue interphases.

Our group has explored enhancing the advantages offered by silk fibroin as a biomaterial for tissue engineering applications via surface modifications [10,22]. First, it was demonstrated that surface modification with lectin wheat germ agglutinin (WGA) increased cell adhesion without affecting the proliferation and differentiation of adipose-derived stem cells (hASC). Hence, suggesting that WGA modification of silk fibroin offers important benefits for the translation of silk fibroin scaffolds into clinical applications [22]. Later, it was shown that heparin functionalization of silk fibroin scaffolds resulted in increased retention of TGF-β2 and GDF5, which allowed for a synergistic effect of biological and structural cues on the differentiation of stem cells *in vitro* [10]. We have already demonstrated *in vivo* the importance of the interconnected structural morphology of our silk fibroin scaffolds on the regeneration and healing of the enthesis [14]. Thus, we will continue to explore the enhancement of such healing capabilities by surface modification using *in vivo* settings in future studies.

### 1.3 miRNAs for enthesis tissue engineering

Upon injury, the mechanisms of enthesis healing elicit the formation of fibrous scar tissue at the site of injury that can extend towards the tendon side of the enthesis, potentially affecting the mechanical properties not only of the injured interphase tissue but also of the adjacent tendon [14,23]. We described in Chapter 5 the occurrence of fibrosis and ectopic ossification in the tendon portion of a rat patellar enthesis after the creation of an injury at the tendon-to-bone insertion site. Fibrosis is a major complication in healing tendons that increases the risk of subsequent chronic tendinopathies and for which there is no effective treatment beyond improvements in surgical and rehabilitation protocols [24,25]. It has been hypothesized that the insufficient healing of enthesis and tendon tissues is related to the low cellularity and vascularity of these tissues, thus suggesting the need for tissue engineering strategies focused on the reduction of fibrosis and the enhancement of the true regeneration of the tendon and/or enthesis, rather than normal fibrotic scar formation [24].

By performing the characterization of the healing process of the injured rat patellar enthesis, we identified a set of dysregulated miRNAs at different time points as a result of the injury. Among these, miR-16-5p was one of the most upregulated [23]. Consequently, in Chapter 6, we investigated the effect of miR-16-5p on the tenogenic commitment of hASCs in a tendon-mimetic microenvironment. Thus, describing a potential therapeutic use for miR-16-5p in the quest against fibrosis and toward the tenogenic differentiation of hASCs. However, each one of the miRNAs found by us to be dysregulated in the injured patellar enthesis samples is worth further investigation as many of them have mRNA targets which are, or can be relevant, for the process of healing, scar formation, and enthesis regeneration [23].

The potential use of miRNAs as therapeutic candidates for tissue engineering is an emerging field of study that holds great promise for the treatment not only of acute tendon and enthesis injuries but also for chronic, degenerative tendinopathies such as Ankylosing Spondylitis [26,27]. However, the development of efficient miRNA-based therapies is hindered by important limitations including poor stability of naked miRNA and the need for efficient and safe delivery methods of the miRNA/inhibitor probes to the injured tissue [28,29]. Consequently, by 2021, less than 20 miRNA-targeting molecules had entered clinical trials and none progressed to phase III [30].

The work described in Chapter 6 involving the use of miRNA mimics and inhibitors was possible thanks to the advances in LNA™ (locked nucleic acid) technology. LNA technology is based on the use of a bicyclic high-affinity RNA mimic in which the sugar ring is locked in the 3'-endo conformation by introducing a methylene

bridge group connecting the 2'-O atom with the 4'-C atom. This modification greatly enhances the affinity of the probe for its complementary target while simultaneously increasing specificity and mismatch discrimination ability [31].

Additionally, a broad range of transfection agents are being investigated for the specific delivery of miRNA to their target cells [32]. Among these, lipid-based transfection agents are the most popular ones, yielding miRNA complexes with variable particle size and charge, which greatly impacts transfection efficiency [33]. Alternatively, other studies show that chemical modification of miRNAs (e.g. internucleotide linkage modifications, sugar modifications, nucleo-base modifications) could enhance the reagent-free delivery capability of miRNA probes and avoid some of the concerns related to the use of transfection reagents like delivery-associated toxicity, poor transfection efficiency, systemic clearance of the delivery agent, and non-specific biodistribution [34-36].

### 1.4 Future directions

The work comprised in this thesis is aimed towards the improvement of enthesis healing. We demonstrated that a detailed characterization of the healthy tissue is necessary and important prior to the design of efficient tissue engineering strategies to deal with the respective injured enthesis tissue. Not every enthesis is created equally and therefore, a carefully tailored strategy to deal with specific enthesis tissues can maximize the outcome of the therapy. To some extent, this personalized treatment approach has been the preferred way to go when researching tissue engineering strategies to treat the most common sites of enthesis injury (*i.e.,* rotator cuff, Achilles tendon, patellar tendon) [37-39]. We can only expect that with the progressive gain in knowledge regarding the molecular and morphological basis of enthesis injury and consequent healing, new therapies will allow for a better, more efficient healing of the tendon-to-bone enthesis in a tailored manner to meet the specific requirements of each enthesis localization.

Similarly, advances in biomaterial science are still needed until we are able to produce enthesis scaffolds for implantation in humans that can emulate the mechanical properties not only of the tendon or the bone individually, but the tendon-to-bone interphase. In Chapter 3, we demonstrated that silk fibroin is a suitable material for treating enthesis defects *in vivo*. However, we did not explore the enhancement of the mechanical properties of the scaffold by modifications with gradients of mineralization or combinations with other biomaterials. On the one hand, mineralization gradients towards the bony side of entheses scaffolds have been proven to induce the desired graded osteogenic differentiation that could lead to better osteointegration [40]. On the other hand, hybrid scaffolds, combining different biomaterials and manufacturing techniques allow for the

fine-tuning of the mechanical properties and the osteogenic, chondrogenic, and tenogenic differentiation required at the tendon-to-bone interphase [15,41].

We finalized this thesis work by investigating the potential use of miRNAs as therapeutic tools to modulate gene expression and aid the process of cell differentiation and ultimately, enthesis healing. We opted for the modulation of miR-16-5p, an antifibrotic miRNA capable of regulating the TGF-β pathway by inhibition of *SMAD*3. When working with miRNAs, modulation is a keyword, as the effects of the modification of the miRNA levels usually induce relatively small changes in gene and protein expression [26,42,43]. Nevertheless, such small changes are often sufficient to elicit the desired response, as we described in Chapter 6.

We explored the delivery of miRNA probes to ASCs encapsulated in a GelMa-based, magnetically responsive bioink. Beyond the potential uses for such bioactive bioink in the 3D printing of tendon or enthesis mimetic structures, it could be an attractive solution for tissue augmentation and the development of injectable systems that would allow for the localized delivery of both miRNA and cells to the site of injury to aid healing and regeneration. The augmentation of tendon healing via the injection of tendon hydrogels has shown promising results *in vivo* [44-46]. Hence, a tendon mimetic hydrogel that is able to deliver miRNA mimic or inhibitor probes, to enhance the tenogenic commitment of the encapsulated cells, holds the great promise of improving tendon and enthesis healing, minimizing fibrosis, and enhancing the regeneration of the native features that characterize the uninjured tissue.

## 2 REFERENCES


1. Warden, S.J. Animal models for the study of tendinopathy. Br J Sports Med 2007, 41, 232-240, doi:10.1136/bjsm.2006.032342.
2. Bryda, E.C. The Mighty Mouse: the impact of rodents on advances in biomedical research. Mo Med 2013, 110, 207-211.
3. Peniche Silva, C.J.; Müller, S.A.; Quirk, N.; De la Vega, R.E.; Coenen, M.J.; Evans, C.H.; Balmayor, E.R.; van Griensven, M. Enthesis: not the same in each localisation - a molecular, histological and biomechanical study. Eur Cell Mater 2022, 44, 43-55, doi:10.22203/eCM.v044a03.
4. Lee, A.H.; Elliott, D.M. Comparative multi-scale hierarchical structure of the tail, plantaris, and Achilles tendons in the rat. J Anat 2019, 234, 252-262, doi:10.1111/joa.12913.
5. Prodinger, P.M.; Foehr, P.; Bürklein, D.; Bissinger, O.; Pilge, H.; Kreutzer, K.; von Eisenhart-Rothe, R.; Tischer, T. Whole bone testing in small animals: systematic characterization of the mechanical properties of different rodent bones available for rat fracture models. European Journal of Medical Research 2018, 23, 8, doi:10.1186/s40001-018-0307-z.
6. Park, J.Y.; Park, S.H.; Kim, M.G.; Park, S.H.; Yoo, T.H.; Kim, M.S. Biomimetic Scaffolds for Bone Tissue Engineering. Adv Exp Med Biol 2018, 1064, 109-121, doi:10.1007/978-981-13-0445-3_7.
7. Huang, L.; Chen, L.; Chen, H.; Wang, M.; Jin, L.; Zhou, S.; Gao, L.; Li, R.; Li, Q.; Wang, H.; et al. Biomimetic Scaffolds for Tendon Tissue Regeneration. Biomimetics 2023, 8, doi:10.3390/biomimetics8020246.
8. Boughton, E.; McLennan, S.V. 6 - Biomimetic scaffolds for skin tissue and wound repair. In Biomimetic Biomaterials, Ruys, A.J., Ed.; Woodhead Publishing: 2013; pp. 153-180.
9. Learn, G.D.; McClellan, P.E.; Knapik, D.M.; Cumsky, J.L.; Webster-Wood, V.; Anderson, J.M.; Gillespie, R.J.; Akkus, O. Woven collagen biotextiles enable mechanically functional rotator cuff tendon regeneration during repair of segmental tendon defects in vivo. Journal of Biomedical Materials Research Part B: Applied Biomaterials 2019, 107, 1864-1876.
10. Font Tellado, S.; Chiera, S.; Bonani, W.; Poh, P.S.P.; Migliaresi, C.; Motta, A.; Balmayor, E.R.; van Griensven, M. Heparin functionalization increases retention of TGF-β2 and GDF5 on biphasic silk fibroin scaffolds for tendon/ligament-to-bone tissue engineering. Acta Biomaterialia 2018, 72, 150-166, doi:https://doi.org/10.1016/j.actbio.2018.03.017.
11. Nowlin, J.; Bismi, M.A.; Delpech, B.; Dumas, P.; Zhou, Y.; Tan, G.Z. Engineering the hard-soft tissue interface with random-to-aligned nanofiber scaffolds. Nanobiomedicine (Rij) 2018, 5, 1849543518803538-1849543518803538, doi:10.1177/1849543518803538.
12. Spalazzi, J.P.; Dagher E Fau - Doty, S.B.; Doty Sb Fau - Guo, X.E.; Guo Xe Fau - Rodeo, S.A.; Rodeo Sa Fau - Lu, H.H.; Lu, H.H. In vivo evaluation of a multiphased scaffold designed for orthopaedic interface tissue engineering and soft tissue-to-bone integration. 2008.
13. Xu, K.; Kuntz, L.A.; Foehr, P.; Kuempel, K.; Wagner, A.; Tuebel, J.; Deimling, C.V.; Burgkart, R.H. Efficient decellularization for tissue engineering of the tendon-bone interface with preservation of biomechanics. PLoS One 2017, 12, e0171577.

14. Peniche Silva, C.J.; Müller, S.A.; Quirk, N.; Poh, P.S.P.; Mayer, C.; Motta, A.; Migliaresi, C.; Coenen, M.J.; Evans, C.H.; Balmayor, E.R.; et al. Enthesis Healing Is Dependent on Scaffold Interphase Morphology-Results from a Rodent Patellar Model. Cells 2022, 11, doi:10.3390/cells11111752.
15. Gottardi, R.; Moeller, K.; Di Gesù, R.; Tuan, R.S.; van Griensven, M.; Balmayor, E.R. Application of a Hyperelastic 3D Printed Scaffold for Mesenchymal Stem Cell-Based Fabrication of a Bizonal Tendon Enthesis-like Construct. Frontiers in Materials 2021, 8.
16. Sensini, A.; Massafra, G.; Gotti, C.; Zucchelli, A.; Cristofolini, L. Tissue Engineering for the Insertions of Tendons and Ligaments: An Overview of Electrospun Biomaterials and Structures. Frontiers in Bioengineering and Biotechnology 2021, 9, 98.
17. Chen, P.; Li, L.; Dong, L.; Wang, S.; Huang, Z.; Qian, Y.; Wang, C.; Liu, W.; Yang, L. Gradient Biomineralized Silk Fibroin Nanofibrous Scaffold with Osteochondral Inductivity for Integration of Tendon to Bone. ACS Biomaterials Science & Engineering 2021, 7, 841-851, doi:10.1021/acsbiomaterials.9b01683.
18. Li, Y.; Zhou, M.; Zheng, W.; Yang, J.; Jiang, N. Scaffold-based Tissue Engineering Strategies for Soft-hard Interface Regeneration. Regenerative Biomaterials 2022, 10, doi:10.1093/rb/rbac091.
19. Vepari, C.; Kaplan, D.L. Silk as a Biomaterial. Prog Polym Sci 2007, 32, 991-1007, doi:10.1016/j.progpolymsci.2007.05.013.
20. Wu, H.; Lin, K.; Zhao, C.; Wang, X. Silk fibroin scaffolds: A promising candidate for bone regeneration. Frontiers in Bioengineering and Biotechnology 2022, 10.
21. Yao, D.; Liu, H.; Fan, Y. Silk scaffolds for musculoskeletal tissue engineering. Experimental biology and medicine 2016, 241, 238-245.
22. Teuschl, A.H.; Neutsch, L.; Monforte, X.; Rünzler, D.; van Griensven, M.; Gabor, F.; Redl, H. Enhanced cell adhesion on silk fibroin via lectin surface modification. Acta Biomaterialia 2014, 10, 2506-2517, doi:https://doi.org/10.1016/j.actbio.2014.02.012.
23. Peniche Silva, C.J.; De La Vega, R.E.; Panos, J.; Joris, V.; Evans, C.H.; Balmayor, E.R.; van Griensven, M. MiRNAs as Potential Regulators of Enthesis Healing: Findings in a Rodent Injury Model. International Journal of Molecular Sciences 2023, 24, doi:10.3390/ijms24108556.
24. Nichols, A.E.C.; Best, K.T.; Loiselle, A.E. The cellular basis of fibrotic tendon healing: challenges and opportunities. Transl Res 2019, 209, 156-168, doi:10.1016/j.trsl.2019.02.002.
25. Derwin, K.A.; Galatz, L.M.; Ratcliffe, A.; Thomopoulos, S. Enthesis Repair: Challenges and Opportunities for Effective Tendon-to-Bone Healing. J Bone Joint Surg Am 2018, 100, e109-e109, doi:10.2106/JBJS.18.00200.
26. Motta, F.; Carena, M.C.; Selmi, C.; Vecellio, M. MicroRNAs in ankylosing spondylitis: Function, potential and challenges. Journal of Translational Autoimmunity 2020, 3, 100050, doi:https://doi.org/10.1016/j.jtauto.2020.100050.
27. Bhaskaran, M.; Mohan, M. MicroRNAs: History, Biogenesis, and Their Evolving Role in Animal Development and Disease. Veterinary Pathology 2013, 51, 759-774, doi:10.1177/0300985813502820.
28. Segal, M.; Slack, F.J. Challenges identifying efficacious miRNA therapeutics for cancer. Expert Opin Drug Discov 2020, 15, 987-992, doi:10.1080/17460441.2020.1765770.

29. Segal, M.; Biscans, A.; Gilles, M.E.; Anastasiadou, E.; De Luca, R.; Lim, J.; Khvorova, A.; Slack, F.J. Hydrophobically Modified let-7b miRNA Enhances Biodistribution to NSCLC and Downregulates HMGA2 In Vivo. Mol Ther Nucleic Acids 2020, 19, 267-277, doi:10.1016/j.omtn.2019.11.008.
30. Momin, M.Y.; Gaddam, R.R.; Kravitz, M.; Gupta, A.; Vikram, A. The Challenges and Opportunities in the Development of MicroRNA Therapeutics: A Multidisciplinary Viewpoint. Cells 2021, 10, doi:10.3390/cells10113097.
31. Roberts, P.; Noerholm, M.; Ståhlberg, N.; Mouritzen, P.; Glue, C. miRCURY™ LNA research tools for microRNA. Nature Methods 2006, 3, I-II, doi:10.1038/nmeth920.
32. Kucharski, M.; Mrowiec, P.; Białka, S.; Misiołek, H.; Misiołek, M.; Sechman, A.; Zięba-Przybylska, D.; Ocłoń, E. Non-viral transfection methods optimized for miRNA delivery to human dermal fibroblasts. Mol Med Rep 2023, 27, 89, doi:10.3892/mmr.2023.12976.
33. Carthew, J.; Donderwinkel, I.; Shrestha, S.; Truong, V.X.; Forsythe, J.S.; Frith, J.E. In situ miRNA delivery from a hydrogel promotes osteogenesis of encapsulated mesenchymal stromal cells. Acta Biomaterialia 2020, 101, 249-261, doi:https://doi.org/10.1016/j.actbio.2019.11.016.
34. Deleavey, G.F.; Damha, M.J. Designing chemically modified oligonucleotides for targeted gene silencing. Chemistry & biology 2012, 19, 937-954.
35. Durso, M.; Gaglione, M.; Piras, L.; Mercurio, M.E.; Terreri, S.; Olivieri, M.; Marinelli, L.; Novellino, E.; Incoronato, M.; Grieco, P.; et al. Chemical modifications in the seed region of miRNAs 221/222 increase the silencing performances in gastrointestinal stromal tumor cells. European Journal of Medicinal Chemistry 2016, 111, 15-25, doi:https://doi.org/10.1016/j.ejmech.2016.01.047.
36. Segal, M.; Biscans, A.; Gilles, M.-E.; Anastasiadou, E.; De Luca, R.; Lim, J.; Khvorova, A.; Slack, F.J. Hydrophobically Modified let-7b miRNA Enhances Biodistribution to NSCLC and Downregulates HMGA2 In Vivo. Molecular Therapy - Nucleic Acids 2020, 19, 267-277, doi:https://doi.org/10.1016/j.omtn.2019.11.008.
37. Aicale, R.; Oliviero, A.; Maffulli, N. Management of Achilles and patellar tendinopathy: what we know, what we can do. Journal of Foot and Ankle Research 2020, 13, 59, doi:10.1186/s13047-020-00418-8.
38. Zheng, Z.; Ran, J.; Chen, W.; Hu, Y.; Zhu, T.; Chen, X.; Yin, Z.; Heng, B.C.; Feng, G.; Le, H. Alignment of collagen fiber in knitted silk scaffold for functional massive rotator cuff repair. Acta biomaterialia 2017, 51, 317-329.
39. Teuschl, A.; Heimel, P.; Nürnberger, S.; van Griensven, M.; Redl, H.; Nau, T. A Novel Silk Fiber–Based Scaffold for Regeneration of the Anterior Cruciate Ligament: Histological Results From a Study in Sheep. The American Journal of Sports Medicine 2016, 44, 1547-1557, doi:10.1177/0363546516631954.
40. Liu, W.; Lipner, J.; Xie, J.; Manning, C.N.; Thomopoulos, S.; Xia, Y. Nanofiber Scaffolds with Gradients in Mineral Content for Spatial Control of Osteogenesis. ACS Applied Materials & Interfaces 2014, 6, 2842-2849, doi:10.1021/am405418g.
41. Baawad, A.; Jacho, D.; Hamil, T.; Yildirim-Ayan, E.; Kim, D.-S. Polysaccharide-Based Composite Scaffolds for Osteochondral and Enthesis Regeneration. Tissue Engineering Part B: Reviews 2022, 29, 123-140, doi:10.1089/ten.teb.2022.0114.
42. Lolli, A.; Sivasubramaniyan, K.; Vainieri, M.L.; Oieni, J.; Kops, N.; Yayon, A.; van Osch, G.J.V.M. Hydrogel-based delivery of antimiR-221 enhances cartilage regeneration by endogenous cells. Journal of Controlled Release 2019, 309, 220-230, doi:https://doi.org/10.1016/j.jconrel.2019.07.040.

43. Yao, Q.; Xing, Y.; Wang, Z.; Liang, J.; Lin, Q.; Huang, M.; Chen, Y.; Lin, B.; Xu, X.; Chen, W. MiR-16-5p suppresses myofibroblast activation in systemic sclerosis by inhibiting NOTCH signaling. Aging (Albany NY) 2020, 13, 2640-2654.
44. Kim, M.Y.; Farnebo, S.; Woon, C.Y.L.; Schmitt, T.; Pham, H.; Chang, J. Augmentation of tendon healing with an injectable tendon hydrogel in a rat Achilles tendon model. Plast Reconstr Surg 2014, 133, 645e-653e, doi:10.1097/prs.0000000000000106.
45. Longo, U.G.; Lamberti, A.; Maffulli, N.; Denaro, V. Tendon augmentation grafts: a systematic review. British Medical Bulletin 2010, 94, 165-188, doi:10.1093/bmb/ldp051.
46. Kaizawa, Y.; Franklin, A.; Leyden, J.; Behn, A.W.; Tulu, U.S.; Sotelo Leon, D.; Wang, Z.; Abrams, G.D.; Chang, J.; Fox, P.M. Augmentation of chronic rotator cuff healing using adipose-derived stem cell-seeded human tendon-derived hydrogel. Journal of Orthopaedic Research® 2019, 37, 877-886.

CHAPTER 8

# Valorization

## 1 VALORIZATION

Tendons and tendon-to-bone entheses play a fundamental role in the movement of the joints upon muscle contraction. Thus, injuries at the tendon or the entheses can significantly impair movement, locomotion, and the quality of life of the injured patient. This can represent a significant societal and economic burden.

Tendinopathies and enthesopathies refer to different pathological conditions that affect the normal physiological function of the tissue. They can result from inflammation and/or chronic degeneration of the tissues and are usually associated with pain and reduced range of motion of the affected joint. Nevertheless, tendon and enthesis injuries can also occur due to a spontaneous rupture of the tendon or the tendon-to-bone attachment at the enthesis (e.g., total or partial tendon/enthesis tear). Although these ruptures can take place without previous symptoms, they are usually attributed to mechanical weakness of the tendon or the enthesis due to pathological changes in the tissues [1]. Such changes can be due to mechanical overuse, vascularisation, or aging. However, tendon rupture can occur in perfectly healthy tendons and entheses when the tissue is subjected to tensile loads exceeding their capacity. This is more likely to happen during the practice of sports. Hence, the majority of tendon and/or enthesis injuries are related to the practice of sports and high-impact physical activities, accounting for 50% of all sports-related injuries [2].

High-contact sports like basketball, football, or hockey are particularly prone to such injuries. Additionally, repetitive movements and strains in sports like tennis and water sports can lead to injuries such as rotator cuff injuries, tennis elbow, and joint dislocation. In the United States alone, more than 3.5 million sports injuries occur annually, with sprains and strains being the most common. Moreover, the incidence of tendon/enthesis ruptures in Europe has been estimated to be about 80 in 100,000, while in the United States the incidence tends to be higher, about 95 in 100,000 [3]. Furthermore, the prevalence of tendon and enthesis injuries is rapidly growing due to, among other reasons, the increase in the practice of sports by the elderly population (> 60 years old) [4].

Interestingly, the incidence of tendon and enthesis injuries has also seen an increase among the less active members of the population where a sedentary lifestyle and rising rates of obesity, diabetes, and the abuse of mutagens like alcohol and tobacco smoke have been correlated with the increase in tendon and enthesis injuries. In total, tendon and enthesis injuries account for about 30% of all musculoskeletal consultations [5,6].

As it has been extensively discussed in this thesis, the mechanisms of healing of injured tendons and enthesis often fail to regenerate the native morphology and mechanical properties of the uninjured tissue. Moreover, patients suffering from tendon and enthesis injury undergo a long and often painful path to recovery [7].

Tendon injuries are currently treated by conservative therapies or surgery with very limited success. Approximately three out of ten patients suffering from tendon or enthesis injuries undergo surgery after failure of conservative therapies. Moreover, some reports indicate that only about 60 % of all restored tendons are functional [7]. All in all, the currently available treatments for tendon and enthesis injuries suffer from significant limitations, ranging from suboptimal healing to the risk of re-injury, and post-operative complications [2,8,9].

The advances in the development and application of tissue engineering strategies aimed to aid the healing of difficult-to-treat tissues hold significant promise for tendon and enthesis healing. In Chapters 2 and 4 of this thesis, we discussed the use of silk as biomaterial to treat tendon and enthesis defects. Silk-based biomaterials, such as silk fibroin, offer remarkable properties that make them ideal for tendon and enthesis healing. Using silk fibroin, it is possible to mimic the extracellular matrix of tendons and tendon-to-bone attachments, while promoting cell adhesion, proliferation, and tissue growth. Moreover, effective tendon healing involves reducing the formation of scar tissue, as excessive scarring can impair tendon function. Silk-based biomaterials, with their ability to guide tissue growth, may help minimize scar formation. This was demonstrated in Chapter 4, where the use of an enthesis-mimetic silk-fibroin scaffold yielded the best healing of an injured patellar enthesis in our rodent model. Furthermore, the use of silk as biomaterial enhances the mechanical properties of the healing tissue, making it more resilient and less prone to re-injury. This could be especially relevant when treating athletes and other patients with high demands on their tendons.



Additionally, in Chapters 5 and 6 we investigated the potential of microRNAs (miRNAs) for tissue engineering applications. miRNA-based therapies allow for the precise regulation of gene and protein expression, which can be crucial in the modulation of the healing response of an injured tissue. In the same way, they can be used to restore lost function or treat diseases. Such potential has encouraged a multitude of miRNA-based therapies targeting a wide range of diseases, some of which have reached clinical trials with promising results, which demonstrates the translational potential of these therapies to the clinic. The LNA-based antagomir Cobomarsen (MRG-106) that targets miR-155, is currently in phase II trials for the treatment of cutaneous T-cell lymphoma and leukaemia [10]. MRG-107, another inhibitor of the miR-155 has alleviated symptoms and extended the survival in preclinical trials of patients suffering from amyotrophic

lateral sclerosis [10]. Moreover, the liposomal formulation of miR-34a known as MRX34 is currently in phase I clinical trial exploring the tumor-suppressing effect of this miRNA for the treatment of a wide range of cancers, including ovarian cancer, colon cancer, cervical cancer, and others [11].

We explored the synergistic effect of a tendon mimetic microenvironment and the modulation of an antifibrotic miRNA to enhance the tenogenic commitment of mesenchymal stem cells with promising results. Thus, giving the first steps towards novel tissue engineering strategies were the combinations of suitable biomaterials with optimized biomimetic morphology and the regulation of gene expression via the modulation of naturally occurring miRNAs brings us closer to the effective healing of tendon-to-bone attachments.

The work summarized in this thesis offers valuable insights into potentially efficient tissue-engineering approaches to aid the healing of the tendon-to-bone enthesis. As the knowledge about the underlying mechanisms of enthesis and tendon healing growths, our understanding of the potential of morphological and molecular cues to aid the process of regeneration increases, opening more opportunities for innovation and the optimization of treatment strategies. Ultimately, offering faster and more effective recovery, minimizing scar tissue formation, and reducing the risk of re-injury of patients suffering from tendon and enthesis injuries.

## 2 REFERENCES


1. Kader, D.; Mosconi, M.; Benazzo, F.; Maffulli, N. Achilles Tendon Rupture. In Tendon Injuries: Basic Science and Clinical Medicine, Maffulli, N., Renström, P., Leadbetter, W.B., Eds.; Springer London: London, 2005; pp. 187-200.
2. Wu, F.; Nerlich, M.; Docheva, D. Tendon injuries: Basic science and new repair proposals. 2017, doi:10.1302/2058-5241.2.160075.
3. Bergamin, F.; Civera, M.; Rodriguez, M.; Burgio, V.; Grimaldo, O.; Surace, C. Worldwide Incidence and Surgical Costs of Tendon Injuries: A Systematic Review and Meta-Analysis. Muscle Ligaments and Tendons Journal 2023, 13, 31, doi:10.32098/mltj.01.2023.05.
4. Kujala, U.M.; Sarna, S.; Kaprio, J. Cumulative incidence of Achilles tendon rupture and tendinopathy in male former elite athletes. Clinical Journal of Sport Medicine 2005, 15, 133-135.
5. Jordan, K.P.; Jöud, A.; Bergknut, C.; Croft, P.; Edwards, J.J.; Peat, G.; Petersson, I.F.; Turkiewicz, A.; Wilkie, R.; Englund, M. International comparisons of the consultation prevalence of musculoskeletal conditions using population-based healthcare data from England and Sweden. Annals of the Rheumatic Diseases 2014, 73, 212, doi:10.1136/annrheumdis-2012-202634.
6. Andarawis-Puri, N.; Flatow, E.L.; Soslowsky, L.J. Tendon basic science: Development, repair, regeneration, and healing. Journal of Orthopaedic Research 2015, 33, 780-784, doi:https://doi.org/10.1002/jor.22869.
7. Rees, J.D.; Wilson, A.M.; Wolman, R.L. Current concepts in the management of tendon disorders. Rheumatology (Oxford) 2006, 45, 508-521, doi:10.1093/rheumatology/kel046.
8. El Hawary, R.; Stanish, W.D.; Curwin, S.L. Rehabilitation of Tendon Injuries in Sport. Sports Medicine 1997, 24, 347-358, doi:10.2165/00007256-199724050-00006.
9. Snedeker, J.G.; Foolen, J. Tendon injury and repair – A perspective on the basic mechanisms of tendon disease and future clinical therapy. Acta Biomaterialia 2017, 63, 18-36, doi:https://doi.org/10.1016/j.actbio.2017.08.032.
10. Iacomino, G. miRNAs: The Road from Bench to Bedside. Genes (Basel) 2023, 14, doi:10.3390/genes14020314.
11. Beg, M.S.; Brenner, A.J.; Sachdev, J.; Borad, M.; Kang, Y.-K.; Stoudemire, J.; Smith, S.; Bader, A.G.; Kim, S.; Hong, D.S. Phase I study of MRX34, a liposomal miR-34a mimic, administered twice weekly in patients with advanced solid tumors. Investigational new drugs 2017, 35, 180-188.

CHAPTER 9

# Public Summary

## PUBLIC SUMMARY

Tendons connect muscle to bone and therefore, they are of paramount importance for the movement and the stabilization of joints. The interphase tissue connecting muscles and tendons is called myotendinous junction, and the interphase between tendons and bones is called enthesis. The tendon-to-bone enthesis is perhaps one of the most challenging interphase tissues to study and treat upon injury. This is due to the fact that the enthesis connects two tissues with very different mechanical properties.

The soft-to-hard transition found at the tendon-to-bone enthesis consists of opposite gradients of collagen alignment and mineralization that allow for a smooth stress transfer from tendons to bone. However, the physiology of the tendon-to-bone enthesis makes this tissue often a site of injury. Unfortunately, the healing process of the enthesis often yields scar tissue with poor mechanical properties, which increases the chance of re-injury of the affected tissue.

The currently available therapies and surgical approaches to treat enthesis injuries suffer from significant failure rates and patients from tendon or enthesis injuries are likely to suffer from re-injuries in the future, even after surgical intervention to reintegrate the tendon to the bone.

Advances in tissue engineering offer the hope of developing novel strategies to enhance the regeneration of the tendon-to-bone attachment site while minimizing scar formation and maximizing the recapitulation of the native morphological and mechanical features of the injured tissue. In **Chapter 2** of this book, we summarized the state of the art in terms of current tendon and enthesis therapies and the use of biomaterials to enhance and promote the healing and regeneration of the enthesis. Furthermore, we stress the potential of silk biomaterials in tendon- and enthesis-tissue engineering applications. Silk is an attractive biocompatible and cost-effective biomaterial with mechanical properties comparable to those of the tendon. Additionally, silk-based biomaterials can be combined with other elements and materials to create hybrid constructs to improve biocompatibility and to better mimic the micro- and macro-environment of the tendon-to-bone attachment site. However, in our bodies, we count hundreds of tendon-to-bone entheses, each one of them with highly specialized morphology, specifically tailored for their anatomical localization and physiology. Thus, in **Chapter 3** we investigated the mechanical properties, histological features, and gene expression levels of several tendon and enthesis markers in three of the most clinically relevant anatomical localizations of enthesis injury. By doing so, we improved our understanding of the biology and morphology of the native tissue at the supraspinatus enthesis,

the patellar tendon enthesis, and the Achilles tendon enthesis. Moreover, from such characterization, we selected the patellar tendon enthesis as our model for future enthesis studies. This selection was mostly based on the adequate mechanical properties of the enthesis at this localization and the large cross-sectional area of the tendon-to-bone insertion site, which facilitated the handling and access to the tissue.

Following the characterization of the three different anatomical localizations, we investigated the regeneration of a tendon-to-bone attachment in a rodent model for enthesis regeneration. This is described in **Chapter 4**. There, a defect was created in rat patellar enthesis and subsequently treated with two versions of a biphasic silk fibroin scaffold. The scaffolds were designed to mimic the tendon-to-bone transition. However, one scaffold exhibited a smooth, interconnected transition between the phases, similar to the native transition characteristic of the healthy patellar enthesis while the second version showed an abrupt transition. The results of this *in vivo* study unequivocally demonstrated the superior capacity of the silk fibroin scaffold with the interconnected transition between the phases to promote the effective healing of the injured patellar enthesis in comparison to the scaffold with the abrupt transition. Hence, demonstrating the relevance of the morphological cues in the healing and regeneration of interphase tissues.

After demonstrating the positive effects that a biomimetic scaffold has in the process of healing and regeneration of an injured enthesis, we decided to research molecular cues that could further aid the regeneration of the enthesis. For this purpose, we dedicated **Chapter 5** to investigate the early healing response of an injured patellar enthesis. We looked into the development of fibrosis at the site of the injury and more specifically, into the potential role of microRNAs (miRNAs) in the regulation of fibrosis and the healing response. MicroRNAs are powerful epigenetic regulators of gene expression and they are known to intervene in many pathways and biological processes. By looking into the expression patterns of fibrosis-related miRNAs, we described a set of at least 13 miRNAs that were dysregulated within the first 10 days after an enthesis injury. Furthermore, target prediction analysis revealed that these miRNAs have the potential to regulate the mRNA expression of several tendon and enthesis markers. From this set of miRNAs, we selected one of the most dysregulated ones, miR-16-5p to investigate its potential use in tendon and enthesis healing applications.

In **Chapter 6**, we loaded a tendon-mimetic magnetic-responsive GelMa hydrogel with mimics or inhibitors of miR-16-5p and human mesenchymal stem cells (hMSCs). We then investigated the expression patterns of its direct target SMAD3 on the encapsulated cells. The 3D-transfections with the miR-16-5p mimic resulted in the sustained downregulation of SMAD3, whilst transfections with the

miR-16-5p inhibitor resulted in the upregulation of this target gene. Moreover, the presence of miR-16-5p mimics promoted the sustained upregulation of key tendon markers such as tenomodulin, tenascin-C, and decorin while decreasing the expression of collagen III. The opposite pattern was observed when the encapsulated cells were transfected with the miR-16-5p inhibitor. The results from this chapter highlight a probable tenogenic role for miR-16-5p that should be further investigated.

All in all, the work comprised in this thesis delves into the intricate world of tendons and entheses healing and the role of different morphological and molecular cues in the healing and regeneration process. The results herein described not only deepen our understanding of the healing mechanisms in play at the tendon and in particular the entheses upon injury, but also pave the way for innovative tissue engineering solutions to address their injuries and enhance their regeneration.

CHAPTER 9

# Publieke Samenvatting

## PUBLIEKE SAMENVATTING

Pezen verbinden spieren met botten en zijn daarom onontbeerlijk voor de beweging en de stabilisatie van gewrichten. Het weefsel dat spieren en pezen verbindt, wordt myotendineuze verbinding genoemd, en de interfase tussen pezen en botten wordt enthese genoemd. De pees-bot-enthese is misschien wel een van de meest uitdagende interfase-weefsels om te bestuderen en te behandelen bij letsel. Dit komt door het feit, dat de enthese twee weefsels met zeer verschillende mechanische eigenschappen verbindt.

De overgang van zacht naar hard bij de pees-bot-enthese bestaat uit tegengestelde gradiënten van collageen-architectuur en mineralisatie, die een soepele spanningsoverdracht van pezen naar bot mogelijk maken. De fysiologie van de pees-bot-enthese zorgt er echter voor, dat dit weefsel vaak verwond wordt. Helaas levert het genezingsproces van de enthese vaak littekenweefsel op met slechte mechanische eigenschappen, wat de kans op hernieuwd letsel van het aangetaste weefsel vergroot.

De momenteel beschikbare therapieën en chirurgische oplossingen voor de behandeling van entheseletsel hebben een aanzienlijk percentage mislukkingen. Patiënten met pees- of entheseletsel zullen in de toekomst waarschijnlijk opnieuw letsel oplopen, zelfs na een chirurgische ingreep om de pees en het bot te re-integreren.

Vooruitgang op het gebied van weefselmanipulatie biedt de hoop nieuwe strategieën te ontwikkelen om de regeneratie van de pees-bot-aanhechtingsplaats te verbeteren, terwijl littekenvorming wordt geminimaliseerd en het herstel van de oorspronkelijke morfologische en mechanische kenmerken van het beschadigde weefsel wordt gemaximaliseerd. In **hoofdstuk 2** van dit boek hebben we de stand van zaken samengevat betreffende de huidige pees- en enthese-therapieën en het gebruik van biomaterialen om de genezing en regeneratie van de enthese te bevorderen. Bovendien benadrukken we het potentieel van zijdebiomaterialen in het tissue engineering van pees- en entheseweefsel. Zijde is een aantrekkelijk biocompatibel en kosteneffectief biomateriaal met mechanische eigenschappen, die vergelijkbaar zijn met die van de pees. Bovendien kunnen op zijde gebaseerde biomaterialen worden gecombineerd met andere elementen en materialen om hybride constructies te creëren om de biocompatibiliteit te verbeteren en om de micro- en macro-omgeving van de pees-bot-overgang beter na te bootsen. In ons lichaam tellen we echter honderden pees-bot-enthesen, elk met een zeer gespecialiseerde morfologie, specifiek afgestemd op hun anatomische lokalisatie en fysiologie. Daarom hebben we in **hoofdstuk 3** de mechanische eigenschappen, histologische

kenmerken en genexpressieniveaus van verschillende pees- en enthese-markers onderzocht in drie van de meest klinisch relevante anatomische lokalisaties waar letsel van enthese voorkomt. Door dit te doen, verbeterden we ons begrip van de biologie en morfologie van het natuurlijke enthese weefsel van de supraspinatus-enthese, de patellapees-enthese en de achillespees-enthese. Bovendien hebben we op basis van deze karakterisering de patellapees-enthese geselecteerd als ons model voor toekomstige enthesestudies. Deze selectie was grotendeels gebaseerd op de adequate mechanische eigenschappen van de enthese op deze lokalisatie en het grote dwarsdoorsnedeoppervlak van de pees-bot-enthese, wat het hanteren van en de toegang tot het weefsel zal vergemakkelijken.

Na de karakterisering van de drie verschillende anatomische lokalisaties onderzochten we de regeneratie van een pees-bot-aanhechting in een knaagdiermodel voor enthese-regeneratie. Dit wordt beschreven in **hoofdstuk 4**. Daar werd een defect gecreëerd in de patella-enthese van ratten en vervolgens behandeld met twee versies van een bifasische zijde-fibroïne-implantaat. De implantaten zijn ontworpen om de overgang van pees naar bot na te bootsen. Eén implantaat vertoonde echter een vloeiende, onderling verbonden overgang tussen de fasen, vergelijkbaar met de oorspronkelijke overgang, die kenmerkend is voor de gezonde patella-enthese, terwijl de tweede versie een abrupte overgang vertoonde. De resultaten van dit *in vivo* onderzoek hebben ondubbelzinnig het superieure vermogen aangetoond van het zijde-fibroïne-implantaat met de onderling verbonden overgang tussen de fasen om de effectieve genezing van de beschadigde patella-enthese te bevorderen in vergelijking met het implantaat met de abrupte overgang. Hiermee wordt de relevantie van de morfologische opbouw voor de genezing en regeneratie van interfase-weefsels aangetoond.



Nadat we de positieve effecten hadden aangetoond, die een biomimetisch implantaat heeft in het proces van genezing en regeneratie van een beschadigde enthese, besloten we moleculaire signalen te onderzoeken die de regeneratie van de enthese verder zouden kunnen helpen. Voor dit doel hebben we **hoofdstuk 5** gewijd aan het onderzoeken van de vroege genezingsreactie van een beschadigde patella-enthese. We hebben gekeken naar de ontwikkeling van fibrose op de plaats van het letsel en meer specifiek naar de potentiële rol van microRNA's (miRNA's) in de regulatie van fibrose en de genezingsreactie. MicroRNA's zijn krachtige epigenetische regulatoren van genexpressie en het is bekend dat ze ingrijpen in veel routes en biologische processen. Door te kijken naar de expressiepatronen van fibrose-gerelateerde miRNA's, beschreven we een reeks van ten minste 13 miRNA's die binnen de eerste 10 dagen na een enthese-beschadiging ontregeld waren. Bovendien onthulde de analyse van mogelijke mRNA doelwitten, dat deze miRNA's het potentieel hebben om de mRNA-

expressie van verschillende pees- en enthesemarkers te reguleren. Uit deze reeks miRNA's hebben we een van de meest ontregelde miRNA's geselecteerd, miR-16-5p, om het potentiële gebruik ervan bij toepassingen voor pees- en enthese-regeneratie te onderzoeken.

In **hoofdstuk 6** hebben we een pees-imiterende, magnetisch reagerende GelMa-hydrogel beladen met imitatiemoleculen of remmers van miR-16-5p en humane mesenchymale stamcellen (hMSCs). Vervolgens onderzochten we de expressiepatronen van het directe doelwit SMAD3 op de ingekapselde cellen. De 3D-transfecties met de miR-16-5p-imitatie resulteerden in de aanhoudende onderdrukking van SMAD3, terwijl transfecties met miR-16-5p-remmer resulteerden in de versterkte expressie van dit doelgen. Bovendien bevorderde de aanwezigheid van miR-16-5p-imitatie de aanhoudende expressie van belangrijke peesmarkers zoals tenomoduline, tenascine-C en decorine, terwijl de expressie van collageen III werd verminderd. Het tegenovergestelde patroon werd waargenomen, toen de ingekapselde cellen werden getransfecteerd met de miR-16-5p-remmer. De resultaten uit dit hoofdstuk benadrukken een waarschijnlijke tenogene rol voor miR-16-5p, die verder onderzocht moet worden.

Al met al duikt het werk in dit proefschrift in de ingewikkelde wereld van pezen en bekrachtigt genezing en de rol van verschillende morfologische en moleculaire signalen in het genezings- en regeneratieproces. De hierin beschreven resultaten verdiepen niet alleen ons begrip van de genezingsmechanismen die een rol spelen bij de pees en in het bijzonder de enthesen bij letsel, maar maken ook de weg vrij voor innovatieve oplossingen voor weefselmanipulatie om verwondingen aan te pakken en weefselregeneratie per se te verbeteren.

CHAPTER 10

# Curriculum Vitae

Carlos Julio Peniche Silva

## BIOGRAPHY

Carlos Julio Peniche Silva was born on 5 July 1990 in Havana, Cuba. In 2008 he enrolled in the Licentiate program "Biochemistry and Molecular Biology" of the Faculty of Biology of the University of Havana. As part of this program, he worked as a visiting student in the Center of Genetic Engineering and Biotechnology (CIGB) on the research project "Development of an expression system for the obtention of recombinant IFN-γ in Escherichia coli". After his graduation in 2014, he joined a two-year research training program a the Center of Biomaterials of the University of Havana. There, he worked on the development of a drug delivery system for the parenteral administration of risperidone under the supervision of Prof. Dr. Carlos Peniche Covas.

In 2017, Carlos moved to Munich, Germany, and joined the Department of Experimental Trauma Surgery at the Klinikum rechts der Isar of the Technical University of Munich as a DAAD scholarship holder. There, he worked for two years on the subject "Dendriplexes as therapeutic tools for bone regeneration" under the supervision of Prof. Dr. Elizabeth Rosado Balmayor in the group of Prof. Dr. Martijn van Griensven.

In 2019, Carlos relocated to Maastricht, the Netherlands, to perform his PhD research at the MERLN Institute of Technology-Inspired Regenerative Medicine of Maastricht University under the supervision of Prof. Dr. Martijn van Griensven as promotor and Prof. Dr. Elizabeth Rosado Balmayor as co-promotor. During this period, Carlos focused on the development of novel tissue-engineering strategies to aid the healing and regeneration of the tendon-to-bone enthesis by exploring the use of biomimetic biomaterials and miRNA-based epigenetic regulation in tendon-to-bone enthesis healing applications. The results of his PhD work are described in this book.

## LIST OF PUBLICATIONS

1. **C.J. Peniche Silva**, E. Rosado Balmayor, and M. van Griensven, Chapter 19 - Silk biomaterials for tendon and tendon-to-bone enthesis tissue engineering, in Silk-Based Biomaterials for Tissue Engineering, Regenerative and Precision Medicine (SECOND EDITION), S.C. Kundu and R.L. Reis, Editors. 2024, Woodhead Publishing. p. 549-565.
2. **C.J Peniche Silva,** R.E. De la Vega, J. Panos, V.Joris, C.H. Evans, E.R. Balmayor, and M. van Griensven. MiRNAs as Potential Regulators of Enthesis Healing: Findings in a Rodent Injury Model. International Journal of Molecular Sciences, 24, 2023.
3. **C.J. Peniche Silva**, S.A. Müller, N. Quirk, R.E. De la Vega, M.J. Coenen, C.H. Evans, E.R. Balmayor, and M. van Griensven, Enthesis: not the same in each localization - a molecular, histological and biomechanical study. Eur Cell and Mater, 44, 2022.
4. **C.J. Peniche Silva**, S.A. Müller, N. Quirk, P.S.P. Poh, C. Mayer, A. Motta, C. Migliaresi, M.J. Coenen, C.H. Evans, E.R. Balmayor, and M. van Griensven. Enthesis Healing is Dependent on Scaffold Interphase Morphology-Results from a Rodent Patellar Model. Cells, 11(11), 2022.
5. R.E. De La Vega, M. van Griensven, W. Zhang, M.J. Coenen, C.V. Nagelli, J.A. Panos, **C.J. Peniche Silva**, J. Geiger, C. Plank, C.H. Evans, Elizabeth R. Balmayor. Efficient healing of large osseous segmental defects using optimized chemically modified messenger RNA encoding BMP-2. Science Advances, 8(7), 2022.
6. Groven, R.V.M., **C.J. Peniche Silva**, E.R. Balmayor, B.N.J. van der Horst, M. Poeze, T.J. Blokhuis, and M. van Griensven, Specific microRNAs are associated with fracture healing phases, patient age and multi-trauma. Journal of Orthopaedic Translation, 37, 2022.
7. **C.J. Peniche Silva**, G. Liebsch, R.J. Meier, M.S. Gutbrod, E.R. Balmayor, M. van Griensven. A New Non-invasive Technique for Measuring 3D-Oxygen Gradients in Wells During Mammalian Cell Culture. Frontiers in Bioengineering and Biotechnology, 8:595, 2020.
8. W. Zhang, R.E. De La Vega, M.J. Coenen, S.A. Müller, **C.J. Peniche Silva**, M.K. Aneja, C. Plank, M. van Griensven, C.H. Evans, E.R. Balmayor. An improved, chemically modified RNA encoding BMP-2 enhances osteogenesis in vitro and in vivo. Tissue Engineering Part A, 25, 2019

## AWARDS AND GRANTS

1. ON/EORS Education Grant - for attending the EORS 2023 Annual Meeting in Porto, Portugal. Prize: 500.00 CHF
2. ESCI Mobility Grant 2022 from the European Society for Clinical Investigation - for the project "Micro RNA as novel therapeutic tools to aid enthesis healing". Prize: 3,000 EUR
3. ON Kick-Starter Grant no. 20-105: "Tendon" (2020) for the project titled: "miRNA signature of injured tendon for developing novel molecular tendon regeneration therapy". Prize: 10,000.00 CHF

## LIST OF PODIUM PRESENTATIONS AT INTERNATIONAL CONFERENCES

1. miRNA-laden magnetic-responsive bioink for tendon and enthesis tissue-engineering. **C. J. Peniche Silva**, R. Dominguez, S.M Bakht, A. Pardo, V. Joris, A.I. Gonçalves, S. P. B. Texeira, E. R. Balmayor, M. E. Gomes, M van Griensven. EORS Annual Meeting 2023, Porto, Portugal. 09/2023
2. miRNAs as potential regulators of enthesis healing in a rodent injury model. **C. J. Peniche Silva**, R. E. De La Vega, V. Joris, C. H. Evans, E.R. Balmayor, M. van Griensven. TERMIS EU 2022, Krakov, Poland. 07/2022
3. Establishment of a Rat Model for Enthesis Regeneration Studies. **C. J. Peniche Silva**, S. A. Müller, N. Quirk, R. E. De la Vega, M. J. Coenen, C. H. Evans, E. R. Balmayor, M. van Griensven. NBTE Annual Meeting, De Werelt, the Netherlands. 04/2022
4. Genetic Signature and Biomechanical characterization of native entheses in a rat model. **C. J. Peniche Silva**, S. A. Müller, N. Quirk, R. E. De la Vega, M. J. Coenen, C. H. Evans, E. R. Balmayor, M. van Griensven. TERMIS World Congress, 2021, Maastricht, the Netherlands (Virtual due to Covid) 11/2021
5. Dendriplexes as tools for gene delivery. **C. J. Peniche,** N. Roumans E. R. Balmayor, M. van Griensven. TERMIS World Congress, 2021, Maastricht, the Netherlands. (Virtual due to Covid) 11/2021
6. miRNA Signature of an injured enthesis in an animal model. **C. J. Peniche Silva,** R.E. De la Vega, J. Panos, V.Joris, C.H. Evans, E.R. Balmayor, and M. van Griensven. Third Achilles Workshop, Porto, Portugal. 10/2021
7. Extracellular matrix gene expression of a tissue-engineered enthesis. **C. J. Peniche Silva,** S.A. Müller, C.H. Evans, E.R. Balmayor, and M. van Griensven. Surgical Research Days, RWTH Aachen University, Aachen, Germany. 09/2019
8. A new non-invasive optical sensor foil-based technique for measuring the 3D-oxygen gradient formation during mammalian cell culture. **C. J. Peniche Silva**, G. Liebsch, R.J. Meier, M.S. Gutbrod, E.R. Balmayor, M. van Griensven TERMIS EU 2019, Rodes, Greece. 04/2019

## POSTERS IN CONFERENCES

1. Characterization of an injured enthesis: insights on the role of miRNAs in tendon fibrosis and ectopic ossification. **C. J. Peniche Silva**, R.E. De la Vega, J. Panos, V.Joris, C.H. Evans, E.R. Balmayor, and M. van Griensven. TERMIS 2023, Manchester, UK. 03/2023
2. MiRNAs modulate enthesis-specific mRNA targets and collagen I and II expression. **C. J. Peniche Silva**, R.E. De la Vega, V.Joris, C.H. Evans, E.R. Balmayor, and M. van Griensven. ORS 2022 Annual Meeting, Tampa, Florida, USA. 2022
3. MiRNAs as potential regulators of enthesis healing in a rodent injury model **C. J. Peniche Silva**, R.E. De la Vega, J. Panos, V.Joris, C.H. Evans, E.R. Balmayor, and M. van Griensven. NBTE Annual Meeting, De Werelt, the Netherlands. 12/2022

CHAPTER 11

# Acknowledgements

## ACKNOWLEDGMENTS

Some people like sports, others prefer reading, and many enjoy both. Some people love the cold, others prefer warmth, and a few always complain. Differences can bring people apart, while common goals bring people together. The journey I have just completed with the work summarized in this book, is the result of the combined effort of very different people working all together for a common goal. This section is dedicated to all of them.

To **Martijn** and **Elizabeth**, I have so much to thank you for. Your guidance, trust, and full commitment throughout my PhD made me feel confident and safe at every step of the way. Martijn, or "Profe" as I often call you, thank you for the infinite patience, for the open discussion, for the encouragement, for the pride with which you always stood by my side. Elizabeth, Eli, thank you for the optimism, for the mentorship, for the shared knowledge and the unconditional support. Thank you, Eli and Martijn for being always there not just to listen, but to make my challenges your challenges and my goals your goals. Having you both as my supervisors, but more importantly, as part of my life, has been the definitive highlight of my PhD. As a couple not only in science but in life, you have nurtured me as your apprentice, your friend, and your family, and by doing so you have transformed my life in every possible way.

To my co-authors and collaborators, thanks for the trust, the help, and the commitment to good science. To **Chris**, **Rodo**, **Joe**, **Michael**, thanks for the feedback, the teamwork, the knowledge, and the support. To **Manuela**, **Rui**, **Mahwish**, **Alberto**, **Ana**, **Simão**, thanks for welcoming me as one of you, and moving heaven and earth to make the best out of my time with you at the 3'Bs.

To my scientist paranymph, **Martyna**, thanks for being a friend, for always being ready and available for me every time I needed your help. Thanks for making me feel that I could always count on you. It never mattered what it was, you were there, ready to deliver a parcel across Europe with extremely short notice, to puppysit Leito during my Colloquium presentation, to share coffee and chocolates between incubation times, or to stand next to me on one of the most important days of my career.

To my second paranymph, "el" **Denis**, thanks for being that piece of Cuba that makes me feel at home every time we are together. My friend, *mi hermano,* thanks for always being proud of me and for celebrating my victories as if they were your own. Thanks for standing always by my side.

To the members of Martijn's & Elizabeth's group, **Virginie, Claudia, Rald, Claire, Steven, Madina, Margot, Fangzhou**, thanks for the discussion and feedback, for the teamwork and help. Our Monday meetings were always a great source of scientific output, ideas, and solutions thanks to all of you.

To **Rald,** thanks for the energy, the friendship, for the crazy fun winter bike rides, for all the help in and out of the labs.

To **Virginie**, thanks for your dedication, the dark humor, for being always willing to help and for always having that extra aliquot of primer or antibody for me.

To **Timo**, **Marloes**, **Nadia**, **Dennie**, **Denis**, thanks for your prompt reply and always quick reaction, your patience in dealing with me every time I forgot a lab duty, and for all the help in the office and/or in the labs. You were always the right person for the right job.

To **Daniel**, **Monize**, **Tristan**, **Julia**, **Stefan, Pere**, **Johana, Anne**, **Shivesh**, **Claudia, Mirco, Gabriele, Paula** thank you for the costume parties, the picnics, the dinners, and drinks together, and the unforgettable weekends of "glamping". To **Adrian** and **Kike**, you truly made my days brighter. To **Fangzhou**, thanks for your contagious positivity and the great Chinese food. Thanks **Claire** and **Mirco** for the amazing brownies… you should have birthdays every month!

To **Francesca** (Giacomini) for sharing your tenocytes with me, for the tips and tricks. To **Sveva, Pierpaolo, Vivek, Alberto, Marie, Liline, Tim, Helen, Elizabetta, Sophia, Dorian, Vini**, **Jaehyeon**, **Fiona** thanks for good vibes. To each and every one at MELRN, that took the time to chat over lunch, to smile back at a greeting, to cheer me up with their positive attitude, I thank you all.

To the **PIs** from MERLN that took time from their busy agenda to catch up, to show interest in how I was progressing and for always offering words of encouragement. Thanks **Paul** and **Niloo**, for being the first people at MERLN to approach me and for making me feel so welcome on my first day in the office.

To those that shared the passion for cycling with me, which was essential to balance the stress of work with the pleasures of life: **Rald** (is not that cold you said?), **Anne** (people don't imagine how brave/crazy you can be on a mountain bike), **Daniel** and **Shivesh** (thanks for the longest ride!), **Fransiska** and **Arianne** (you girls are really fast!), **Pere** and **Marione** (thanks for sharing the road with me), **Martijn** (always a pleasure to ride with you).

To the bouldering crew, **Daniel** (this time Pereira), **Jasia**, **Rald**, **Gabriela**, **Omar**, **Francesca**, **Tom**, and the new and ever-growing generation of climbers from MERLN. Thanks for pushing me to my limits, to overcome my fears and be better every day.

To **Franciska** for the friendship and all the pictures we took together, we indeed made a great team, that magazine turned out beautifully!

And of course, to my family:

We have reached this milestone together, **mimi, mami, pipo, Irmi, tata**. Thank you for the love and unconditional support. To my parents, thanks for the education you gave me and the examples you set me to follow. Thanks to my invincible mimi for teaching me that there are no limits to what we can achieve.

And to my partner in life, the love of my life, **Brendi**, you have danced with me every step of the way. You have shared with me all my ups and downs. You have supported me, encouraged me, pushed me, and loved me at my best and my worst. Thanks for the strength and courage with which you followed me to the unknown. Thanks for taking a pile of bricks in the cloudy Maastricht and transforming it into the warmest home. Thanks for Leito, thanks for saying "yes, I'll go with you".